UNIVERSIDADE ESTADUAL DE CAMPINAS
INSTITUTO DE QUÍMICA

PAULLA BEATRIZ FRANÇA DE SOUSA

ACIDITY OF 2D LAMELLAR ALUMINOSILICATES IN THE PRESENCE AND ABSENCE OF WATER

ACIDEZ DE ALUMINOSSILICATOS LAMELARES 2D NA PRESENÇA E NA AUSÊNCIA DE ÁGUA

CAMPINAS
2024

PAULLA BEATRIZ FRANÇA DE SOUSA

ACIDITY OF 2D LAMELLAR ALUMINOSILICATES IN THE PRESENCE AND ABSENCE OF WATER

ACIDEZ DE ALUMINOSSILICATOS LAMELARES 2D NA PRESENÇA E NA AUSÊNCIA DE ÁGUA

Dissertação de Mestrado apresentada ao Instituto de Química da Universidade Estadual de Campinas como parte dos requisitos exigidos para a obtenção do título Mestra em Química na área de Química Inorgânica.

Master's Dissertation presented to the Institute of Chemistry of the University of Campinas as part of requirements to obtain the title of Master in Chemistry in the area of Inorganic Chemistry.

Supervisor: Dr. Heloise de Olivera Pastore Jensen
Co-supervisor: Dr. Marco André Fraga

O arquivo digital corresponde a versão final da dissertação defendida pela aluna Paulla Beatriz França de Sousa e orientada pela Profa. Dra. Heloise de Oliveira Pastore Jensen e coorientada pelo Prof. Dr. Marco André Fraga.

CAMPINAS
2024

Ficha catalográfica
Universidade Estadual de Campinas (UNICAMP)
Biblioteca do Instituto de Química
Simone Luiz Alves - CRB 8/9094

So85a
Sousa, Paulla Beatriz França de, 1999-
Acidity of 2D lamellar aluminosilicates in the presence and absence of water / Paulla Beatriz França de Sousa. – Campinas, SP : [s.n.], 2024.

Orientador(es): Heloise de Oliveira Pastore Jensen.
Coorientador(es): Marco André Fraga.
Dissertação (mestrado) – Universidade Estadual de Campinas (UNICAMP), Instituto de Química.

1. RUB-18. 2. Sítio ácido. 3. Óxido de trimetilfosfina. 4. Conversão de biomassa. 5. Ressonância magnética nuclear de fósforo-31. I. Jensen, Heloise de Oliveira Pastore, 1962-. II. Fraga, Marco André. III. Universidade Estadual de Campinas (UNICAMP). Instituto de Química. IV. Título.

Informações complementares

Título em outro idioma: Acidez de aluminossilicatos lamelares 2D na presença e na ausência de água
Palavras-chave em inglês:
RUB-18
Acid site
Trimethylphosphine oxide
Biomass conversion
Phosphorus-31 nuclear magnetic resonance
Área de concentração: Química Inorgânica
Titulação: Mestra em Química na área de Química Inorgânica
Banca examinadora:
Heloise de Oliveira Pastore Jensen [Orientador]
Paulo Cesar de Sousa Filho
Jean Marcel Ribeiro Gallo
Data de defesa: 07-11-2024
Programa de Pós-Graduação: Química

Identificação e informações acadêmicas do(a) aluno(a)
- ORCID do autor: https://orcid.org/0000-0002-5050-3429
- Currículo Lattes do autor: http://lattes.cnpq.br/5713269061250256

BANCA EXAMINADORA

Prof.ª Dr.ª Heloise de Oliveira Pastore Jensen (Orientadora)

Prof. Dr. Paulo Cesar de Sousa Filho (Universidade Estadual de Campinas - UNICAMP)

Prof. Dr. Jean Marcel Ribeiro Gallo (King Abdullah University of Science and Technology - KAUST)

A Ata da defesa assinada pelos membros da Comissão Examinadora, consta no SIGA/Sistema de Fluxo de Dissertação/Tese e na Secretaria do Programa da Unidade.

Este exemplar corresponde a redação final da Dissertação de Mestrado defendida pela aluna **Paulla Beatriz França de Sousa**, aprovada pela Comissão Julgadora em 07 de novembro de 2024.

I dedicate this work to my family, Arinaldo de Sousa, Luzimar F. Sousa, Janaína F. Sousa, and Childebergue C. Matos, whom I deeply admire and who have unconditionally accompanied me, even at a distance, during another academic journey.

ACKNOWLEDGMENTS

I am very thankful to God for guiding me on this intriguing and challenging path, full of ups and downs, that is life, and for giving us such a vast, beautiful, and mysterious universe. It motivates me to try to understand it. That is why I have chosen science to be always by my side. I consider myself blessed. He always showed me that no matter how difficult my path was, it was the right one for me to grow.

To my beautiful family from Natal/RN and Rio de Janeiro/RJ: Arinaldo de Sousa, Luzimar F. Sousa, Janaína F. Sousa, Childebergue Matos, Jóbson F. Sousa, Hibson Sousa, Ana Maria A. Sousa, Edimilson A. Sousa, Lúcia Sena (*In memoriam*), Katiene Sena, Emerson Sena, Kelly Sena, Cláudio Mota, Christopher Sena, Cleber Sena and Tayani Sena. I could not have done it without you. Thanks for your concern, affection, patience, attention, and especially, for the emotional, spiritual, and mental support! For the moments of leisure during trips and concerts, lunches and dinners with the family, and celebrations of special occasions. Every time that I felt lost, you helped me get back on track and feel stronger. Even if you are not part of the academic world, please know that you have been fundamental to the development of this work! To my dear Aunt Lucia, I want it on record. I am sorry you are not here, especially for the eight months in 2023 when I went to Rio to work and study. But I would like to thank you for the opportunity to live with you and your family for those two months in 2020-2021. I got to know you and created a stronger, lovely, and meaningful family bond. I am deeply grateful for this!

To my supervisor and co-supervisor, Dr. Heloise O. Pastore (Lolly) and Dr. Marco A. Fraga, for providing me with the invaluable opportunity to work in your laboratory. I am profoundly grateful for your confidence in my work, the comprehensive experimental support you have provided to develop this research, the knowledge you have shared, the guidance you have offered, and your attention and patience. You played a crucial role in enabling me to complete this academic stage. During this period, I was able to grow professionally and personally, I realized my dream of studying and working at IQ/UNICAMP and I had a wonderful time working at INT. I had access to analyses and equipment, especially the opportunity to operate them, that I would never have imagined I could have. I will be eternally grateful for all of this!

To the professor Dr. Sibele B. C. Pergher, for her academic guidance during my undergraduate degree in Chemistry, for celebrating and being happy with me for my achievements during this period, and for the support that I needed for my transition from the Federal University of Rio Grande do Norte (UFRN) to the University of Campinas (UNICAMP).

To my co-workers, “ex co-workers” and friends from GPM^3/UNICAMP: Dr. Erica Munsignatti, Dr. Flavia de Sousa, Marcelo Brasil, Dr. Lanousse Petiote, Dr. Juliana Floriano, Dr. Bruna N. Silva, M.Sc. Débora Pinheiro, Dr. Monize Picinni, Dr. Ricardo Passini, Lorena Lima, and M.Sc. Guilherme Campos. These almost two years and six months were unique! You are the best! The most exceptional professionals I have ever had the pleasure and opportunity to work with, share knowledge with, learn from, and talk to. Thank you for all the *happy hours*, snacks, lunches, skewers with beers at Toca, and the most wonderful cakes with coffee! For your incredible support and patience, for listening to me, and for putting up with my craziness! Also, I would like to thank Flávia and Erica (*“Fraviaaa e Ericaaaa”*) for always being willing to help me whenever I needed it. It isn't easy losing family support due to distance, thus I will be eternally grateful for everything!

To my catalytic fellows of the Catalysis Division at the National Institute of Technology (INT - Rio de Janeiro), especially the Fraga's team: M.Sc. Paola Oliveira, Dr. Elise Albuquerque, Dr. Leon Feitosa, Dr. Simone Canhaci, Dr. Kryslaine Santos, Dr. Vinicius W. Faria, Dr. Camila G. Silva, Dr. Camila Lopes, M.Sc. Cleuber Mendes, and M.Sc. Karina Lima. Wow! It's been an incredible eight months! All those breakfasts, lunches, *happy hours*, for accompanying me on the academic trips (CBCAT-2023 and RASBQ-2024), and the activities at the lab were pretty fun and made me feel at home. Thank you for the experimental support and expertise in the catalytic tests. It was an honor that our paths crossed and that I had the opportunity to work with you!

To my friend M.Sc. Fernando Azevedo, and my friends of the LEEDS laboratory at the IQ/UNICAMP, especially Felipe Barbosa, Neuryelen Bandeira, M.Sc. Raul Artisiani, Dr. Lucas Silva, and Dr. João Damasceno. Who would have thought that an analytical chemistry course could allow me to meet and get to know some spectacular people? That is right! I am grateful for the company, the relaxed chats on all possible and unimaginable topics, the coffee time, the advice and venting, laughter, and the like!

To my friends at Natal/RN, mainly Lucas M. Nascimento, Davis V. Nascimento, M.Sc. Janaína Gomes, M.Sc. Francisco Emanuel Silva, Waltécio Cortez, Rohdriggo Cardoso, Júlia Oliveira, Arlan Dantas (and his family), Lara Souza, Mariana Teixeira, and my friends at Analytical Center - IQ/UFRN and LABPEMOL/UFRN. Also, to my dear scientist colleagues, spread around the world, Prof. Dr. Roberto Lima and M.Sc. Vitor Greati. I am grateful for sharing with me the experiments, knowledge, advice, and conversations about everything, including the most important: life, science, the academic world, papers, coffee, wine, and artesian beer! You have been with me for a long time and particularly mean a lot to me. I am thankful for all the times we have met, the fun moments, the trips to the beach, and the bars/restaurants/coffee shops. Each time I went home, I recharged "my batteries" and returned to Campinas feeling focused and determined. I am also grateful for cheering me on and being happy about my achievements.

I thank the Institutional Laboratory of Nuclear Magnetic Resonance (LIRMN) technical team at the IQ/UNICAMP, especially the B.Sc. Anderson Pedrosa and M.Sc. Carolina Galuppo, for teaching, training, sharing experiences and knowledge, fun moments, and performing the NMR analyses. You are the best, guys! Thanks for everything!

To the Analytical Chemistry Testing and Development Laboratory (LADEQ) of the Chemistry and Biotechnology Division at the INT/RJ, I am grateful to Natália Guimarães, Agape Mattos, and Dr. Camila Lopes for the performance of my chromatographic analyses.

I should not forget to thank Marcos Magalhães and Wilson Gonçalves (Glassware Repair and Mechanic Divisions at IQ/UNICAMP) for their expertise on my Schlenk and autoclaves whenever I need them! To the Institute of Chemistry (UNICAMP) and the National Institute of Technology (INT) for the experimental support to develop this research.

To the professors at the Institute of Chemistry at UNICAMP and the Department of Chemical Engineering at the State University of Rio de Janeiro (UERJ), especially Dr. Jackson Megiatto, Dr. William Araújo, Dr. Lauro Kubota (*In memoriam*), Dr. Amelie Rochet, and Dr. Deborah Vargas, who have worked assiduously with the excellence of my academic education, instigating the knowledge through classes and advice to achieve my goals.

"Last but not least, I wanna thank me. I wanna thank me for believing in me, doing all this hard work, having no days off, never quitting, tryna do more right than wrong, and just being me at all times." (Snoop Dogg)

This work was supported by the São Paulo Research Foundation (FAPESP), grant n° 2022/05743-0 and project n° 2021/12058-0.

The author also acknowledges the Coordenação de Aperfeiçoamento de Pessoal de Nível Superior – Brasil (CAPES) for partial financial support - Finance Code 001.

“A scientist in his laboratory is not a mere technician: she/he is also a child confronting natural phenomena that impress her/him as though they were fairy tales.”

(Marie Skłodowska-Curie)

RESUMO

Além dos silicatos lamelares serem conhecidos como excelentes trocadores iônicos, a substituição isomórfica (IS) do Si^{4+} por um átomo-T^{3+} na estrutura confere propriedades ácidas. Assim, esses materiais podem ser aplicados em processos catalíticos que demandem acessibilidade aos sítios ácidos por moléculas volumosas. Sabe-se que os sítios de alumínio estrutural (sítios Al_{Td} - $(SiO_4)_4Al$) com acidez de Brönsted (BAS) nos materiais H-[Al]-RUB-18 foram ativos na desidratação do etanol. Porém, a acidez dos sítios de alumínio parcialmente-estruturais (sítios Al_{Oh} ou aluminol - $(SiO_4)_3Al\text{-}(OH)(H_2O)_2$) não é completamente conhecida. as propriedades ácidas dos sítios aluminol presente no RUB-18 foram elucidadas utilizando a técnica espectroscópica de caracterização das propriedades ácidas, ^{31}P-NMR do óxido de trimetilfosfina (TMPO) adsorvido, em conjunto com testes catalíticos na presença e ausência de água. Os catalisadores lamelares não-semeados e semeados foram sintetizados com razões molares nominais Si/Al iguais a ∞, 15, 30, 60, e caracterizados por DRX, FRX, ^{29}Si- e ^{27}Al-RMN. Os valores das razões das espécies de Si^{4+} (Q^3/Q^4) nos materiais lamelares Na-[Al]-RUB-18 indicam defeitos estruturais devido a uma grande presença de grupos silanol, influenciando no processo de IS com a incorporação de espécies de Al_{Td}/Al_{Oh} em diferentes proporções na estrutura. Com isto, a análise espectroscópica indicou que os sinais ^{31}P resultam de TMPO adsorvido na superfície das lamelas, nos sítios silanol/aluminol e nos sítios ácidos de Brönsted. O grau de cristalinidade da estrutura, a quantidade e as espécies de alumínio presentes na estrutura, e a variação da concentração de TMPO nas análises na presença e na ausência de água conduziram a alterações nas ressonâncias ^{31}P. Dois sinais de ressonância na região de sítios ácidos de Brönsted foram atribuídos às espécies de Al_{Td} e Al_{Oh}. Uma correlação clara entre a capacidade de adsorção dos sítios ativos e as intensidades dos picos na região de BAS prova a influência da água no processo de adsorção. O nosso estudo traz evidências adicionais de que as espécies $(SiO_4)_4Al$ and $(SiO_4)_3Al\text{-}(OH)(H_2O)_2$ desempenharam um papel crucial nas reações de conversão derivados de biomassa. A identificação do levulinato de etila como produto final na alcoólise do álcool furfurílico é indicativo da sua formação apenas em BAS de força média. Para as reações-modelo de conversão da di-hidroxiacetona e piruvaldeído, foi revelada a atividade simultânea dos sítios ácidos de Brönsted/Lewis, com a possibilidade dos sítios aluminol atuarem como LAS. O presente estudo esclarece as caraterísticas de acidez dos sítios aluminol no material lamelar RUB-18 e chama a atenção para a avaliação desses parâmetros nos catalisadores sólidos em fase aquosa.

ABSTRACT

In addition to lamellar silicates being known by their ion exchange properties, the isomorphous substitution (IS) of Si^{4+} by T^{3+}-atoms in the structure confers acidic properties. Thus, these materials can be applied in catalytic processes that demand the accessibility of bulky molecules to the acid sites. While framework-Al (Al_{Td} - $(SiO_4)_4Al$) sites on [Al]-RUB-18 materials with Brönsted acidity were active in ethanol dehydration, the acidity of partial framework-Al sites (Al_{Oh} or aluminol sites - $(SiO_4)_3Al\text{-}(OH)(H_2O)_2$) remains unknown. ^{31}P-NMR of adsorbed trimethylphosphine oxide (TMPO) was used together with catalytic reactions in the presence and absence of water to elucidate the acidity features of aluminol sites on lamellar RUB-18. Acidic non-seeded and seeded lamellar catalysts (nominal Si/Al molar ratios = ∞, 15, 30, 60) were synthesized and characterized by XRD, XRF, ^{29}Si- and ^{27}Al-MAS-NMR. The synthesis of lamellar Na-[Al]-RUB-18 yielded materials with Si^{4+} species ratios (Q^3/Q^4) ≥ 2, indicating structural defects due to the large presence of silanol groups. This influenced the process of IS with the incorporation of Al_{Td}/Al_{Oh} species in different proportions into its structure. Herein, spectroscopic analysis indicates the ^{31}P signals arise from TMPO adsorbed on the lamellar surface, silanol/aluminol sites, and Brönsted acid sites. The crystallinity degree of the structure, amount of aluminum in the structure, completely and partially framework-Al species, and TMPO loadings, under wet and dry conditions, all lead to changes in ^{31}P resonances. Two resonance signals at the BAS range were attributed to Al_{Td} and Al_{Oh} species. A clear correlation between the adsorption capacity of the active sites and peak intensities in the BAS region proves the influence of water in the adsorption process. This study brings additional evidence that the $(SiO_4)_4Al$ and $(SiO_4)_3Al\text{-}(OH)(H_2O)_2$ species played a crucial role in biomass-derivative conversion reactions. The identification of ethyl levulinate as the final product in the furfuryl alcohol reaction is indicative of the presence of medium-strength BAS. For the dihydroxyacetone and pyruvaldehyde conversions, it was revealed the simultaneous activity of Brönsted/Lewis acid sites, with the possibility of the aluminol sites acting as Lewis acid sites. The present study clarifies the acidity features of aluminol sites on lamellar [Al]-RUB-18 and brings attention to the evaluation of these features in the solid catalysts under aqueous-phase conditions.

LIST OF FIGURES

Figure 1.1: A graphical simplified representation of the (A) Na-RUB-18 and (B) H-RUB-18 unit cell in the [101] directions [4, 5]. **24**

Figure 1.2: Scientific papers about the lamellar silicate RUB-18, published until September 2022 with the terms (A) "ilerite" or "octosilicate", and (B) "rub-18" or "na-rub-18". The following colors designate the main research groups and researchers: Wilhelm Schwieger - light purple, Makoto Owaga - dark cyan, Hermann Gies – yellow, and GPM^3/Heloise O. Pastore – light red. Source: Scopus Elsevier Database (Accessed: Sep. 2022). **25**

Figure 1.3: A graphical simplified representation of the Si^{4+} (Q^3 and Q^4 sites) and Al^{3+} (Al_{Td} and Al_{Oh} sites) species on the lamella surface of the acidic RUB-18 (structural unit: cavities [5^4] in [101] directions). **28**

Figure 1.4: Different scenarios to adsorbed trialkylphosphine oxide (R_3PO, with R = CH_3) on an acidic solid surface: (a) -SiOH groups, (b) Lewis acid sites (LAS from tricoordinate-Al) and (c) Brönsted acid sites (BAS from tetracoordinate-Al)....................................... **31**

Figure 1.5: Reaction schemes for evaluating the activity and strength of Brönsted (BAS) and Lewis (LAS) acid sites: Model reaction A - through alcoholysis of furfuryl alcohol; Model reaction B - through reaction of pyruvaldehyde to lactic acid; Model reaction C - through cascade reaction converting dihydroxyacetone to lactic acid. **33**

Figure 1: XRD patterns for (A) sodium and (B) acidic lamellar RUB-18, with *[Al y]* are the lamellar aluminosilicates with *y* equal to the experimental Si/Al molar ratios **45**

Figure 2: (A) ^{29}Si- and ^{27}Al-MAS-NMR spectra for sodium and acidic lamellar RUB-18, with different Si/Al molar ratios. *[Al y]* are the lamellar aluminosilicates with *y* equal to the experimental Si/Al molar ratio. The values between the parentheses *(x)* are the Q^3/Q^4 and Al_{Td}/Al_{Oh} molar ratios for the ^{29}Si- and ^{27}Al-NMR spectra, respectively. (B) Graphical representation of the Si^{4+} and Al^{3+} species on a structural unit of RUB-18 (cavities [5^4] in [101] directions). **46**

Figure 3: ^{31}P-MAS-NMR spectra for H-R18 and H-[Al]-R18 non-seeded samples in the absence of water, with different Si/Al and Al_{Td}/Al_{Oh} molar ratios and P/Al molar ratio equal (A) 1.20 and (B) 0.50. The values between the parentheses *(x)* are the proportional percentages concerning the ^{31}P resonance signals above 50 ppm (For details, see the percentage values for all signals in the spectra in Table S.2.). **48**

Figure 4: ^{31}P-MAS-NMR spectra for H-R18 and H-[Al]-R18 seeded samples in the absence of water, with different Si/Al and P/Al molar ratio = (A) 1.4, (B) 0.50, and (C) 0.25. The deconvoluted signals were magnified 4x. **51**

Figure 5: ^{31}P-MAS-NMR spectra for H-R18 and H-[Al]-R18 non-seeded samples in the presence of water (2 mol H_2O: 1 mol Al_{Oh}), with different Si/Al and Al_{Td}/Al_{Oh} molar ratios, and P/Al molar ratio = 0.50. The values between the parentheses *(x)* are the proportional percentages concerning the ^{31}P resonance signals above 50 ppm (For details, see the percentage values for all signals in the spectra in Table S.2.). **52**

Figure 6: ^{31}P-MAS-NMR spectra for hydrated materials, saturated with physisorbed H_2O molecules: (A) H-R18 and H-[Al]-R18 seeded samples, with different Si/Al and Al_{Td}/Al_{Oh} molar ratios, and P/Al molar ratio = 1.40; (B) H-[Al16]-R18 and (C) H-[Al47]-R18$_{(seeded)}$ samples, with different TMPO loadings (P/Al molar ratio). The deconvoluted signals for (B) and (C) graphs were magnified 3x concerning (A) graphs. The values between the parentheses *(x)* are the proportional percentages concerning the ^{31}P resonance signals above 50 ppm (For details, see the percentage values for all signals in the spectra in Table S.2.). **53**

Figure 7: Boxplot of δ^{31}P (ppm) values for TMPO absorbed over non-seeded and seeded lamellar RUB-18 as a function of the following possible site types: physisorbed TMPO (o – light red), ≡SiOH/≡AlOH groups (o – dark cyan), BAS(1) from Al_{Oh} (o – light purple), BAS(2) from Al_{Td} (o – purple). The box represents one standard deviation (SD) according to the distribution of the values. The gray dash-dot line is the limit of molecular interactions (Chem. = chemisorption, and Phys. = physisorption). **55**

Figure 8: (A) FTIR spectra for pure dehydrated (a) H-R18 and (b) H-[Al16]-R18 non-seeded samples. (B) Schemes of a chain of H-bonds on lamella surface of H-R18 and H-[Al16]-R18 non-seeded samples in [010] direction. **56**

Figure 9: Conversion (X, %) and Selectivity (S, %) values, and respective graphs of the relation between structural properties and selectivity ratios for H-[Al]-R18 catalysts: (A) Alcoholysis of FFA (3 h of reaction), (B) PA reactions (values for 3 h of reaction), (C) Hydrolysis of DHA (average values of 3 h and 6 h of reaction in duplicate). Carbon balance was determined within the range of 86% - 96%, based on measurements obtained through CG-FID and HPLC-RID techniques. In the catalyst axis, the autothermal reactions are represented by *AT*, and *[Al y]* are the aluminosilicate catalysts with *y* equal

to the Si/Al molar ratio before the reaction. 58

Figure 10: Illustration of pyruvaldehyde adsorption by displacement of water molecules on aluminol sites (as Lewis acid sites) in the lamellar surface of H-[Al]-RUB-18. 61

Figure S.1: Digital image of home-built Schlenk: (a) valves and taps to achieve high vacuum; (b) main cell; (c) secondary cell. 72

Figure S.2: TG and differential TG curves of (A) sodium and (B) acidic seeded lamellar RUB-18, with different Si/Al molar ratios. To guarantee the maintenance of the structure with -OH groups on the lamellar surface of RUB-18, the maximum temperatures used for the treatment of these materials were as follows: 140 °C (*H-R18*), 250 °C (*H-[Al32]-R18*), 280 °C (*H-[Al29]-R18*), and 290 °C (*H-[Al16]-R18*). 73

Figure S.3: XRD patterns spectra of sodium and acidic lamellar acidic seeded lamellar RUB-18. 75

Figure S.4: FTIR spectra of sodium lamellar samples. The inner graph corresponds to samples after ion exchange (— *solid curve*) and acid form (--- *dashed curve*): (ii) NH_4- and (i) H-R18$_{(Seeded)}$; (iv) NH_4- and (iii) H-[Al25]-R18$_{(Seeded)}$; (vi) NH_4- and (v) H-[Al47]-R18$_{(Seeded)}$. 75

Figure S.5: ^{27}Al- and ^{29}Si-MAS-NMR spectra of sodium and acidic lamellar acidic seeded lamellar RUB-18. 76

Figure S.6: TG and differential TG curves of sodium and acidic seeded lamellar RUB-18, with different Si/Al molar ratios: Na- and H-R18$_{(Seeded)}$ (— *solid curves*); Na- and H-[Al25]-R18$_{(Seeded)}$ (--- *dashed curves*); Na- and H-[Al47]-R18$_{(Seeded)}$ (··· *dotted curves*). *To guarantee the maintenance of the structure with -OH groups on the lamellar surface of RUB-18, the maximum temperature used for thermal treatment of these materials was 250 °C. 76

Figure S.7: Proposal for reaction pathways to the alcoholysis of furfuryl alcohol, according to the compounds observed by GC-MS. 77

Figure S.8: Structural characterization by XRD analysis of catalysts before (--- *dashed curves*) and post-DHA (— *solid curves*) and PA (··· *dotted curves*) reactions, with different experimental Si/Al molar ratios before reaction. 78

Figure S.9: Structural characterization by ^{27}Al-MAS-NMR analysis of catalysts before (--- *dashed curves*) and post-DHA (— *solid curves,* ··· *dotted curves* = reactions in duplicate), and PA reactions (— *solid curves*), with different experimental Si/Al molar ratios before reaction. **78**

Figure S.10: Evaluation of variation of the tetrahedral and octahedral Al species concentration for each catalyst in the function of total Al concentration (mmol g^{-1}) before reaction: (A) data from the DHA reaction (average values ± standard deviation), and (B) data from the PA reaction. **79**

Figure A.1: Experimental apparatus for adsorption procedure of TMPO as probe molecule: (a) oven; (b) schlenk with sample connected to a vacuum line; and (c) turbomolecular pump to achieve high vacuum. **90**

Figure A.2: Digital image of schlenk: (a) valves and taps to achieve high vacuum; (b) main cell; and (c) secondary cell. **90**

Figure A.3: Digital image of (a) batch multi-reactor system: (b) manometer; (c) gas flow; (d) carousel with the reactors; and (e) digital temperature controller. **91**

Figure A.4: Digital image of continuous flow reaction system: (a) HPLC pump with the substrate solution; (b) digital temperature controller; (c) manometer; (d) oven with the reactor; and (e) sampler. **91**

Figure B.1: Analytical curve for Na^+ at λ = 589.592 nm employed for quantification of the metal in synthesized lamellar samples. **92**

Figure C.1: Analytical curve of substrate solutions and the respective regression data for alcoholysis reactions. **93**

Figure C.1: (Cont.) Analytical curve of substrate solutions and the respective regression data for alcoholysis reactions. **94**

Figure C.2: Chromatogram of the analytical curve of 0.250 mol L^{-1} of substrate solutions and the compound retention times (RT): Pyruvaldehyde (PA, RT = 10.2 min); Lactic acid (LA, RT = 10.8 min); and Dihydroxyacetone (DHA, RT = 11.9 min). **95**

Figure C.3: Analytical curve of substrate solutions and the respective regression data for DHA and PA reactions. **96**

Figure D.1: Aliquots from FFA alcoholysis reaction (multi-reactor - batch process): 0h = blank aliquot at 0 h, r2 = H-[Al16]-R18, r4 = H-R18, r6 = H-[Al29]-R18, r8 = autothermal, r10 = H-[Al32]-R18. .... **97**

Figure D.2: Chromatogram obtained by GC-MS of the FFA to EL reaction (Catalyst = H-[Al16]-R18). **98**

Figure E.1: Aspects of the catalysts before and post-PA and post-DHA reactions. **99**

Figure E.2: Aliquots of PA in continuous flow reaction (fixed-bed in a tubular reactor). **100**

Figure E.3: Aliquots of DHA in continuous flow reaction (fixed-bed in a tubular reactor). **101**

Figure E.4: Chromatograms of the pyruvaldehyde to lactic acid reactions (time of reaction = 3 h). **102**

Figure E.5: Chromatograms of the dihydroxyacetone to lactic acid reactions (time of reaction = 6 h). **103**

LIST OF TABLES

Table 1.1: Characteristics values of chemical shifts to the trimethylphosphine oxide (TMPO) adsorbed on acid catalyst solids [40]. **30**

Table 1.2: Comparison of the methods for acidity characterization of solid acid catalysts. Legend: + superior, ± satisfactory, - inferior; R = $C_nH_{(2n+1)}$, (*n* = 1, 2, 4, and 8); B = BAS and L = LAS. Reproduced from [41]. **31**

Table S.1: Determination of Si^{4+} and Al^{3+} species molar ratios and the molar chemical composition of the unit cell for acidic non-seeded lamellar materials. **73**

Table S.2: Percentage of resonance signals for ^{31}P-NMR spectra of dehydrated and hydrated lamellar materials. The values between parentheses are the respective chemical shifts... **74**

Table S.3: Si/Al and Al_{Td}/Al_{Oh} molar ratios, and concentration of Al species before and after catalytic reactions. **77**

Table D.1: Compounds and the respective retention time analyzed in GC-MS (Catalyst used in FFA reaction = H-[Al16]-R18). **97**

LIST OF ABBREVIATIONS

AIMD	***a***_b_ ***i***_nitio_ **M**olecular **D**ynamics
Al$_{Oh}$	Octahedrally coordinated aluminum
Al$_{Td}$	Tetrahedrally coordinated aluminum
AS	**A**cid **S**ites
BAS	**B**rönsted **A**cid **S**ites
BEA	Zeolite Beta
CBU	**C**omposite **B**uilding **U**nit
DFT	**D**ensity **F**unctional **T**heory
DHA	**Dih**ydroxy**a**cetone
DPE	**D**eprotonation **E**nergy **V**alues
DTG	**D**ifferential **T**hermo**g**ravimetry
EFAL	**Extra-f**ramework **A**luminum
EL	**E**thyl **L**evulinate
EMF	2-ethoxy**m**ethyl-**f**uran
FFA	**F**urfuryl **A**lcohol
FID	**F**lame **I**onization **D**etector
FTIR-Py	**F**ourier-**T**ransform **I**nfra**r**ed spectroscopy of adsorbed **Py**ridine
GPM^3	*__G__rupo de __P__eneiras __M__oleculares __M__icro e __M__esoporosas* (Micro and Mesoporous Molecular Sieves Group)
GC	**G**as **C**hromatograph
HPDEC	**H**igh **P**ower **Dec**oupling
HPLC	**H**igh-**P**erformance **L**iquid **C**hromatography
ICP-OES	**I**nductively **C**oupled **P**lasma **O**ptical **E**mission **S**pectrometry
IS	**I**somorphous **S**ubstitution
LA	**L**actic **A**cid
LAS	**L**ewis **A**cid **S**ites
MAS-NMR	**M**agic-**a**ngle **S**pinning **N**uclear **M**agnetic **R**esonance spectroscopy
MCM-41	**M**obil **C**omposition of **M**atter - forty-one
MFI	Code for zeolite ZSM-5
M.P.	**M**elting **P**oint
MS	**M**ass **S**pectrometer
PA	**P**yruv**a**ldehyde

PTFE	**P**oly**t**etra**f**luoro**e**thylene
RID	**R**efractive **I**ndex **D**etector
RUB-18	**R**uhr **U**niversity **B**ochum - eighteen
SS-NMR	**S**olid-**s**tate **N**uclear **M**agnetic **R**esonance spectroscopy
TPD-NH_3	**T**hermo-**p**rogrammed **d**esorption of ammonia
TMPO	**T**ri**m**ethyl**p**hosphine **o**xide
XRD	**X**-**r**ay **D**iffraction
XRF	**X**-**r**ay **F**luorescence
ZSM-5	**Z**eolite **S**ocony **M**obil - **f**ive

CONTENTS

1. INTRODUCTION 23

1.1. Context and relevance of the study 23

1.1.1. Lamellar silicate: RUB-18 23

1.1.2. Catalytic reactions: the *"active"* acidity 26

1.1.3. Techniques for the determination of acidity in solid catalysts: Nuclear Magnetic Resonance Spectroscopy of trisubstituted phosphine oxides 29

1.1.4. Additional characterization of acid properties: Catalytic model reactions to convert biomass derivatives 32

1.2. Objectives 34

2. DOCUMENTS TO BE PUBLISHED 36

2.1. Original research article entitled "Partial framework-Al in lamellar H-[Al]-RUB-18: acidity by probe TMPO adsorption and catalytic study in the presence and absence of water" 36

3. FINAL CONSIDERATIONS 80

3.1. Conclusions 80

3.2. Future perspectives 81

REFERENCES 83

ANNEX A: EXPERIMENTAL APPARATUS FOR ADSORPTION AND CATALYTIC PROCESSES 90

ANNEX B: ANALYTICAL CURVE FOR ICP-OES ANALYSIS 92

ANNEX C: ANALYTICAL CURVES FOR FFA, DHA, AND PA CONVERSION REACTIONS 93

ANNEX D: ALIQUOTS AND CHROMATOGRAMS OF FFA CONVERSION REACTIONS 97

ANNEX E: CATALYSTS, ALIQUOTS AND CHROMATOGRAMS OF DHA AND PA

CONVERSION REACTIONS 99

ANNEX F: DECLARATION FOR ALTERNATIVE FORMAT FOR DISSERTATION AND THESIS 104

1. INTRODUCTION

1.1. Context and relevance of the study

1.1.1. Lamellar silicate: RUB-18

The crystal structure of Na-RUB-18 was described by Gies and co-authors in 1997 [1]. RUB-18 are two-dimensional solids whose structure consists of double sheets of silicates. The structure is formed by the union of cavities [5^4], and its basic unit consists of four 5-membered rings with SiO_4 tetrahedral, which is similar to the composite building unit (CBU) ***mor*** of the MFI and MOR zeolites.

The chaining of these cavities generates silicate sheets that are interspersed with chains of Na^+ ions octahedrally coordinated with H_2O molecules. The surface of the lamella contains silanol (≡SiOH) and silanolate (≡SiO^-) groups, with a thickness of approximately 1.1 nm in the [001] direction. The interlayer space is filled by negatively charge-compensating hydrated Na^+ ions from the ≡SiO^- groups and their shared edges form parallel one-dimensional chains in the [100] and [010] directions. Thus, the following chemical composition describes the unit cell:

$$Na_8[Si_{32}O_{64}(OH)_8] \cdot 32\,H_2O$$

Subsequently published work [2, 3] provided information about the hydrogen bond network on the lamella surface formed by Si–O–H···($^-$O)–Si bridges, which gives the three-dimensional structure of the silicate lamellar, as well as the dynamics and conduction of protons in this network as a function of temperature variation. It was only in 2008 that Gies and coauthors [4] summarized the existing results and added new information, providing a complete structural characterization of Na-RUB-18. **Figure 1.1** shows a simplified representation of the unit cell of Na- and H-RUB-18 in the [101] directions.

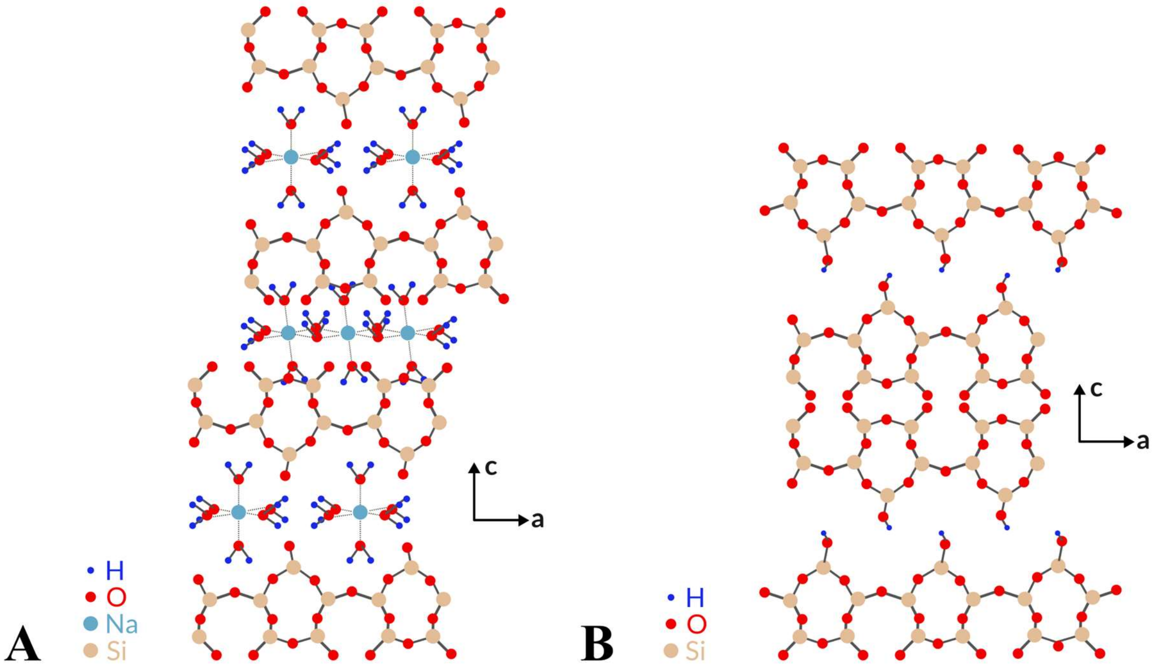

Figure 1.1: A graphical simplified representation of the **(A)** Na-RUB-18 and **(B)** H-RUB-18 unit cell in the [101] directions [4, 5].

In addition, the potential to chemically and geometrically modify the interlayer space of hydrated lamellar silicates provides a wide range of applications. The reactivity of the ≡SiOH groups enables their functionalization, and their basic unit is the main structural element of microporous materials with high silica content [6, 7].

Several papers have been published about the transformation of the lamellar structure into another silicate, zeolites, and mesoporous molecular sieves through topotactic recrystallization, hydrothermal restructuration assisted by surfactants, and pillarization [8-11]. The isomorphous substitution (IS) of Si^{4+} by T^{3+}-atoms, such as Al^{3+} ions, through hydrothermal synthesis generates acid sites without changing its structure. The acidic properties of these lamellar solids are created which endow the structure with new functionalities, with application in heterogeneous catalysis [12-14].

According to the data catalogued up to September 2022 by Scopus (Elsevier Database), 141 documents have been identified, with 114 articles published in scientific journals related to three nominations for the lamellar silicate RUB-18 (“*ilerite”*, *“octosilicate”* and *“Na-RUB-18 or RUB-18”*). **Figure 1.2** shows the number of publications on RUB-18 since 1988, highlighting the research groups that have continued to work on this material. The published works generally include studies on the definition of structural characteristics, changes in the synthesis route, incorporation of metals into the structure, intercalation and grafting with organic molecules, pillarization, and transformation of the lamellar structure into another silicate and zeolites.

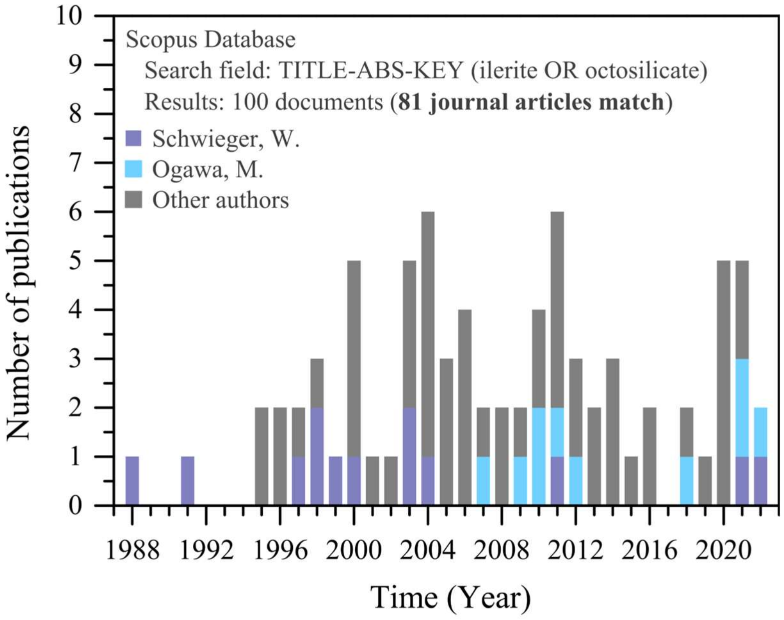

(A)

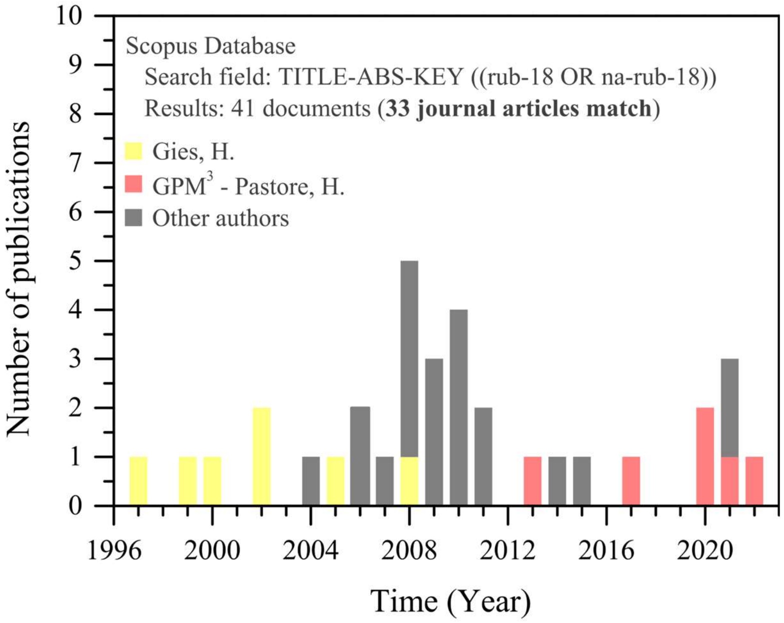

(B)

Figure 1.2: Scientific papers about the lamellar silicate RUB-18, published until September 2022 with the terms **(A)** “ilerite” or “octosilicate”, and **(B)** “rub-18” or “na-rub-18”. The following colors designate the main research groups and researchers: Wilhelm Schwieger - light purple, Makoto Owaga - dark cyan, Hermann Gies – yellow, and GPM^3/Heloise O. Pastore – light red. Source: Scopus Elsevier Database (Accessed: Sep. 2022).

The [Al]-RUB-18 materials were prepared only recently [15-19]. Although there are three or four other research groups in the world that are studying diligently the lamellar silicate RUB-18, the synthesis strategy for the lamellar aluminosilicates RUB-18 presented in the Brazilian researcher group's papers is original (the papers are highlighted in light red as seen in **Figure 1.2.B**). These researchers developed the synthesis methodology and are still investigating the acidity of these two-dimensional aluminosilicates.

The acidic and structural properties introduced by the presence of aluminum in these solids were demonstrated by rigorous characterization and using some specific acidic model reactions. In this way, the active sites available on the surface of the lamellar solids allow them to be used in interesting catalytic reactions. However, the acidic properties of [Al]-RUB-18 are not yet completely known, especially concerning the correlation with the structure and composition of the lamella when compared with zeolites, their 3D-analogues, and the influence of Al-species on the structure.

1.1.2. Catalytic reactions: the *"active"* acidity

Lamellar aluminosilicates possess distinct advantages over zeolitic materials: they do not exhibit spatial limitations regarding catalytic site location. The structure of 2D materials is composed of thin lamella; thus, their active catalytic sites are exposed in the interlamellar space and on the surface of the crystals. Because of the easy access of interlayer space, these spaces can be enlarged by intercalation of bulky molecules [17-20]. It is now possible to carry out reactions that could not be catalyzed on zeolites due to the large size of the reactants and products.

Many gas-phase reactions using acidic solid catalysts have been investigated and successfully deployed by the chemical industry [21]. Most heterogeneous catalytic processes are conducted under elevated temperature and pressure conditions, and the characteristics of the active sites on these catalysts employed in the gas-phase processes have been widely discussed in the literature [21, 22]. However, active sites acting in liquid-phase transformations, where the water is the final product, the solvent/cosolvent, or still part of the biomass, are not completely understood [23].

Special attention is given to the need for water-tolerant acid sites in aqueous phase transformations over heterogeneous catalysts. It is essential to gain insight into the reactant/solvent-catalyst interactions and deactivation mechanisms, including phenomena such as leaching, carbon deposition, poisoning, phase transition, and restructuring of active sites. This knowledge can be obtained by probing these sites under aqueous-phase processes, which is crucial for the development of stable catalysts [23, 24].

In this regard, alternative chemical routes are researched for using bio-renewable, sustainable, and low-cost feedstocks. Biomass valorization represents a pathway for upgrading sustainable raw or pretreated feedstock into value-added products [25]. The residual biomass, originating from industry and as agriculture waste, is an alternative, renewable, and abundant carbon source [25, 26]. In this context, hydrolysis of biopolymers that constitute biomass has emerged as a promising sustainable energy source to produce fuels and fine chemicals, reducing the global economy's reliance on fossil fuels [27, 28].

Biomass conversion processes are commonly conducted in aqueous phases at temperatures less than 300 °C, with chemical reactions including hydrolysis, dehydration, isomerization, aldol condensation, and hydrodeoxygenation [23, 25]. The hydrothermal stability of the active sites in solid acid catalysts has become increasingly important in the last years, and aqueous-phase biomass transformations require catalyst design strategies to avoid deactivations and improve durability [24]. Moreover, aqueous-phase systems represent an effective and environmentally sustainable medium for biomass conversion [29]. The use of water as a non-toxic and clean solvent renders this process greener for the chemical industry [30].

Campos and collaborators [20] demonstrated the excellent performance of H-[Al]-magadiite, an acidic lamellar aluminosilicate, for catalytic reactions of hydrolysis of cellobiose. The results indicate the presence of active and stable Lewis acid sites (LAS) in the catalyst, even in the aqueous-phase continuous flow reaction, at high temperature and pressure. Besides, the stability and maintenance of the magadiite structure during and after the reaction made this catalyst a greater option for the conversion of biomass-derived molecules.

Magadiite and Na-RUB-18 belong to the same family of hydrous sodium layer silicates [4]. These lamellar silicates have some similar properties. However, one difference is the presence of Q^3 and Q^4 silicon sites in different proportions, hence the lamella thickness. In this way, the incorporation of Al^{3+} ions into the lamellar framework ends up generating different Al species, such as framework-Al (tetrahedrally coordinated aluminum - Al_{Td}) and partial framework-Al sites (octahedrally coordinated aluminum - Al_{Oh} as aluminol sites or

$(SiO_3)_3$-Al(OH)$(H_2O)_2$) [16]. Such species could form different active acid sites on the lamella surface. **Figure 1.3** illustrates the Si^{4+} and Al^{3+} species on the lamella surface of the RUB-18.

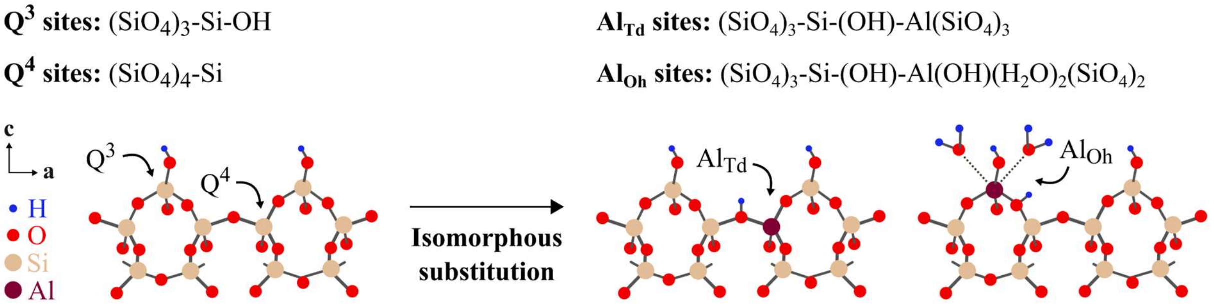

Figure 1.3: A graphical simplified representation of the Si^{4+} (Q^3 and Q^4 sites) and Al^{3+} (Al_{Td} and Al_{Oh} sites) species on the lamella surface of the acidic RUB-18 (structural unit: cavities [5^4] in [101] directions).

According to the Brönsted-Lowry and Lewis concepts on acidity and basicity [31,32], Brönsted acids are species that tend to lose a hydrogen ion (H^+), and Brönsted bases are species with the tendency to gain a hydrogen ion (H^+). Conversely, Lewis acids are defined as electron-pair acceptor species, and Lewis bases are electron-pair donor species. Also, a Lewis adduct is formed by the sharing of the electronic density of the frontier molecular orbitals, from the base's HOMO orbitals to the acid's LUMO orbitals.

In this regard, the structure and composition of acidic solid catalysts, such as molecular sieves and metal oxides, will be critical to forming and identifying Bronsted (BAS) and Lewis (LAS) acid sites. For example, the formation of BAS and/or LAS can occur after Si atoms are partly substituted by Al atoms in silicates. As illustrated in **Figure 1.3**, BAS arises from acidic bridging hydroxy groups (≡Al−(OH)−Si≡), and LAS are generated by complete (tri-coordinate Al) or partial coordination (octa-coordinate Al – Al_{Oh} species) of aluminum to the structure, or even by extra-framework aluminum species (Aluminum oxide, Al_2O_3 – Al_{Oh} species) [33,34].

It was proved that the acidic lamellar aluminosilicate magadiite and RUB-18 contain aluminum structural sites with Brönsted acidity, and these sites were active in the ethanol dehydration reaction [17,19,35]. Nevertheless, these reactions were conducted in the gas phase, and the acidic properties of [Al]-RUB-18, mainly the aluminol sites $(SiO_3)_3$-Al(OH)$(H_2O)_2$), in the presence of water still remain to be fully evaluated.

1.1.3. Techniques for the determination of acidity in solid catalysts: Nuclear Magnetic Resonance Spectroscopy of trisubstituted phosphine oxides

Acid/base strength measurements are determined by thermodynamic parameters of acidity and basicity in the gas phase [32, 36]. In this context, an increase in proton affinity (expressed as an enthalpy, ΔH) and gas-phase basicity magnitudes (expressed as an entropy, ΔG = Gas-Phase Basicity and Acidity – GB and GA, respectively) indicates an increase in the difficulty of removing the hydrogen from BAS. In other words, the more positive the value of the thermodynamic parameters, the stronger the base will be, while the weaker its conjugated acid will be. Thus, the use of strong bases in acidity measurements allows for the identification of active center heterogeneity in terms of strength (strong, medium, or weak) and nature (Brönsted or Lewis).

Several analytical and spectroscopical techniques are applied to characterize acid properties in solid catalysts: Hammett acid-base titration, microcalorimetry, thermo-programmed desorption of ammonia (TPD-NH_3), Fourier-transformed infrared spectroscopy of acid-sites adsorbed pyridine (FTIR-Py), and solid-state nuclear magnetic resonance spectroscopies (SS-NMR) [37]. The last three techniques above are based on the adsorption/desorption of basic probe molecules on the catalyst acid sites. The acidic properties are determined by direct or indirect detection of acid-active centers, including the nature/type, concentration, strength, or location/accessibility.

In the case of TPD, the heat associated with the ammonia adsorption/desorption process on the acid sites is evaluated through variable temperature measurements [38]. TPD-NH_3 provides data about the concentration and strength of the total acid sites from the amount of ammonia desorbed and the associated temperature during the heating process.

For the FTIR technique, pyridine molecules or their analogous substitutes are used [39]. FTIR-Py offers insights into the nature (Brönsted or Lewis) and concentration of the sites. The vibrational frequency of each pyridine species formed after adsorption on the catalyst is related to the observed position of the stretching bands in the spectrum. These species include the pyridinium ion derived from BAS (PyH^+) and the pyridine that is coordinatively bound to LAS. The acidic sites are also quantified by combining the intensity of the bands and the corresponding molar extinction coefficient (ε) using the Lambert-Beer law. The ability to retain pyridine at higher temperatures reflects the presence of stronger acid sites in the desorption process.

Trisubstituted phosphine (R_3P) or phosphine oxides (R_3PO) species are used in SS-NMR experiments of the ^{31}P nucleus [40, 41]. Any alterations in the chemical environment of the ^{31}P nucleus after the adsorbed probe interacting with active sites on the catalyst surface are discernible by signals in the resonance spectrum. Thus, solid-state ^{31}P-NMR gives quantitative and qualitative evaluations of Brönsted/Lewis's acidity [42]. It is commonly applied to the adsorption processes on zeolites, heteropolyacids, and pure or modified metal oxides [41]. It has been widely employed because ^{31}P is a naturally abundant nucleus (100%) with a wide chemical shift range and high sensitivity in the interactions between the probe molecules and active sites [43-49]. The ^{31}P spectra give information about strength (weak, medium, or strong), nature (Brönsted or Lewis), concentration, and spatial distribution/accessibility of the active sites (inside of the pores or on the surface of the crystals) by linear correlation with the chemical shifts, the peak positions, the spectrum/peaks integration, and by using different probe molecule sizes, respectively [41].

Trimethylphosphine oxide (TMPO - M.P. = 140 °C) is extensively used in this process due to its kinetic diameter (0.55 nm) allowing adsorption on many catalysts, especially on microporous solids [50]. Also, this phosphine oxide (proton affinity = 910 kJ mol^{-1}) is a base with intermediate force when compared with other probe molecules applied in acid properties measurements, such as pyridine (proton affinity = 930 kJ mol^{-1}) and ammonia (proton affinity = 854 kJ mol^{-1}) [51].

Attribution	**$\delta^{31}P$, ppm**
Crystalline TMPO	39 ppm
Physisorbed TMPO	45 ppm
-SiOH groups	52 – 59 ppm [49]
LAS	50 – 60 ppm
BAS	50 – 100 ppm
Superacidity	> 86 ppm

Table 1.1: Characteristics values of chemical shifts to the trimethylphosphine oxide (TMPO) adsorbed on acid catalyst solids [40].

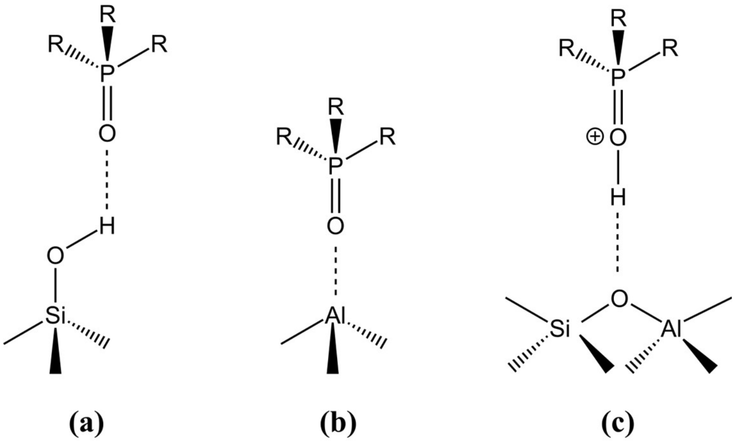

Figure 1.4: Different scenarios to adsorbed trialkylphosphine oxide (R_3PO, with R = CH_3) on an acidic solid surface: **(a)** ≡SiOH groups, **(b)** Lewis acid sites (LAS from tricoordinate-Al) and **(c)** Brönsted acid sites (BAS from tetracoordinate-Al).

Table 1.1 illustrates the assignments of the chemical shift of the resonance signals when TMPO is adsorbed on acid-catalytic solids. **Figure 1.4** shows the different chemical environments of the ^{31}P nucleus of the trialkylphosphine oxide molecules when they are chemisorbed and physisorbed on acidic solids with structural Si and Al atoms. These structures may be a little oversimplified in relation to the surface of lamellar solids.

Method	**Type**		**Location**	**Concentration**	**Strength**
	Brönsted	**Lewis**			
Hammett titration	+	-	-	-	+
TPD-NH_3	+	±	-	+	±
FTIR	+	-	-	-	+
FTIR-Py	+	+	-	±	-
FTIR-CO	-	+	-	-	+
^1H-NMR	+	-	-	+	-
^1H-NMR (pyridine-d_5)	+	-	-	±	+
^{31}P-NMR (TMP)	+	+	-	+ (B); + (L)	- (B); + (L)
^{31}P-NMR (TRMPO)	+	+	+	+ (B); + (L)	+ (B); - (L)

Table 1.2: Comparison of the methods for acidity characterization of solid acid catalysts. Legend: + superior, ± satisfactory, - inferior; R = $C_nH_{(2n+1)}$, (n = 1, 2, 4, and 8); B = BAS and L = LAS. Reproduced from [41].

Some experimental techniques do not allow a complete acid characterization of the solid catalysts. **Table 1.2** exhibits the effectiveness of the main methods for measuring acidity in providing information on the properties of the active sites (type, location, concentration, and strength). TPD and FTIR spectroscopy are complementary techniques used to evaluate the acidity parameters of a catalyst [33, 52, 53]. In addition, these conventional methods cannot provide information about spatial correlations of acid sites as can be given by the two-dimensional homo/heteronuclear correlation SSNMR techniques [41].

Another important aspect is the acidity characterization when the solid catalysts are conditioned in a hydrated environment. A change in the local properties of acid sites can occur in the presence of water, making it necessary to understand these effects better to design solid acid catalysts for technological applications [24, 54]. Experimental limitations of conventional techniques make it difficult to select an appropriate acidity characterization method for the analysis in the presence of water.

In FTIR-Py analysis, the literature has reported many ε values for each pyridine species that are used for quantification in an anhydrous medium [39, 55], which may differ when the analysis is performed on hydrated samples, resulting in inaccurate quantitative results. In contrast, the TMPO ^{31}P-NMR technique facilitates analysis in the presence and absence of water, adjusts temperature treatments, and avoids damaging the structure of the catalyst. Some authors have used this approach to study the "invisible acid nature", comparing the spectra of dehydrated and hydrated probe-loaded samples [56, 57].

In this context, the ^{31}P-NMR technique on dehydrated and hydrated TMPO-loaded samples will provide new insights into the acidic properties of partial framework-Al sites on H-[Al]-RUB-18. To evaluate the acid sites on silicate and aluminosilicate materials, adsorption experiments were carried out in the presence and absence of water with distinct TMPO loadings.

1.1.4. Additional characterization of acid properties: Catalytic model reactions to convert biomass derivatives

For the catalytic tests, three model reactions were selected to investigate the nature, activity, and strength of the active sites on H-[Al]-RUB-18. These reactions have known mechanisms and have been extensively studied in the literature: the alcoholysis of furfuryl alcohol [58], pyruvaldehyde conversion to lactic acid [59], and the hydrolysis of dihydroxyacetone to lactic acid [60]. The reaction schemes are shown in **Figure 1.5**.

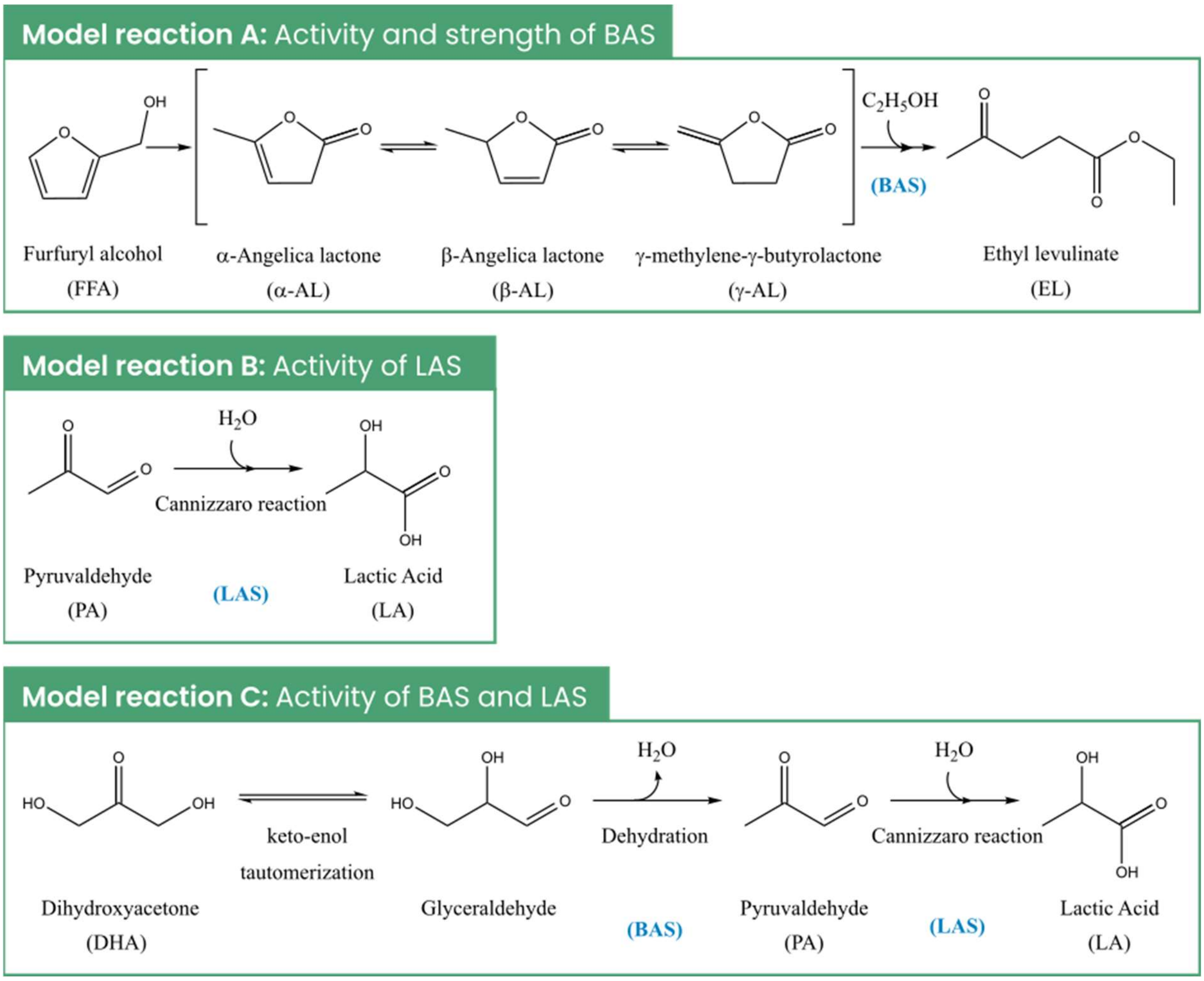

Figure 1.5: Reaction schemes for evaluating the activity and strength of Brönsted (BAS) and Lewis (LAS) acid sites: **Model reaction A** - through alcoholysis of furfuryl alcohol; **Model reaction B** - through reaction of pyruvaldehyde to lactic acid; **Model reaction C** - through cascade reaction converting dihydroxyacetone to lactic acid.

The activity and strength of the Brönsted acid sites (BAS) were evaluated using the alcoholysis reaction of furfuryl alcohol (FFA) to produce ethyl levulinate (EL). In general, alkyl levulinates attracted more attention due to their wide applications as chemical solvents, flavorings, and fuel additives [61-63]. One of the most important routes to the synthesis of EL is from renewable and low-cost feedstocks. Lignocellulosic biomass is a promising green alternative route for obtaining FFA to produce EL [61, 64]. The details of reaction mechanisms are reported by the literature. Faria *et al.* [58] investigated that the hydrolysis of FFA to levulinic acid occurs in two steps catalyzed by BAS, with no contribution from Lewis centers. Angelica lactones are the reaction intermediates, in which BAS strength is critical for this conversion. Then, EL can be formed by Fischer esterification of levulinic acid with ethanol. In this work, the reaction parameters used in FFA hydrolysis will be applied to the alcoholysis reaction (**Figure 1.5** - Model reaction A). Anhydrous ethanol will be the solvent in order to evaluate the acid sites without the presence of water.

Other two model reactions were chosen to investigate only LAS activity and simultaneous LAS/BAS activity. **Figure 5** provides a schematic representation of the conversion of pyruvaldehyde (PA) and dihydroxyacetone (DHA) into lactic acid (LA). Lactic acid is an important chemical compound for many industries, mainly related to its use in food additives and the production of biodegradable polymers (PLA - poly(lactic acid)) [65]. Alternative chemical routes are researched for the use of bio-renewable feedstock for trioses conversion into LA. Special attention is given to the need for water-tolerant acid sites in aqueous phase transformations over heterogeneous catalysts. Few recent studies are using this system to produce LA [54, 66-67]. Thus, cascade reactions of DHA (**Figure 1.5** - Model reaction C) occur in two principal steps, the first one requires BAS to form PA, and the last step exclusively requires LAS to convert PA into LA (**Figure 1.5** - Model reaction B and C) [59,60].

In this study, non-seeded and seeded H-[Al]-RUB-18 materials were synthesized with different Si/Al and Al_{Td}/Al_{Oh} molar ratios. The structural and compositional properties of these lamellar aluminosilicates were determined. Acidic properties in the presence and absence of water were first studied by the TMPO adsorption process as a probe molecule. Subsequently, solid-state ^{31}P-MAS-NMR spectroscopy of the TMPO-loaded samples was applied to the structural evaluation of the partial framework-Al acidity on H-[Al]-RUB-18. Furthermore, the “active acidity” of the lamellar materials was also probed by using model reactions for the conversion of biomass derivatives. The activity and strength of the Brönsted acid sites (BAS) were evaluated using the alcoholysis reaction of FFA to produce EL. Additionally, a continuous flow aqueous-phase reaction system was used to evaluate only the Lewis acid site (LAS) activity, and simultaneous activity of BAS and LAS. This involved the corresponding catalytic reactions: pyruvaldehyde conversion to LA, and cascade reaction of dihydroxyacetone to form LA.

1.2. Objectives

This work aims to investigate the acidity of the lamellar aluminosilicates RUB-18 in the presence and absence of water. To achieve this, the study steps will include:

- Synthesis of the lamellar silicate and aluminosilicates, with different Si/Al nominal molar ratios = ∞, 15, 30, and 60.

- Structural, compositional, and thermal characterization of the materials by: XRD, solid-state NMR of ^{27}Al and ^{29}Si nucleus, XRF, FTIR, ICP-OES, and TG/DTG.
- To measure the acidity of TMPO absorbed as probe molecules on lamellar [Al]-RUB-18 using ^{31}P-MAS-NMR analysis:
    - Evaluation of different TMPO concentrations: P/Al ratio = 1.40 to 0.25.
    - Analysis in the presence and absence of water.
- To acquire information about the "active" acidity using catalytic model reactions:
    - Activity and strength of Brönsted acid sites (BAS): alcoholysis of furfuryl alcohol to ethyl levulinate.
    - Activity of Lewis acid sites (LAS): pyruvaldehyde to lactic acid conversion via Cannizzaro mechanism.
    - Activity of Brönsted and Lewis acid sites (BAS/LAS): Cascade reaction to converting dihydroxyacetone to lactic acid.

2. DOCUMENTS TO BE PUBLISHED

The following study details the findings of an experimental investigation into the acidity features of partial framework Al-type species on acidic lamellar material [Al]-RUB-18. It also includes a comprehensive discussion of the results. ^{31}P-NMR spectroscopic analyses were performed in combination with catalytic tests to probe the active sites under dry and wet conditions. The objective is to comprehend the effect of dimensionality and structural connection on the nature and strength of the aluminum sites inserted into the structures of solids. In addition, this study highlights the importance of exploring the acidity properties of solid catalysts under aqueous-phase conditions, particularly in the context of lamellar materials.

2.1. Original research article entitled “Partial framework-Al in lamellar H-[Al]-RUB-18: acidity by probe TMPO adsorption and catalytic study in the presence and absence of water”

The author will publish the following documents (the Manuscript and Supplementary Information) to RSC Catalysis Science and Technology or Applied Surface Science.

- **Graphical Abstract**

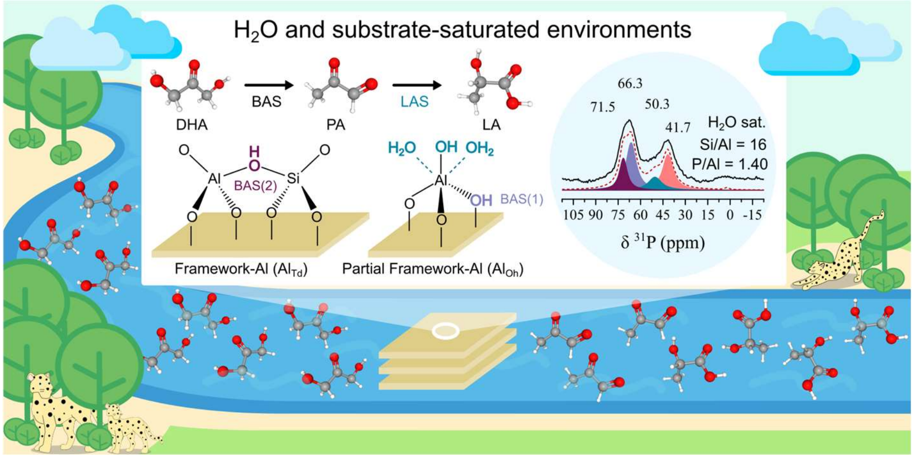

Partial framework-Al in lamellar H-[Al]-RUB-18: acidity by probe TMPO adsorption and catalytic study in the presence and absence of water

Paulla B. F. Sousa[1,2], Elise M. Albuquerque[2], Marco A. Fraga[2,3*], and Heloise O. Pastore[1*]

[1]*Micro and Mesoporous Molecular Sieves Group, Institute of Chemistry, University of Campinas, Campinas-SP,13083-862, Brazil.*
[2]*Instituto Nacional de Tecnologia (INT), Laboratory of Catalysis, Rio de Janeiro-RJ, 20081-312, Brazil.*
[3]*Department of Chemical and Materials Engineering, Pontifical Catholic University of Rio de Janeiro (PUC-Rio), 22453-900 Rio de Janeiro, RJ, Brazil.*

*Corresponding authors: marco.fraga@int.gov.br (M.A. Fraga); lolly@unicamp.br (H.O. Pastore)

Abstract

While framework-Al (Al_{Td}) sites on [Al]-RUB-18 materials with Brönsted acidity were active in ethanol dehydration, the acidity of partial framework-Al sites (Al_{Oh} or aluminol sites) remains unknown. ^{31}P-MAS-NMR of ^{31}P nucleus of adsorbed trimethylphosphine oxide (TMPO) was used together with catalytic reactions, in the presence and absence of water, to elucidate the acidity features of aluminol sites on lamellar RUB-18. Herein, spectroscopic analysis indicates the ^{31}P signals arise from TMPO adsorbed on the lamella surface of RUB-18 ($\delta^{31}P = 40 – 49$ ppm), silanol/aluminol sites ($\delta^{31}P = 49 – 56$ ppm), and Brönsted acid sites (60 – 75 ppm). The crystallinity degree of the structure, Si/Al and Al_{Td}/Al_{Oh} molar ratios, and TMPO loadings, under wet and dry conditions, all lead to changes in ^{31}P resonances. Two resonance signals at 69 ppm and 64 ppm were attributed to Al_{Td} and Al_{Oh} species. A clear correlation between the adsorption capacity of the active sites and peak intensities in the BAS region proves the influence of water in the adsorption process. This study brings additional evidence that the $(SiO_4)_4Al$ and $(SiO_4)_3Al\text{-}(OH)(H_2O)_2$ species played a crucial role in biomass-derivative conversion reactions. The simultaneous activity of Brönsted/Lewis acid sites was revealed, with the possibility of the $(SiO_4)_3Al\text{-}(OH)(H_2O)_2$ sites acting as LAS. The present study clarifies the acidity features of aluminol sites on lamellar [Al]-RUB-18 and brings attention to the evaluation of solid catalysts under aqueous-phase conditions.

KEYWORDS: RUB-18, Partial framework-aluminum, BAS/LAS, TMPO adsorption, Biomass conversion

1. Introduction

The lamellar silicate Na-RUB-18 is built by the union of [5^4] cavities that consist of four 5-membered rings of tetrahedral SiO_4. Lamella surfaces display silanolate/silanol groups, the interlamellar space is filled by hydrated Na^+ charge-compensating ions, which, by shared edges, form 1-dimensional parallel chains in [100, 010] directions [1-2]. The potential to chemically modify the framework of layered silicates increases the possibility of applications [3-4]. The isomorphous substitution (IS) of Si^{4+} by T^{3+}-atoms, such as Al^{3+} ions through hydrothermal synthesis, generates acid sites without changing their structure. The acidic properties of lamellar solids are created which endow the structure with new functionalities, with application in heterogeneous catalysis [5-8].

[Al]-RUB-18 materials were prepared only recently [9-13]. Therefore, their acidic properties are not yet completely known, especially concerning the correlation with the structure and composition of the lamella when compared with zeolites, their 3D-analogues. Lamellar aluminosilicates possess active catalytic sites exposed in the interlamellar space and on the surface of the crystals. Due to the easy access to interlayer space, they can be enlarged by intercalation of bulky molecules [11,14]. Thus, these 2D materials have distinct advantages over zeolitic materials.

Many gas-phase reactions using acidic solid catalysts have been investigated and successfully deployed by the chemical industry [15]. Most heterogeneous catalytic processes are conducted under elevated temperatures and pressures conditions, where water is absent. However, active sites acting in liquid-phase transformations, where the H_2O is the final product, the solvent or still part of the biomass, are not completely understood [16]. The hydrothermal stability of the active sites in solid acid catalysts has become increasingly important in the last years, and aqueous-phase biomass transformations require catalyst design strategies to avoid deactivation and improve durability [17].

Special attention is given to the need for water-tolerant acid sites in aqueous phase transformations over heterogeneous catalysts. In this regard, alternative chemical routes are researched for the use of bio-renewable and low-cost feedstocks. The residual biomass, originating from industry and as agriculture waste, is an alternative, renewable, and abundant carbon source [18-19]. In this context, hydrolysis of biopolymers that constitute biomass has emerged as a promising sustainable energy source to produce fuels and fine chemicals, reducing the global economy's reliance on fossil fuels [20-21]. In general, alkyl levulinates attracted more attention due to their wide applications as chemical solvents, flavorings, and fuel additives [22-24]. Lactic acid (LA) is an important chemical compound for many industries, mainly related to its use in food additives and the production of biodegradable polymers (PLA - poly(lactic acid)) [25]. Thus, lignocellulosic biomass is a promising route for obtaining furfuryl alcohol (FFA) to produce ethyl levulinate (EL) [24,26]. Additionally, trioses are converted into lactic acid (LA), also using aqueous phase system [27-29]. Moreover, aqueous-phase systems represent an effective and environmentally sustainable medium for biomass conversion [30].

In this way, the incorporation of Al^{3+} ions into the lamellar framework ends up generating different Al species, such as framework-Al (tetrahedrally coordinated aluminum - Al_{Td}) and partial framework-Al sites (octahedrally coordinated aluminum - Al_{Oh} as aluminol sites or $(SiO_4)_3$-$Al(OH)(H_2O)_2$) [10]. Such species could form different active acid sites on the lamella surface. It was proved that these acidic lamellar aluminosilicates contain aluminum structural sites (Al_{Td} sites) with Brönsted acidity, and these sites were active in the ethanol dehydration reaction [11,13,31]. Nevertheless, these reactions were conducted in the gas phase, and the acidic properties of [Al]-RUB-18, mainly aluminol sites, in the presence of water still remain to be fully evaluated.

Several analytical techniques were applied to characterize acid properties in catalyst solids: Hammett acid-base titration, microcalorimetry, thermo-programmed desorption of ammonia (TPD-NH_3), Fourier-transformed infrared spectroscopy acid-sites adsorbed pyridine (FTIR-Py), and solid-state nuclear magnetic resonance spectroscopies [32-35]. Some experimental techniques do not allow a complete acid characterization of the solid catalysts (nature, concentration, strength, and location of acid sites) [32].

However, solid-state ^{31}P-NMR gives quantitative and qualitative evaluations of Brönsted/Lewis's acidity. This technique is based on the adsorption/desorption of trisubstituted phosphines or phosphine oxides as probe molecules on acid sites [35-36]. It has been widely employed because ^{31}P is a naturally abundant nucleus (100%) with high sensitivity in the interactions between the probe molecules and active sites [37-42]. The ^{31}P

spectra give information about strength, nature, concentration, and spatial distribution/accessibility of the active sites (inside of the pores or on the surface of the crystals) by linear correlation with the chemical shifts, the peak positions, the spectrum/peaks integration, and by using different probe molecule sizes, respectively [43]. Trimethylphosphine oxide (TMPO - M.P. = 140 °C) is extensively used in this process due to its kinetic diameter (0.55 nm) allowing adsorption on many catalysts, especially on microporous solids [44]. Also, this phosphine oxide (proton affinity = 910 kJ mol^{-1}) is a base with intermediate force when compared with other probe molecules applied in the measurements of acid properties, such as pyridine (proton affinity = 930 kJ mol^{-1}) and ammonia (proton affinity = 854 kJ mol^{-1}) [45]. The advantageous aspect of this technique is its capacity to facilitate analysis in the presence and absence of water, adjust temperature treatments, and avoid damaging the structure of the catalyst.

In this study, the TMPO adsorption on H-[Al]-RUB-18 was performed in the presence and absence of water. Subsequently, solid-state ^{31}P-MAS-NMR spectroscopy of the phosphine oxide adsorbed as a probe molecule was applied to the structural evaluation of the partial framework-Al acidity on H-[Al]-RUB-18. Furthermore, the “active acidity” of the lamellar materials was also probed by using model reactions for the conversion of biomass derivatives. The activity and strength of the Brönsted acid sites (BAS) were evaluated using the alcoholysis reaction of FFA to produce EL [46]. Additionally, a continuous flow aqueous-phase reaction system was used to evaluate only the Lewis acid site (LAS) activity, and simultaneous activity of BAS and LAS. This involved the corresponding catalytic reactions: pyruvaldehyde conversion to LA [47], and the cascade reaction of dihydroxyacetone to form LA [48].

2. Experimental

2.1. Syntheses of acidic lamellar silicate and aluminosilicates RUB-18

The analytical grade reactants employed in synthesis procedures were amorphous silica (Silica-fumed, powder, 0.2 - 0.3 µm, Sigma-Aldrich), sodium hydroxide (Pellets, 98% purity, Sigma-Aldrich), aluminum isopropoxide (98% purity, Alfa Aesar), and distilled water.

The silicate and aluminosilicate materials were synthesized according to the literature [9,10], with modifications. A sodium metasilicate solution (Na_2SiO_3, Molar composition: 0.05 SiO_2: 0.10 NaOH: 1.31 H_2O) was prepared by dissolving NaOH in distilled water, followed by the addition of silica under magnetic stirring at room temperature (22 °C) for 15 min. The well-dispersed suspension was transferred to a Teflon-lined stainless-steel autoclave and heated for 24 h at 100 °C. Silica (0.16 mol) was slowly added to the total volume of Na_2SiO_3 solution and kept under mechanical stirring at 22 °C for 60 min. The homogeneous, viscous, and bright gel (molar composition 0.05 Na_2SiO_3: 0.16 SiO_2: 1.36 H_2O) was completely transferred to a stainless-steel autoclave lined with Teflon® and hydrothermally treated in the oven for 14 days at 100 °C. The products (named *Na-R18*) were washed with distilled water, filtered until neutral pH, and dried in the oven for 12 h.

The post-synthesis method to incorporate Al^{3+} on lamellar silicates (Si/Al nominal ratio = 15, 30, 60) was applied sequentially based on [10]. In the hydrothermal treatment step, it is essential to maintain a proportion of 77.8% of the volume used for NaOH solution concerning the autoclave capacity for synthesis reproduction (*e.g.*, 7 g of RUB-18 to 70 mL of 0.1 mol L^{-1} NaOH solution in an autoclave with a total capacity of 90 mL). The final products were named *Na-[Al x]-R18*, with *x* as the Si/Al experimental ratio.

The ion exchange procedures [13] were carried out by dispersing sodium lamellar materials in a 0.06 mol L^{-1} of HCl solution (J.T. Baker, 36.5% - 38.0% w/w), maintaining the proportion of 0.0473 L g^{-1}, with magnetic stirring at room temperature (22 °C) for 30 min. The samples were filtered and washed with distilled water until a negative test for chloride ions using $AgNO_3$. The products (*H-[Al y]-R18*, with *y* as the experimental Si/Al molar ratio) were dried in the oven for 12 h.

2.2. Structural and compositional characterizations

The samples were analyzed by powder X-ray diffraction (XRD) in a Shimadzu diffractometer (XRD7000 model, CuKα radiation, $\lambda = 1.54$ Å, voltage 40 kV, current of 30 mA, detector SSD160-1D, inlet scattering slits of 1 mm), in a range of $2\theta = 5°$ to $50°$ and at a scan rate of 0.5° 2θ min^{-1}.

The experiments of solid-state 1D-MAS-NMR were carried out with a Bruker Avance II^+ 400 MHz Spectrometer using High Power Decoupling (HPDEC, $B_0 = 9.4$ T, with 10 kHz rotation at 22 °C, probe 2R, Zr rotor of 4 mm). The ^{29}Si-NMR spectra were obtained at a resonance frequency of 79.459 MHz, $\pi/2$ pulse (3.5 μs), and 60 s delay, using kaolinite as the reference. The ^{27}Al-NMR spectra were obtained at a resonance frequency of 104.261 MHz, $\pi/12$ pulse (1.25 μs), and 2 s delay, using aqueous acid $Al(NO_3)_3$ as the reference.

The elemental analyses were performed by X-ray fluorescence (XRF) in a Shimadzu (XRF 1800 model, Rh tube, 40 kV and 95 mA). The scan rate was 8° min^{-1} in a range of 10° to 140° using a diffraction crystal of LiF and a detector FPC to lightweight elements ($Z \leq 21$). The quantification of the elements was performed by the fundamental parameters protocol.

Na element was quantified by Inductively Coupled Plasma Optical Emission Spectrometry (ICP-OES). The dissolution of the samples was carried out according to the methodology defined by [49]. The ICP-OES analyses were performed in a Perkin Elmer spectrometer (Optima 8300 model), with the following operating conditions: 1.3 kW power, a plasma gas flow rate of 0.5 L min^{-1}, λ^{-1} = 589.592 nm of emission line and axial viewing for Na element.

Thermogravimetric (TG) and differential analyses (DTG) were obtained in SETSYS Evolution SETARAM. The samples (~14 mg) were heated in a flow of N_2 (16 mL min^{-1}), at a heating rate of 10 °C min^{-1} from room temperature to 1000 °C.

2.3. Evaluation of acidic properties in the presence and absence of water

2.3.1. TMPO adsorption experiments and solid-state ^{31}P-MAS-NMR spectroscopy

TMPO adsorption experiments were carried out in the following steps [42-43]. A portion of 300 mg of acid lamellar solids was placed into a Schlenk tube (See **Figure S.1**) and connected to a vacuum line. The samples were heated up to a certain temperature (according to TG/DTG data - **Figures S.2 and S.6**) for 15 h to remove physisorbed water and other impurities. For the analysis in the presence of water, the re-hydration procedure was applied in the same Schlenk under vacuum, heating another cell with a calculated mass of $CoCl_2 \cdot 6H_2O$ (Sigma-Aldrich) at 140 °C for 90 min. The mass of water in the hydrated metallic complex was equivalent to the proportion of 2:1 mol of H_2O to Al_{Oh} sites based on each Al content in acidic lamellar solids. Further experiments were conducted in selected samples to saturation with physisorbed H_2O, by the respective TG/DTG data. A specific volume of 54.3 mmol L^{-1} of $(CH_3)_3PO/CH_2Cl_2$ solution (TMPO - Alfa Aesar/CH_2Cl_2 Solvent - Synth, 99.5% anhydrous) was used for each sample, adjusted to achieve different TMPO loading (P/Al molar ratio = 1.4, 1.2, 0.50 and 0.25). Afterward, this portion of the solution and 30 mL of CH_2Cl_2 were added to the sample in a dry glovebox under an argon atmosphere. The suspension was maintained for 1 h in the sealed Schlenk, after which the Schlenk tube was again connected to the vacuum line to remove the solvent, at 50 °C for 1 h. Following that, the TMPO@sample was treated at 165 °C for 1 h to ensure uniform diffusion and distribution of the probe molecules on the active sites. Finally, the Schlenk was opened in a dry glovebag under argon and the TMPO@sample was packed into MAS-NMR zirconia rotor (ø = 4 mm), and sealed with a gas-tight Kel-F cap. The High-Power Decoupling (HPDEC) ^{31}P-MAS-NMR spectra were obtained in a resonance frequency of 161.9 MHz (Bruker Avance II^{+} 400 MHz, with 10 kHz at 22 °C), a pulse $\pi/2$ (1.931 µs), a delay of 20 s and 5400 scans, using concentrated H_3PO_4 as the reference. Lorentz deconvolution spectral analysis results are shown as red dashed curves, and the asterisks denote spinning sidebands on the graphs.

2.4. Additional characterization of acidic properties: Catalytic model reactions to convert biomass derivatives

2.4.1. Reaction in batch process

The alcoholysis reaction of furfuryl alcohol (FFA) was performed in a batch multi-reactor at 150 °C for 3 h, under 15 bar of N_2 pressure [46]. For that, 0.029 g of each H-[Al]-R18 catalyst was added to the reactors with 5 mL of 0.2 mol L^{-1} of FFA (Sigma-Aldrich, 98% purity) solution in ethanol (EtOH, Sigma-Aldrich, anhydrous, <0.003% de H_2O; extra-pure absolute). Previously, inert gas was used to purge the system. The reactors were then sealed, and pressure and temperature were adjusted. Time and magnetic stirring were counted after the system reached the desired temperature. Products were collected at the end of the reaction, filtered with PTFE filters (22 µm), quantified, and analyzed on an Agilent Technologies gas chromatograph using a flame ionization (GC-FID, model 7890B) or a mass spectrometer (GC-MS) detector. The method of GC-MS analysis is found in the Supporting Information. In CG-FID, the products were separated by an HP-Innowax column (30 m x 530 µm x 1 µm), 1 mL min^{-1} of N_2 flow, and a heating ramp from 80 °C to 240 °C. The inlet temperature was 280 °C, with 1 µL of injection volume in triplicate, a 10:1 split ratio, and 11 mL min^{-1} of total flow.

2.4.2. Reactions in the continuous flow system

The conversions of 1,3-dihydroxyacetone (DHA, dimer, Sigma-Aldrich, 97% purity) and pyruvaldehyde (PA solution, 40% wt. in H_2O, Sigma-Aldrich) to lactic acid were performed in a fixed-bed continuous flow reaction system in aqueous medium [47,48]. The 0.2 mol L^{-1} substrate solution was pumped at a flow rate of 0.3 mL min^{-1} using an HPLC Gilson 307 pump. The back pressure Swagelok valve maintained a 10 bar of pressure in the system. The 316 stainless steel reactor ($ø_{\text{inner}}$ = 4.15 mm) was heated at the desired temperature (130 °C).

H-[Al]-R18 catalyst (300 mg, h_{bed} = 7 cm, and τ = 9 min) was secured with quartz wool at the inlet and outlet of the reactor. Products were collected in a time range of the reaction, filtered with PTFE filters (22 μm), quantified, and analyzed on a High-Performance Liquid Chromatography system (HPLC), using an Agilent Technologies 1110 instrument equipped with a refractive index detector (RID) at 50 °C. Aliquots of 5 μL were injected in triplicate, and the products were separated on an HPX-87H column at 65 °C, with a flow of 0.7 mL min^{-1} of 5 mmol L^{-1} H_2SO_4 solution as the mobile phase.

2.4.3. Equations for catalytic performance

All compounds were identified based on their respective retention times. Substrate conversion (X_r), product selectivity (S_p), and carbon balance (CB) were determined by **Eqs. (1)** to **(3)**, respectively:

$$(1)\ X_r = \left(\frac{[r_0]-[r_t]}{[r_0]}\right)\cdot 100\%$$

$$(2)\ S_p = \left(\frac{n\cdot[p_t]}{n\cdot[r_0]-n\cdot[r_t]}\right)\cdot 100\%$$

$$(3)\ CB = \left(\frac{n\cdot[r_t] + \sum n\cdot[p_t]}{n\cdot[r_0]}\right)\cdot 100\%$$

where *n* is the number of carbon atoms in the molecule, $[r]_0$ is the initial concentration of the reactant, $[r]_t$ and $[p]_t$ are the concentrations of the reactant and products at time (*t*), respectively.

3. Results and discussions

3.1. Structural characteristics of lamellar materials

The chemical compositions of acidic samples are summarized in **Table S.1**. The partial substitution of Si^{4+} to Al^{3+} ions on the RUB-18 structure is indicated by the final Si/Al molar ratios for the products, and the 90-99% ion exchange efficiency.

The structural properties of the lamellar silicate and aluminosilicate materials are displayed in **Figures 1** and **2**. XRD patterns for sodium samples (**Figure 1.A**) show a peak around 2θ = 7.9° corresponding to the basal space of the lamella in the c direction [004] (d_{004} = 1.1 nm). The peak range from 2θ = 15° to 35° characterizes the crystalline structure of Na-RUB-18 [9-10]. Amorphization of the structure, indicated by a halo in the range between 20-30° 2θ, was not observed. There were some changes in the relative intensities and shifted peaks, but a unique crystalline phase was observed in the samples prepared in this work. The removal of hydrated interlamellar cations $[Na(H_2O)_6]^+$ from the interlayer spaces caused the appearance of a typical intrinsic structural order for H-RUB-18 [50] and reduced the interlayer space (**Figure 1.B**). The diffractograms indicate that the basal space in H-RUB-18 is 0.74 nm (peak at 2θ = 12°).

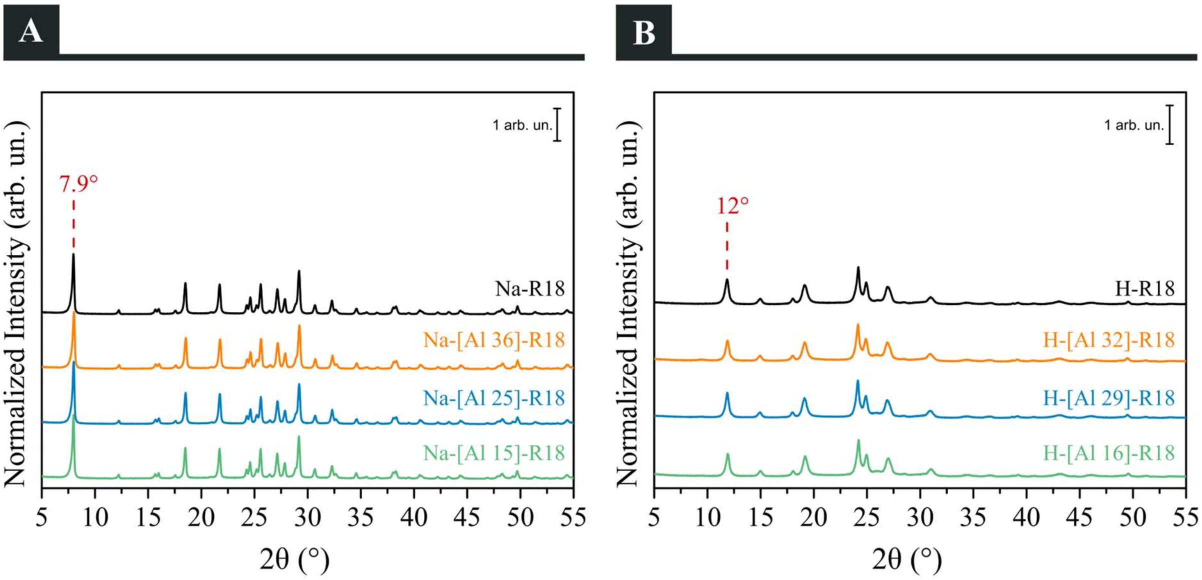

Figure 1: XRD patterns for **(A)** sodium and **(B)** acidic lamellar RUB-18, with *[Al y]* are the lamellar aluminosilicates with *y* equal to the experimental Si/Al molar ratios.

According to ^{29}Si-MAS-NMR spectra (**Figure 2.A**), two resonance signals at -99 ppm and -111 ppm are visualized. These signals are characteristic of Q^3 $[(SiO_4)_3\text{-Si-}(OH)/(SiO_4)_3\text{-Si-O-}Na^+]$ and Q^4 $[(SiO_4)_4\text{-Si}]$ type-Si^{4+} sites found in Na-RUB-18 structure, respectively [1,9-10,51]. A larger presence of silanol/silanolate groups, given by the highest signal intensity of the Q^3 sites and the Q^3/Q^4 molar ratio > 2 (See values in the ^{29}Si spectrum for sodium samples - **Figure 2.A**), suggests structural defects and smaller crystal sizes than standard RUB-18 (Q^3/Q^4 ratio = 1) [2,10]. Moreover, only slight changes in peak shapes (height and width) were observed after Al insertion demonstrating that the presence of Al in the structure did not cause order disturbances in these samples. Contrarily, peaks broadening and variation in the intensity of the resonance signals were observed for H-[Al]-R18 samples. These features demonstrate changes in the local order of sites, probably indicating different angles of T-O-T bonds for Si^{4+} species upon Al introduction and ion exchange. In addition, a small resonance signal at -101 ppm is attributed to Si(3Si, 1Al) species [52]. A decrease in the Q^3/Q^4 ratio in H-[Al]-R18 samples in relation to Na-[Al]-R18 was observed, which depends on the aluminum concentration in the materials (See values in the ^{29}Si spectra - **Figure 2.A** and the **Table S.1** for details).

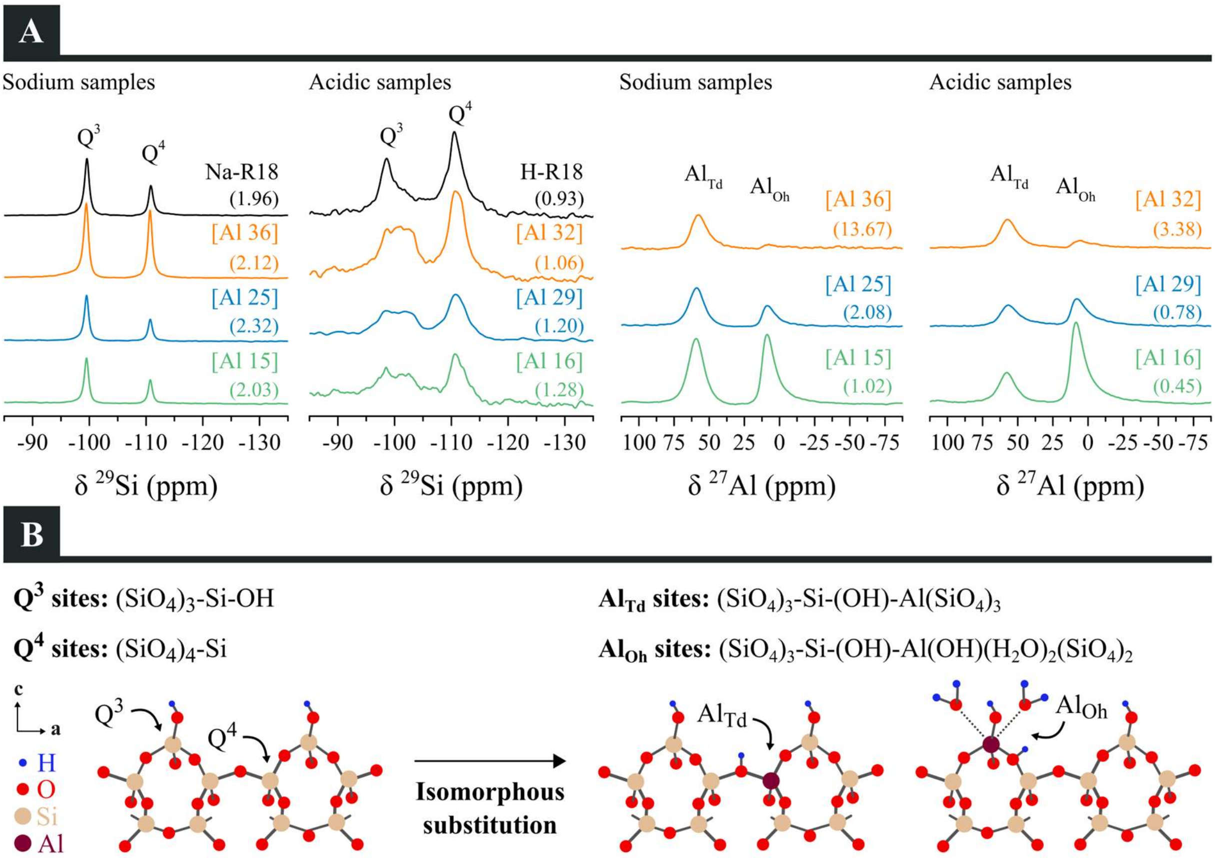

Figure 2: (A) ^{29}Si- and ^{27}Al-MAS-NMR spectra for sodium and acidic lamellar RUB-18, with different Si/Al molar ratios. *[Al y]* are the lamellar aluminosilicates with *y* equal to the experimental Si/Al molar ratio. The values between the parentheses *(x)* are the Q^3/Q^4 and Al_{Td}/Al_{Oh} molar ratios for the ^{29}Si- and ^{27}Al-NMR spectra, respectively. **(B)** Graphical representation of the Si^{4+} and Al^{3+} species on a structural unit of RUB-18 (cavities [5^4] in [101] directions).

The formation of Al_{Td} and Al_{Oh} species and the influence of Q^3 sites in the isomorphous substitution (IS) process on the RUB-18 structure were verified by ^{27}Al-MAS-NMR analysis. As illustrated in **Figure 2.A**, the peaks corresponding to tetrahedral (Al_{Td}) and octahedral (Al_{Oh}) aluminum sites for Na- and H-[Al]-R18 samples were observed at ca. 60 ppm and 8 ppm, respectively [51]. It was shown before that framework (Al_{Td}) and partial-framework (Al_{Oh}) Al species in RUB-18 structure correspond to $(SiO_4)_4Al$ and $(SiO_4)_3Al\text{-}(OH)(H_2O)_2$ species (**Figure 2.B**), respectively [13,53]. The coordination of water in aluminol sites was already observed in sodium lamellar aluminosilicate RUB-18 and confirmed by DFT calculations [53,13]. The combination of variations in Q^3 site content and the IS results in fluctuations of Al_{Td} to Al_{Oh} species concentrations (See values in the ^{27}Al spectra - **Figure 2.A** for details). A higher content of Al_{Td} species was found when reducing total Al content (Na-[Al36]-R18 sample), resulting in better dispersion of these species on the lamellar structure. In contrast, Al_{Oh} species increased in relation to Al_{Td} species due to a higher Al content on the RUB-18 lamellar surface (Na-[Al15]-R18 sample). The ^{27}Al-MAS-NMR spectra of acidic solids exhibited analogous characteristics to those observed in sodium materials. However, the signal areas of the framework tetrahedrally coordinated Al sites decreased in comparison to the peaks for aluminol sites. This finding suggests that the ion exchange method induced a partial hydrolysis of the Al-O bonds, which led to the Al(Td) → Al(Oh) transformation [54]. The final Al_{Td}/Al_{Oh} ratios of acidic non-seeded samples prepared in this work are also reported in **Table S.1** and **Figure 2** for all non-seeded samples.

It is essential to understand the type of acid sites (AS) formed on the lamellar surface of RUB-18, particularly those originating from aluminol sites, and if AS becomes more or less acidic or even loses activity under wet conditions. Furthermore, the presence of a large number of silanol/aluminol groups in the RUB-18 structure makes it difficult to determine the acidity properties at elevated temperatures. Given this information, the subsequent characterizations were conducted to appropriately assess the acidity of H-[Al]-RUB-18 lamellar solids.

3.2. Acidity properties analyzed by ^{31}P-MAS NMR

3.2.1. Evaluation of ^{31}P Chemical Shifts of TMPO adsorbed on RUB-18

In light of the aforementioned results and the data published by [10-13], the isomorphous substitution process of Si^{4+} to Al^{3+} atoms in RUB-18's structure occurs on the lamellar surface. As a result, Al species were formed in tetrahedral (Al_{Td}) and octahedral (Al_{Oh}) coordination. Typical Brönsted acid sites (BAS) are originated by one acidic proton introduced in the form of Si-O(H)-Al or bridging -OH groups for each substituted framework (Al_{Td} sites) or partial-framework atom (Al_{Oh} or aluminol sites) [13]. In this way, the adsorption experiments were conducted with TMPO as a probe molecule because it is more sensitive to the strength of BAS than LAS (Lewis acid sites) in solid acid catalysts [35]. The chemical shift range to the reaction products of TMPO with BAS is $\delta^{31}P = 50 - 100$ ppm [44], the larger the chemical shift the stronger the acidity. ^{31}P-NMR resonances above 86 ppm have been assigned as the threshold for superacidity [36]. Between 50 ppm to 60 ppm, the peak could be indicative of LAS in zeolites [40-41] or -SiOH internal/external groups in zeolite without LAS [42].

The ^{31}P-MAS-NMR spectra of the dehydrated samples with different Si/Al and P/Al molar ratios are shown in **Figure 3**. No resonance signals were visualized at 31 ppm and 39 ppm associated with mobile and crystalline TMPO [41]. This is indicative that the probe molecules were physisorbed and chemisorbed with δ^{31}P values around 40 - 49 ppm and 50 ppm to 80 ppm, respectively [44].

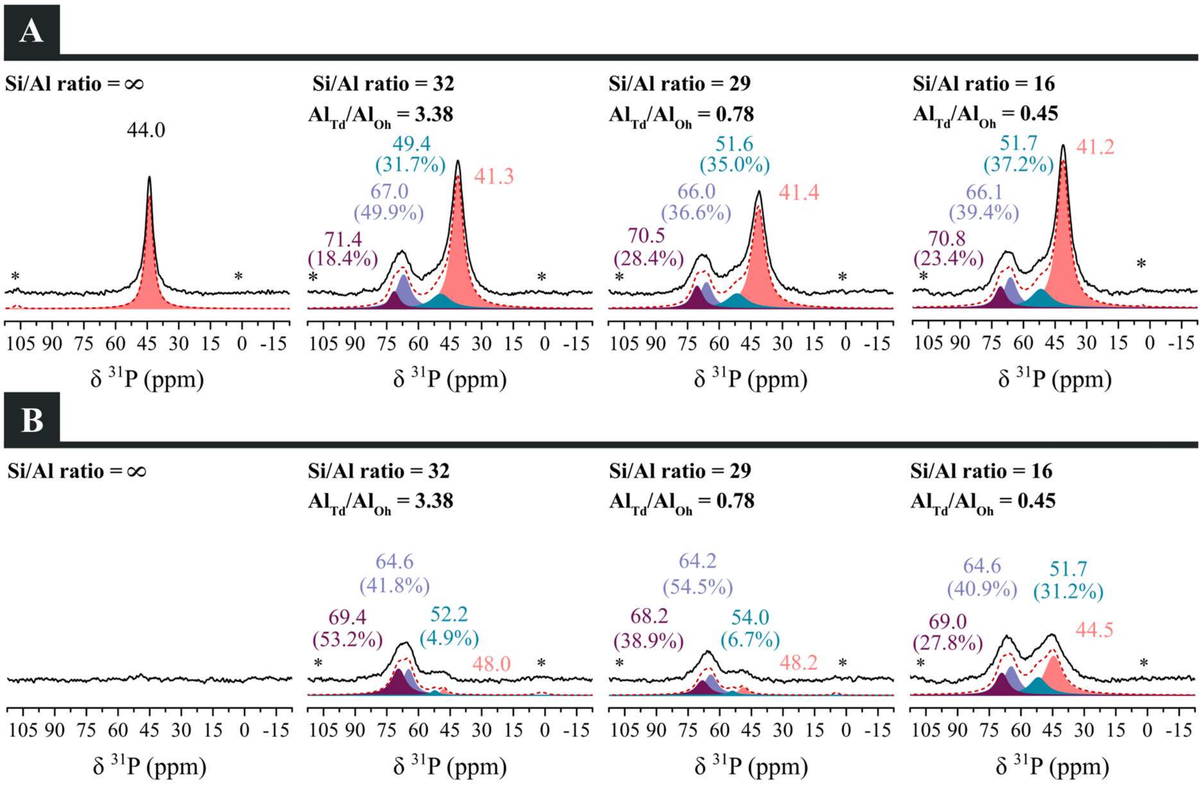

Figure 3: ^{31}P-MAS-NMR spectra for H-R18 and H-[Al]-R18 non-seeded samples in the absence of water, with different Si/Al and Al_{Td}/Al_{Oh} molar ratios and P/Al molar ratio equal **(A)** 1.20 and **(B)** 0.50. The values between the parentheses *(x)* are the proportional percentages concerning the ^{31}P resonance signals above 50 ppm (For details, see the percentage values for all signals in the spectra in **Table S.2.**).

As seen in **Figure 3.A**, the spectrum with high TMPO loading (P/Al ratio = 1.20) for acidic lamellar silicate exhibits one resonance signal. The symmetric and thin peak at 44 ppm is relative to the physisorbed TMPO [43]. The rise of resonance signals in the BAS region proves the insertion Al in framework positions of RUB-18, with chemical shift values in the region between δ^{31}P = 60 ppm - 80 ppm. Thus, four signals were visualized for the three spectra of acidic aluminosilicate samples (H-[Al]-R18, with Si/Al ratio = 32, 29, and 16). The presence of the Al in the RUB structure causes an upfield shift in the $TMPO_{(Phys.)}$ signal to 41 ppm. Also, the appearance of a small resonance peak at ca. 49 ppm could be attributed to TMPO complexes interacting with ≡SiOH/≡AlOH on the surface and edges of the lamella. The increase in aluminol site content (Al_{Td}/Al_{Oh} molar ratio = 3.38 to 0.45) leads to a downfield shift ($\delta^{31}P = 51.4$ ppm) and a rise in intensity of this peak. The peaks above ca. 60 ppm identified the $TMPOH^+$ ions formed by the interaction of TMPO with BAS. Moreover, the narrowing and shifting of this chemisorbed signal can be explained by the uniform distribution of Al_{Td} species on the lamella surface. Therefore, the reduction of Al concentration facilitates the insertion of stronger BAS into the structure of the solid [36,41].

The adsorption of TMPO with P/Al molar ratio = 0.5 in dehydrated acidic samples is shown in **Figure 3.B**. The reduction of TMPO concentration allowed a better resolution of the signals. This is reflected in the intensity of the signals when the physisorbed peak decreases and the other ones increase accordingly. No resonance signal was identified in the spectrum of silicate H-R18 (Si/Al = ∞). One explanation for this phenomenon is that the adsorption process in these materials occurs first in stronger acid sites, the BAS, and only when they are filled, the physisorption occurs and H-R18 presents no strong acid sites [43].

Equivalent results were obtained for the H-[Al]-R18 samples (Si/Al = 32 and 29), whereby only medium to strong intermolecular interactions were observed in the spectrum. For the H-[Al16]-R18, the amount of TMPO solution was doubled as a function of the increased Al concentration, thus the expected physisorption signal was observed at 44 ppm. The small peak characteristic of TMPO adsorbed on ≡SiOH/≡AlOH sites was shifted from ca. 49 ppm to around 52 ± 1 ppm. This downfield-shifted peak at ca. 52 ppm can be explained by the interactions of the ≡SiOH groups that make the chain-connected groups via hydrogen bonds, see discussion about FTIR spectra in the *Summary of spectroscopic analysis of Al-sites* section.

The results of TMPO interaction with a BAS site in low TMPO concentration were identified by the two peaks at ca. 64 ppm and 69 ppm. It is known that the peak positions in the spectrum are indicative of the varying strengths of BAS [36,55]. Overall, the peak at 69 ppm becomes more intense with low total aluminum content, and consequently, with a high Al_{Td}/Al_{Oh} molar ratio (sample with Si/Al ratio = 32 and Al_{Td}/Al_{Oh} ratio = 3.38), in accordance with the presence of stronger BAS. **Table S.2** exhibits the variation in signal percentages in the BAS region for dehydrated samples with P/Al molar ratio = 0.50 when changing the Si/Al ratio. Bornes *et al.* [41] identified changes in ^{31}P-NMR spectra of HZSM-5 by probing TMPO with P/Al ratios = 0.21 to 0.75. According to those authors, the percentage of spectral intensity in the Brönsted region varied with changes in the TMPO content. Also, the BAS resonance signals identified by the authors around δ^{31}P = 64 - 87 ppm arise from the confinement effect of protonated TMPO in HZSM-5 pores.

3.2.2. Additional TMPO analysis in lamellar seeded RUB-18 materials: proof of concept

The following discussion pertains to lamellar samples synthesized with seed crystals. Experimental data about long/short-range structural ordering for acidic seeded materials are found in Supporting Information (**Figures S.3 to S.6**).

According to Wright [56], high supersaturation and the seeding technique made it possible to control the final products, including the distribution of crystals' sizes. This resulted in the production of crystallites that were significantly smaller in size [56]. Thus, the excess of ≡SiOH sites on the lamellar surface is caused by the diminishing of crystallite size. In parallel, the formation of aluminol species (Al_{Oh}) in high concentration is favored. ^{27}Al- and ^{29}Si-NMR spectra for sodium and acidic lamellar samples are displayed in **Figure S.5**. The final Al_{Td}/Al_{Oh} molar ratios of Al^{3+} species in solids were: 0.35 for H-[Al47]-R18$_{(seeded)}$, and 0.15 for H-[Al25]-R18$_{(seeded)}$.

Furthermore, the ion exchange process, followed by ammonia thermo-decomposition, resulted in variations of diffraction pattern that are characteristic of the RUB-18 structure as seen in **Figure S.3**. The fluctuations of intensity, broadening of the peaks, and reduction in the signal/noise ratio are all in agreement with previous studies of H-RUB-18 prepared with this procedure [11]. Despite the partial amorphization of the structure, the adsorption range between 1300 cm^{-1} to 400 cm^{-1} in FTIR spectra shows that the structural units of the RUB have been preserved after the calcination step (**Figure S.4**) [9], thus local organization of the sites is intact.

The partially framework-coordinated Al species (aluminol sites) on seeded RUB-18 were also probed by the TMPO ^{31}P-MAS-NMR spectroscopy technique (**Figure 4**).

When the samples are saturated with TMPO (P/Al molar ratio = 1.4), the physisorbed probe molecules on the lamella surface are also seen in the spectra by the peak at 42 ppm - 44 ppm. In addition, the small resonance shoulder appeared in spectra at 49.5 ppm - 53 ppm even for the silicate H-R18$_{(Seeded)}$ sample. Small crystals' size, thus abundant external surface, and large content of ≡SiOH groups, all confer distinct strengths of interaction between adsorbate and active sites. Hence, the chemical environment of the ^{31}P nucleus is changed, which is reflected in the position and shape of the signals in the spectrum.

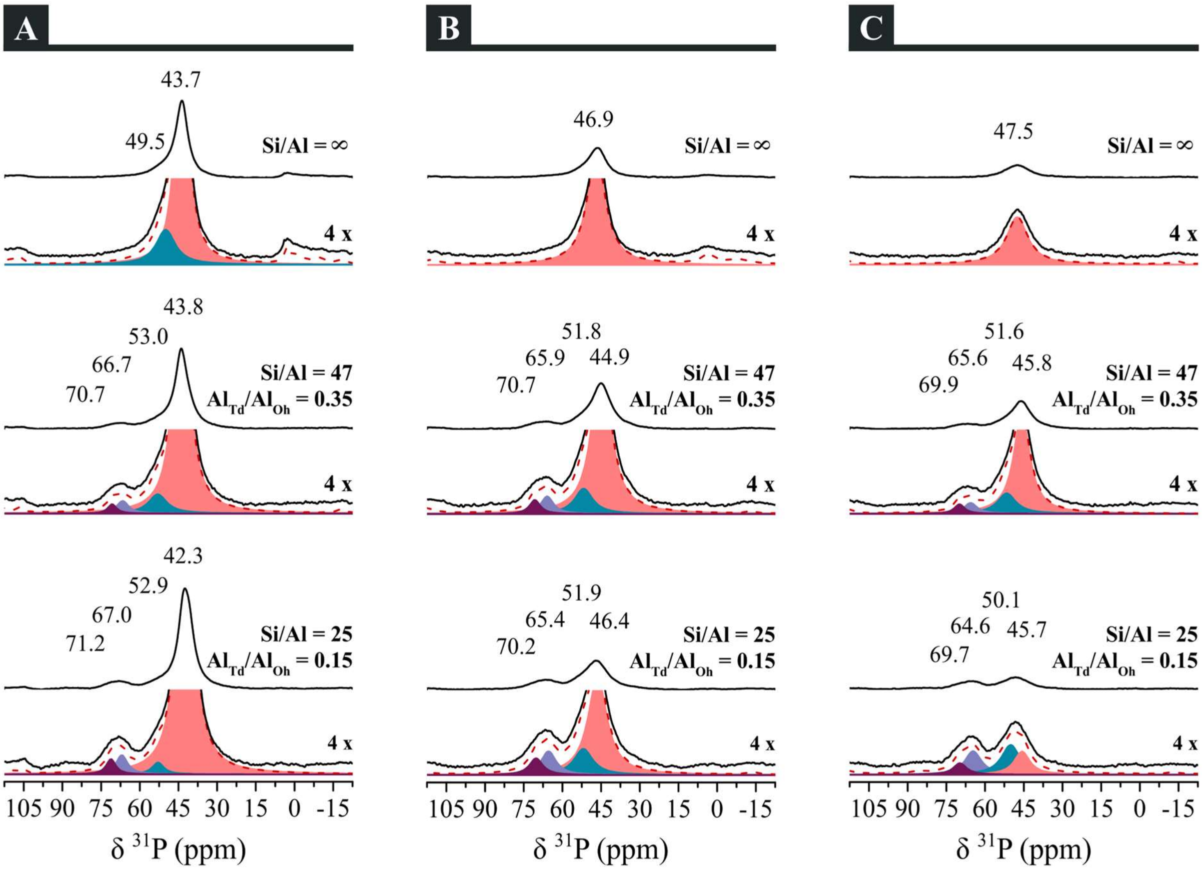

Figure 4: ^{31}P-MAS-NMR spectra for H-R18 and H-[Al]-R18 seeded samples in the absence of water, with different Si/Al and P/Al molar ratio = **(A)** 1.4, **(B)** 0.50, and **(C)** 0.25. The deconvoluted signals were magnified 4x.

In relation to the non-seeded synthesis, the higher the Al_{Oh} concentration and/or less crystalline the structure both observed in seeded samples, the higher will be the signal corresponding to ≡SiOH and ≡SiOH/≡AlOH: it goes from $\delta^{31}P$ = 49.4 – 51.7 ppm in non-seeded aluminosilicate samples to 49.5 - 53 ppm on seeded silicate and aluminosilicate ones. Also, two peaks were again observed above 60 ppm, for all TMPO concentrations (P/Al ratio = 1.40 to 0.25). These BAS peaks arise from $TMPOH^+$ species. In summary, the spectroscopic analysis of non-seeded H-[Al]-R18 samples (See **Figure 3**) can be used to explain the behavior of adsorption sites and chemical shift values for ^{31}P obtained for acidic seeded solids.

3.2.3. Influence of water in adsorption process and spectroscopic analysis

The TMPO is prone to deliquescence and, consequently, the standard procedure requires a dehydration step before the adsorption process [44]. However, an alternative approach to study the "invisible acid nature" using trimethyl phosphines and phosphine oxides ^{31}P-NMR technique is to conduct experiments on dehydrated and partially hydrated probe-loaded samples and compare the spectra [57-59].

In the present study, the influence of water was investigated to further clarify acid site behavior. The experiments were initially conducted with 2:1 mol of H_2O to aluminol sites (Al_{Oh}). The initial idea is to create the initial hydrated Al_{Oh} sites and analyze the effects on the acidity of these sites. The spectra for H-[Al]-R18 samples with low TMPO loading and different Si/Al ratios are presented in **Figure 5**.

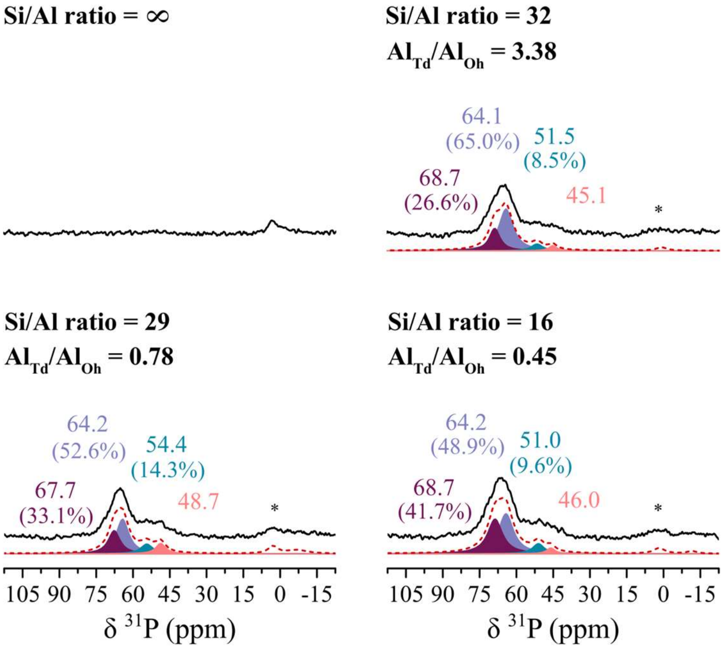

Figure 5: ^{31}P-MAS-NMR spectra for H-R18 and H-[Al]-R18 non-seeded samples in the presence of water (2 mol H_2O: 1 mol Al_{Oh}), with different Si/Al and Al_{Td}/Al_{Oh} molar ratios, and P/Al molar ratio = 0.50. The values between the parentheses *(x)* are the proportional percentages concerning the ^{31}P resonance signals above 50 ppm (For details, see the percentage values for all signals in the spectra in **Table S.2.**).

As expected, all aluminosilicate lamellar solids present a decline in the intensity of the $TMPO_{(Phys.)}$ signal in relation to the signals associated with chemisorbed TMPO above $\delta^{31}P$ = 60 ppm. This is more evident in the H-[Al16]-R18 spectrum by comparison to its dehydrated spectrum (See **Figure 3.B,** and for details, see the percentages for all signals in **Table S.2**). As illustrated in the lamellar silicate spectrum, H_2O molecules do not affect the ≡SiOH groups in the sense of favoring probe molecule adsorption. However, the aluminosilicate spectra indicate that the peak at 64 ppm is significantly enhanced in intensity, even concerning the peaks at 68 ppm (see **Table S.2** and compares hydrated and dehydrated non-seeded samples with P/Al = 0.50). These experimental results provide information on the identity of the Al species, in which the $\delta^{31}P$ = 64 ppm and 68 ppm signals could be associated with Al_{Oh} and Al_{Td} species, respectively.

Supplementary experiments to simulate the saturated environment with water/adsorbent were performed in seeded samples and H-[Al16]-R18 (**Figure 6**). Upon exposure to humidity, the samples with high TMPO concentration had shifted peaks at $\Delta\delta^{31}P$ = 1 - 2 ppm and an increase in the relative intensity of these signals in the spectra (**Figure 6.A**).

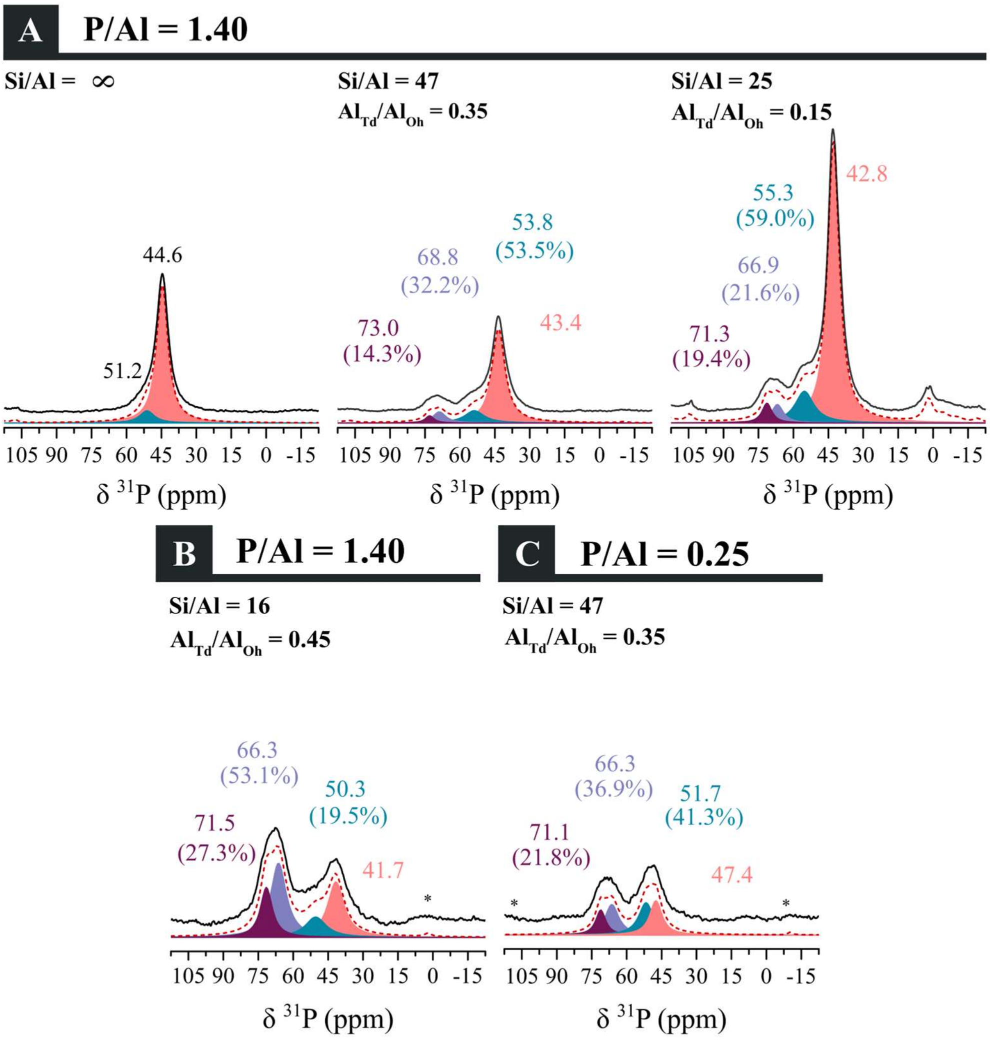

Figure 6: ^{31}P-MAS-NMR spectra for hydrated materials, saturated with physisorbed H_2O molecules: **(A)** H-R18 and H-[Al]-R18 seeded samples, with different Si/Al and Al_{Td}/Al_{Oh} molar ratios, and P/Al molar ratio = 1.40; **(B)** H-[Al16]-R18 and **(C)** H-[Al47]-R18$_{(seeded)}$ samples, with different TMPO loadings (P/Al molar ratio). The deconvoluted signals for **(B)**

and **(C)** graphs were magnified 3x concerning **(A)** graphs. The values between the parentheses *(x)* are the proportional percentages concerning the ^{31}P resonance signals above 50 ppm (For details, see the percentage values for all signals in the spectra in **Table S.2.**).

Moreover, an evident reduction in the TMPO$_{(Phys.)}$ signal is accomplished with intensity increase of BAS signals in the H-[Al16]-R18 sample (**Figure 6.B**). When the P/Al ratio was reduced in the same H_2O saturated environment (**Figure 6.C**), the BAS sites for H-[Al47]-R18$_{(seeded)}$ (Al_{Td}/Al_{Oh} = 0.35) retained their acidic features (peaks at $\delta^{31}P$ = 66 - 71 ppm). A similar acidic behavior is observed in H-[Al16]-R18 (Al_{Td}/Al_{Oh} = 0.45), even for P/Al molar ratio = 0.5 and H_2O/Al_{Oh} molar ratio = 2 (**Figure 5**). Published works [60,61] affirm the existence of ≡Si-O-H···($^{-}$O)-Si≡ bridges that form a network of hydrogen bonds on the lamella surface, as well as enabling the dynamics and conduction of protons in this region as a function of temperature variation. Thus, the peak values displayed indicate large H-bond interactions of probe molecules with these sites in a saturated environment with H_2O molecules, resulting in the considerable deshielding of ^{31}P resonances to downfield.

In general, TMPO adsorption analysis in aqueous media suggests the maintenance of acid sites, easing the interactions of the probe molecules with the RUB-18 structure. The activity of these sites was not adversely affected, in other words, there was neither deactivation nor loss of acidity in the presence of water. Contrarily, this solvent favored the interactions of the probe molecules with the acid sites in the RUB-18 structure. The coordination of H_2O molecules to aluminol sites, or even by saturation with water, enhances both acidity and the adsorption capacity of the acid sites. This finding suggests that these sites in lamellar material could be used in aqueous-phase catalytic reactions, as already shown for H-[Al]-magadiite [14].

3.3. Summary of spectroscopic analysis of Al-sites

Many authors have extensively studied experimental and computational modeling to probe acid site distributions in various solid acid catalysts, principally in zeolites [44]. In our study, the absence of channels and cavities simplifies the attribution of configuration modes of TMPO adsorbed on RUB-18 based on the existent information about the zeolites.

Despite the information on zeolites, the resonance signals as a function of the typical lamellar structure are not completely clarified by the literature. An alternative approach is exploring the data from TMPO adsorbed on MCM-41 [36,62], BEA [42,63], and H-ZSM-5 [64,65]. The goals are to identify the TMPO resonance signals observed in spectra and to establish a correlation between the RUB-18 structure with the mesoporous/microporous structures that contain few signals at the same $\delta^{31}P$ region, ≡SiOH groups, and BAS/LAS in different proportions, and the same structural unit (cavities [5^4]).

Thus, the spectroscopic analysis by ^{31}P-NMR gave us interesting information about acidic features, mainly structural-activity correlation in lamellar solid acid catalysts. Notably, we have observed the influence of some factors that can change resonance peak positions and intensities (height and width). These factors are as follows: crystallinity degree of the structure, amount of aluminum (Si/Al molar ratio), complete and partial framework-Al species, adsorption under wet or dry conditions, and varying TMPO loadings.

Figure 7 displays the distribution of the dataset relative to chemical shift values ^{31}P nucleus of the resonance signals from non-seeded and seeded lamellar materials. Overall, three main regions of the $\delta^{31}P$ (ppm) were identified with TMPO adsorption modes, with one of them containing a subgroup: physisorbed TMPO (40 – 50 ppm), TMPO strongly absorbed on ≡SiOH/≡AlOH and possible LAS (50 – 60 ppm), and TMPO interacting with Brönsted acid sites from Al_{Oh}, BAS(1), and Al_{Td}, BAS(2), species (60 – 80 ppm).

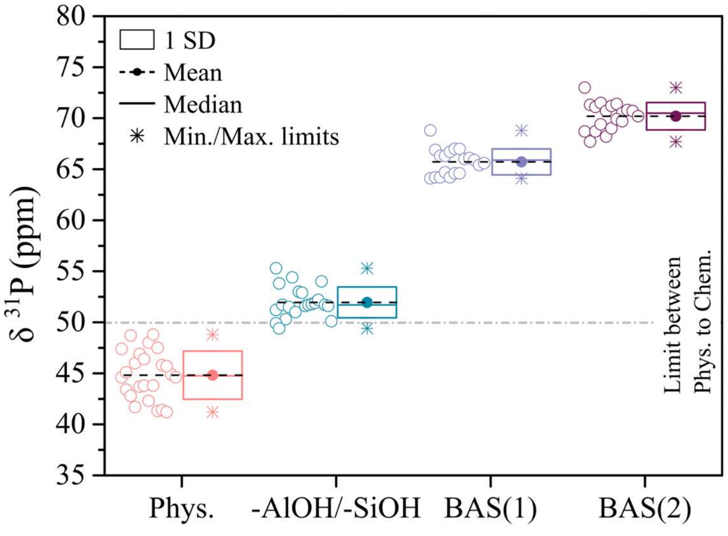

Figure 7: Boxplot of $\delta^{31}P$ (ppm) values for TMPO absorbed over non-seeded and seeded lamellar RUB-18 as a function of the following possible site types: physisorbed TMPO (o – light red), ≡SiOH/≡AlOH groups (o – dark cyan), BAS(1) from Al_{Oh} (o – light purple), BAS(2) from Al_{Td} (o – purple). The box represents one standard deviation (SD) according to the distribution of the values. The gray dash-dot line is the limit of molecular interactions (Chem. = chemisorption, and Phys. = physisorption).

It is important to show that the presence of Al_{Oh} is also indicated by the interaction of its hydroxyl group with the neighboring silanol sites by H-bonding. For that, FTIR of the pure lamellar silicate was used in comparison with aluminosilicate. **Figure 8** shows the result.

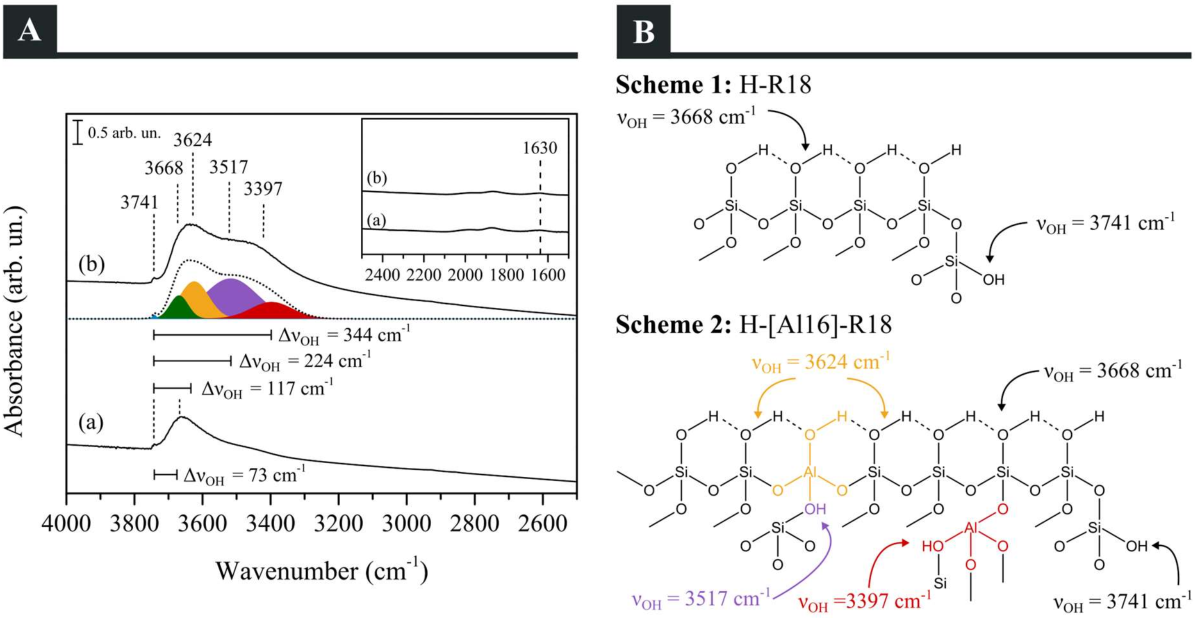

Figure 8: (A) FTIR spectra for pure dehydrated (a) H-R18 and (b) H-[Al16]-R18 non-seeded samples. **(B)** Schemes of a chain of H-bonds on lamella surface of H-R18 and H-[Al16]-R18 non-seeded samples in [010] direction.

The samples were dehydrated at 350 °C for 15 h under high vacuum (~ 10^{-6} mmHg). The FTIR spectra shown in **Figure 8.A** (insert) demonstrates, by the absence of peaks in the 1630 cm^{-1}, region that the samples do not have water molecules. The profile in the region from 3800 cm^{-1} to 3000 cm^{-1} is the one typical of zeolites and was also observed in H-[Al]-magadiite [6].

The first point to call attention is that, despite the absence of water, the bands are broad. This is the typical consequence of extensive H-bonding. The H-bonding displaces the OH stretching vibration to lower wavenumbers, the displacement is proportional to the proton transfer to the atom that is making the H-bond, that is, the more basic the atom with which the proton is shared or the more acid the proton, the larger the displacement. In the same lines, the larger will be the vibration molar absorptivity, ε [66]. The result is that the bands are shifted to lower wavenumbers and increase in intensity.

The spectrum in **Figure 8.A**, curve (a), shows one very low intensity band at 3741 cm^{-1}, due to a minute concentration of isolated Si-OH groups [6]. In the cases where these groups are really isolated, the band is very narrow, and at approximately the same position. The more intense band at 3668 cm^{-1} corresponds to the OH vibration of SiOH involved in a chain of H-bonds, as indicated in **Figure 8.B**, Scheme 1. The frequency difference, $\Delta\nu_{OH}$, is only 73 cm^{-1}, indicating a small proton displacement.

The addition of aluminum to the RUB-18 structure causes changes in the FTIR curve, **Figure 8.A(b)**. The bands observed in H-RUB-18 are still present; the sample presents a small amount of isolated SiOH groups and the chain of H-bonded SiOH groups. However, as was discussed in this work, there will be aluminol, AlOH, groups, isolated bridging acid sites, ≡Si(OH)Al≡, and acidic groups neighboring aluminol sites. Besides these, H-bonded silanol groups that neighbor aluminol sites will be disturbed by them and are expected to appear slightly shifted. Because of that, the bands at 3741 and 3668 cm^{-1} are still seen. The slightly disturbed SiOH will show a slightly larger displacement from the isolated SiOH than the purely H-bonded SiOH, thus the band at 3624 cm^{-1} can be caused by this effect, the $\Delta\nu_{OH}$ is 117 cm^{-1}, the presence of Al atom causes the H on SiOH to be more acidic in that situation.

Naturally, the largest displacement will be that of the band at 3397 cm^{-1}, that corresponds to the isolated, bridging acid site, the ≡Si(OH)Al≡ group (in red, Scheme 2, **Figure 8.B**), in this case, the $\Delta\nu_{OH}$ is 344 cm^{-1} in relation to the isolated Si-OH. Finally, the acidic groups neighboring aluminol sites, in purple, Scheme 2 in **Figure 8.B**, will appear in between the two bands, this is the cause of the elevated baseline. A band around 3517 cm^{-1} is suggested as the result of the presence of this group; it would afford a $\Delta\nu_{OH}$ of 224 cm^{-1} in relation to the isolated silanol group. The acidity of this group is situated between that of the proton in SiOH in the chain of silanol groups disturbed by the presence of Al-OH (in orange, Scheme 2 in **Figure 8.B**) and that of the isolated acidic site in red, Scheme 2 in **Figure 8.B**.

Each one of these groups corresponds to a peak of TMPO NMR spectra (**Figure 3.A**), the TMPO adsorbed in SiOH/AlOH at 51.7 ppm corresponds to the band at 3624 cm^{-1}, the acid site at the aluminol groups adsorbs TMPO and shows a peak at 66.1 ppm that appears at 3517 cm^{-1} and finally, the most acidic site, the isolated ≡Si(OH)Al≡ adsorbs TMPO and causes a ^{31}P chemical shift of 70.8 ppm and a FTIR band at 3397 cm^{-1}.

3.4. Catalytic tests

3.4.1. Strength of BAS through batch process

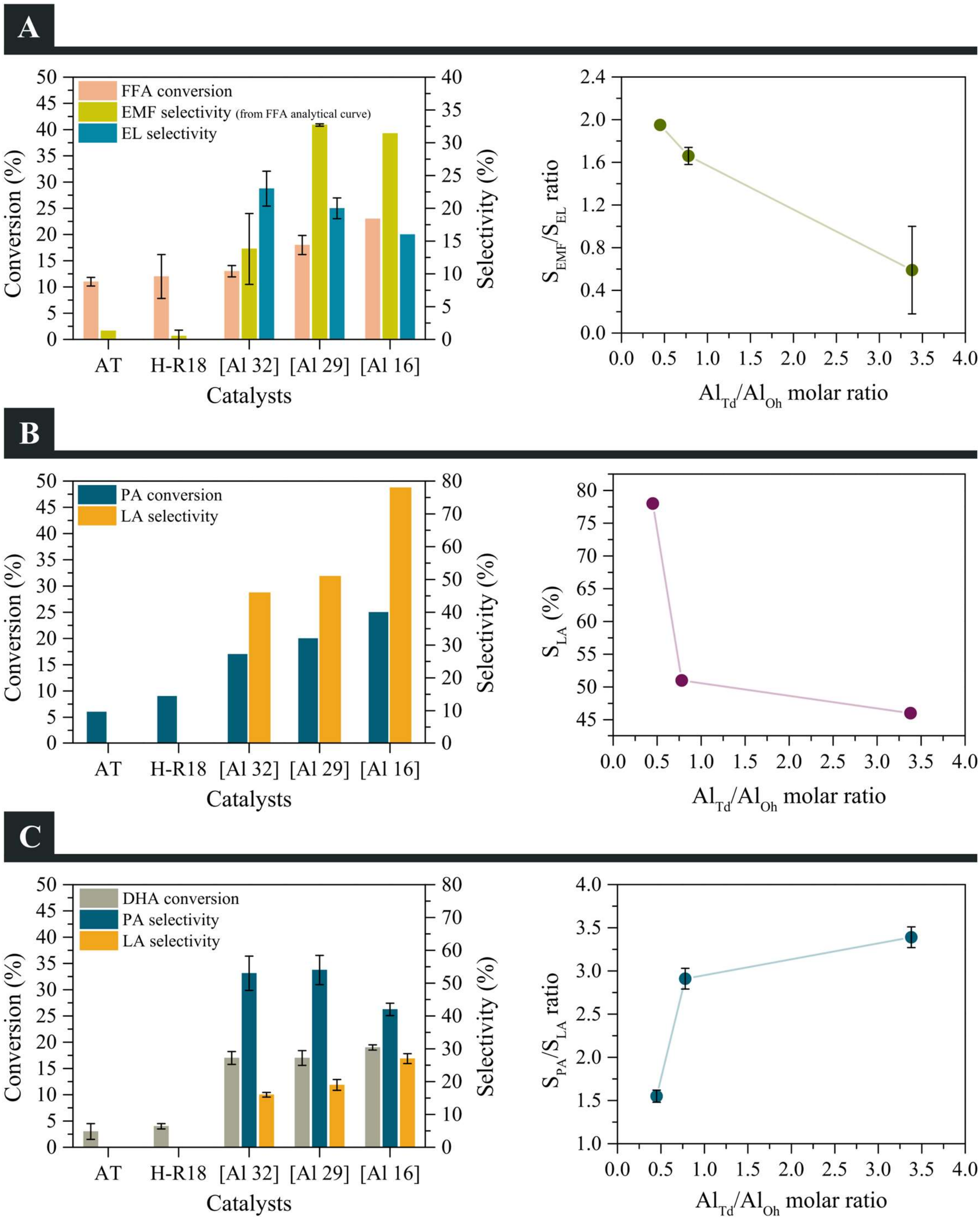

Figure 9: Conversion (X, %) and Selectivity (S, %) values, and respective graphs of the relation between structural properties and selectivity ratios for H-[Al]-R18 catalysts: **(A)** Alcoholysis of FFA (3 h of reaction), **(B)** PA reactions (values for 3 h of reaction), **(C)** Hydrolysis of DHA (average values of 3 h and 6 h of reaction in duplicate). Carbon balance was determined within the range of 86% - 96%, based on measurements obtained through CG-FID and HPLC-RID techniques. In the catalyst axis, the autothermal reactions are represented by *AT*, and *[Al y]* are the aluminosilicate catalysts with *y* equal to the Si/Al molar ratio before the reaction.

The results of the alcoholysis of furfuryl alcohol (FFA) to form ethyl levulinate (EL) are shown in **Figure 9.A**. Autothermal reactions or those using non-acidic catalysts (H-R18) have a small contribution to FFA conversion. It was observed that FFA conversion increased when the reaction was catalyzed over lamellar aluminosilicate samples with larger Al content. The selectivity values to both products increased as Al content increased (Si/Al = 32 to 16).

The EL and 2-ethoxymethyl-furan (EMF) have been identified after 3 h of reaction, while the conventional hydrolysis products, angelica lactones, and levulinic acid, were not detected. GC-MS was used to confirm these products (method in Supporting Information). A reaction pathway for EL and EMF production that requires BAS with medium strength was proposed in **Figure S.7**.

Figure 9.A demonstrated the relationship between the structural properties of the catalysts and the ratio between EMF and EL selectivity. The selectivity for EL is enhanced when the Al_{Oh} content is reduced, and the Si/Al ratio is increased in the catalysts. According to the literature [67-70], the ethanolysis of FFA could occur in two steps depending on the catalysts used. The first step involves BAS and/or LAS for the etherification of FFA. The second step involves the hydrolysis of EMF over BAS with higher strength to form EL. Li and collaborators [69] confirm the dependence on the strength/nature of the active sites in ethanolysis reactions catalyzed over ZSM-5 with different Si/Al ratios. According to these authors, strong sites in the catalyst associated with the highest BAS/LAS ratio produce more EL than EMF compared to catalysts with the lowest strength of sites and also, with low BAS/LAS ratio.

Thus, the partial Al-framework and framework-Al species in the RUB-18 structure played a crucial role in this reaction. The H-[Al16]-R18 sample exhibited greater selectivity towards EMF. In contrast, the selectivity to EL was correlated with a higher concentration of Al_{Td} species and a relative medium strength of Brönsted acid sites in the H-[Al32]-R18 sample. These results are in line with previous studies on zeolites [67-70] and evidence the activity of H-[Al]-R18 as Brönsted acid catalysts as foreseen from the acidity characterization.

3.4.2. Activity of BAS and/or LAS through continuous flow aqueous-phase system

The transformation of pyruvaldehyde (PA) into lactic acid (LA) is a typical Lewis acid-catalyzed reaction [27,47]. The results are presented in **Figure 9.B**. The blank experiments revealed that AT and H-R18 had a negligible contribution to PA conversion, and LA was not even identified as a product in these reactions. On the other hand, all H-[Al]-R18 catalysts were active, disclosing the Lewis activity of these lamellar solids, and consistently, a selectivity to LA. It is worth mentioning that in the presence of water, the TMPO adsorption also revealed the concentration increase in the Lewis acid sites (compare **Figure 3.B** with **Figures 6.B** and **6.C**). The catalyst H-[Al16]-R18 (with a lower Si/Al ratio) showed a selectivity to LA above 75%.

The PA conversion and LA selectivity increase with the higher concentration of Al_{Oh} species and the lower Si/Al ratio. The relationship between LA selectivity and Al_{Td}/Al_{Oh} molar ratios of the catalysts can be seen in **Figure 9.B**. The results state that the presence of Al^{3+} in octahedral coordination as aluminol sites in the RUB-18 structure influenced the reaction pathway. The reaction catalyzed by H-[Al32]-R18 and H-[Al29]-R18 have comparable LA selectivity.

For this reason, it is suggested that partial framework-Al sites (Al_{Oh} as aluminol sites) in the RUB-18 catalyst structure behaved as Lewis acid sites. In **Figure 10**, the proposed reaction pathway follows the coordination of the pyruvaldehyde on Al^{3+}, in Al_{Oh} sites, instead of, or displacing, H_2O molecules, forming a cyclic intermediate. The H_2O molecules in the reactional medium act as nucleophiles and proton donors for the Cannizzaro reaction in a concerted mechanism or by its self-dissociation[1]. It is important to indicate that the H_2O molecules are continuously re-coordinated to the Al site, thereby recovering these acid sites [27].

---

[1] As exemplified below, the H_2O molecules in the reactional medium may undergo self-dissociation via protonation with other water molecules, forming OH^- (the nucleophile) and H_3O^+ (proton donor) ions which act in the Cannizzaro reaction [73,74].

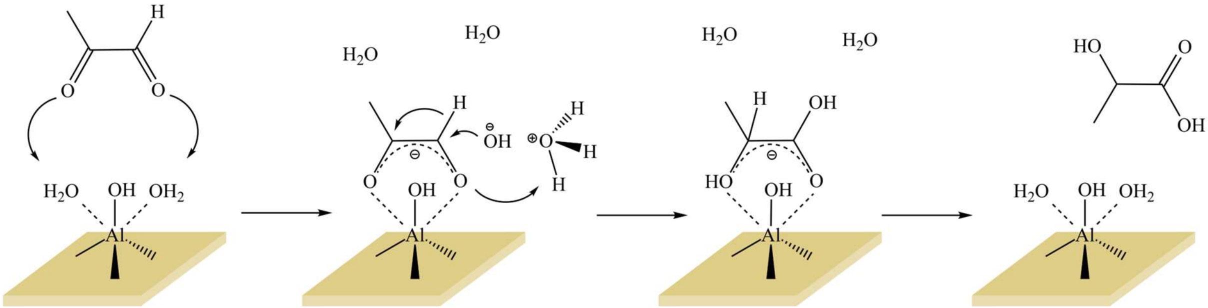

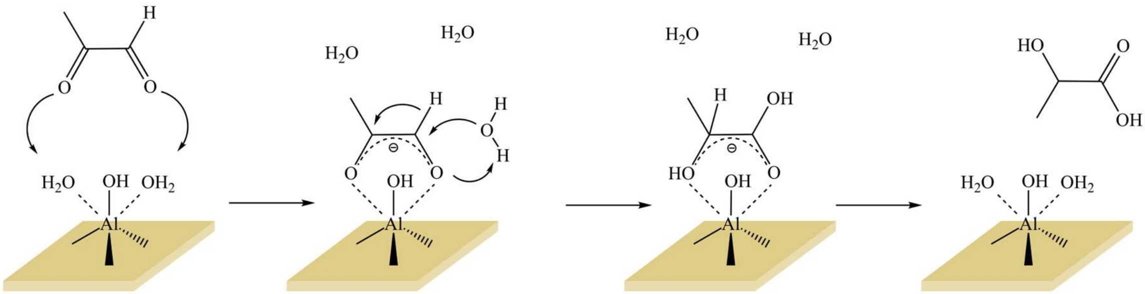

Figure 10: Illustration of pyruvaldehyde adsorption by displacement of water molecules on aluminol sites (as Lewis acid sites) in the lamellar surface of H-[Al]-RUB-18.

According to Albuquerque and co-workers [47], there is a correlation between the strength of the acid sites and the reaction rate. The authors noted that medium-strength sites are the minimal requisition for the Cannizzaro reaction. Therefore, it can be inferred that the H-[Al]-R18 samples contain medium-strength Lewis acid sites needed to cause the intramolecular rearrangement of pyruvaldehyde to form lactic acid.

BAS are required for the dehydration step of DHA to form PA, and the intramolecular rearrangement of PA to form LA only occurs via LAS [48]. This reaction was used as another continuous aqueous-phase transformation to evaluate the simultaneous activity of the BAS and LAS over silicate and aluminosilicate catalysts (**Figure 9.C**).

The blank experiments presented low conversions, and thus their PA selectivity, or selectivity to any other organic compound, could not be assertively quantified. Catalysts H-[Al]-R18 were active to convert DHA, with 17% - 19% ± 2% of conversion. The PA and LA were the main products. The presence of pyruvaldehyde (PA) proves the insertion of BAS in the RUB-18 structure, corroborating the initial results in furfuryl alcohol alcoholysis. The dehydration of DHA resulted in an increased PA selectivity, ΔS_{PA}, of 12% when the Si/Al ratio was increased, from 42% to 54%.

Lactic acid (LA) was also produced in the next step as could be anticipated from the reaction runs using pyruvaldehyde as feedstock. As commented, Lewis acid sites are required to promote the Cannizzaro mechanism and transform PA into LA. The following final selectivity values were ~16% to ~27% when the Si/Al ratio of the catalysts was decreased from 32 to 16. Therefore, as in the case of FFA and PA conversion reactions, the intrinsic relationship between the products' selectivity and the catalysts' structural properties was observed once again. As seen in **Figure 9.C**, a higher concentration of Al_{Oh} sites results in a considerable consumption of PA to form LA. Thus, H-[Al16]-R18 is the best catalyst among the ones prepared in this work for the DHA into LA transformation via the cascade reaction. Meanwhile, H-[Al32]-R18 is a better acidic solid that promotes the first step reaction, with high PA selectivity.

These findings reinforce the hypothesis that the aluminol, $(SiO_4)_3Al\text{-}(OH)(H_2O)_2$, sites in the RUB-18 structure act as LAS in the aqueous phase reactions. Furthermore, the X_{DHA}, S_{PA}, and S_{LA} values remained constant during the investigated reaction timeframe, indicating an effective simultaneous activity of BAS and LAS, and that these lamellar catalytic systems are stable.

The structural properties of H-R18 and H-[Al]-R18 catalysts before and post-PA and DHA reactions are discussed below and summarized in **Table S.3**. The XRD pattern (**Figure S.8**) indicates that the long-range structural order characteristic of H-RUB-18 was preserved. For the H-R18 sample, peaks at $2\theta = 13°$ and $26°$ suggest the presence of residual quartz wool recovered from the reactor with the catalyst. A slight broadening of the baseline was observed around the $2\theta = 15°$ to $30°$, which might also be attributed to residual wool. Moreover, a slight reduction in the intensity of the peaks above $2\theta = 20°$ indicates a possible partial loss of the crystalline structure for RUB-18.

The ^{27}Al-NMR analysis (**Figure S.9**) shows a modification of short-range structural order. An increase in the peak area relative to Al_{Oh} species and a reduction of Al_{Td} content for both reactions were observed. A partial hydrolysis of Al-O bonds has been considered. If the conversion and selectivity values and the structure by XRD pattern are kept, the variation can be related to the creation of $(SiO_4)_3Al(OH)(H_2O)_2$ species. As a result, the BAS activity is not eliminated. Also, the LAS activity in aluminol sites was maintained. **Figure S.10** shows the tendency of variation in the Al species concentration as a function of the initial Al concentration for each catalyst. For DHA reactions, the positive $\Delta[Al_{Oh}]$ and negative $\Delta[Al_{Td}]$ confirm the transformation of the species without loss of structural Al. On the other hand, a negative Δ[total Al species] detected after PA reaction catalysts infers the loss of the Al framework of the structure.

3.5. Summary of catalyst reactivity

It is also clear that the catalysts exhibit BAS/LAS acidity, which affords the interactions between the substrate (FFA, DHA, PA) and acid sites on the RUB-18 lamellar surface. Higher selectivity and conversion were observed in aqueous-phase transformations, in which the acidity behavior arises from an H_2O and substrate-saturated environment. These results are consistent with the results of the ^{31}P spectra discussed in **Figure 6**. Some authors have proposed several types of LAS, such as framework LAS from tri-coordinate aluminum, extra-framework (EFAL with octahedral coordination), and framework-associated aluminum (Al_{Td} to Al_{Oh} reversible coordination) [54,63,71,72]. According to the authors [54], the latter type becomes kinetically allowed and thermodynamically stable under wet conditions, allowing for a reversible transition between BAS and coordinatively saturated LAS. Thus, these authors propose that three H_2O molecules in the 1st coordination shell are firmly bound to partially framework-Al_{Oh} in $Al(SiO_3)_3(H_2O)_3$ arrangement [54].

Our study, contrarily, suggests that the partial framework-Al species as $(SiO_4)_3$-Si-(OH)-Al(OH)$(H2O)_2(SiO_4)_2$ sites (or aluminol sites - Al_{Oh}) (as seen in **Figure 2.B**) on the lamella surface of RUB-18 could be assigned either as Brönsted and/or Lewis acid sites, depending on the experimental conditions used. Brönsted acidity is the only one found in anhydrous environment without coordinating reactants while Lewis acidity will also be present, together with Bronsted one, in the presence of water or any coordinating solvent or reactant.

4. Conclusions

A larger concentration of silanol/silanolate groups influenced the isomorphous substitution process (Si^{4+} to Al^{3+} ions) that occurs on the lamellar silicate surface of RUB-18, with a direct correlation between the Si/Al molar ratio in the synthesis and aluminum species in the structure. The present work shows that the experiments carried out using the ^{31}P-NMR technique on dehydrated and hydrated TMPO-loaded samples in combination with catalytic tests provide new insights into the acidic properties of partial framework-Al sites on non-seeded and seeded H-[Al]-RUB-18.

We believe that some factors lead to changes in ^{31}P-NMR resonances, such as the crystallinity degree of the structure, the amount of aluminum (Si/Al ratio), completely and partially framework-Al species, adsorption under wet or dry conditions, and varying TMPO loadings. The spectroscopic analysis of the ^{31}P nucleus indicates that the resonance signals arise from TMPO adsorbed on the lamellar surface ($\delta^{31}P$ = 40 – 49 ppm), silanol/aluminol sites ($\delta^{31}P$ = 49 – 56 ppm), and Brönsted acid sites (60 – 75 ppm). In lower TMPO concentrations, the spectral data revealed at least the existence of two types of BAS with different strengths at ca. 64 ppm and 68 – 69 ppm. Upon exposure to humidity, the coordination of water molecules to aluminol sites enhanced the adsorption capacity of the active sites. This resulted in an increase in the resonance peak intensities, for both the Al_{Td} and Al_{Oh} species, associated with the peaks at 69 and 64 ppm, respectively. A water and TMPO-saturated environment induced changes in the signals above 50 ppm, both in position and intensity, implying that no loss of acidity, and possibly no deactivation, occurs in the presence of water. This would result in enhanced catalytic activity when subjected to similar experimental conditions.

The "active acidities" of the H-[Al]-R18 lamellar non-seeded samples were tested in both batch and flow systems in the presence and absence of water. It is worth noting that the $(SiO_4)_4Al$ and $(SiO_4)_3Al\text{-}(OH)(H_2O)_2$ species present in the RUB-18 structure played a crucial role in biomass-derivative conversion reactions. The H-[Al32]-R18 catalyst has a better performance in producing ethyl levulinate in ethanolysis reaction and pyruvaldehyde in DHA dehydration. This is attributed to the uniform distribution of Al_{Td} species due to the smaller Al content in the RUB structure, which facilitates the insertion of stronger BAS. Conversely, the H-[Al16]-R18 catalyst exhibited a significant selectivity towards 2-ethoxymethyl-furan (an intermediate in the ethanolysis reaction). This indicates that the BAS sites are not sufficiently strong for complete 2-ethoxymethyl-furan hydrolysis. Finally, the production of lactic acid (the final product of DHA and PA conversions) over lamellar aluminosilicates RUB-18 under aqueous conditions reveals the possibility of the $(SiO_4)_3Al\text{-}(OH)(H_2O)_2$ sites (Al_{Oh} sites) acting as Lewis acid sites.

The ^{31}P-NMR spectroscopic analysis and catalytic tests approach reinforce the improvement in acidity under wet conditions and highlight the acid behavior of partial framework-Al sites in the RUB-18 structure. This work initiates the effort to create a consistent protocol for acidity analysis in lamellar solids, comparable to the existing ones for zeolites, and brings the importance of evaluating the acidity characteristics of solid catalysts under aqueous-phase conditions.

Acknowledgments

P.B.F.S. and H.O.P. acknowledge the Fundação de Amparo à Pesquisa do Estado de São Paulo (FAPESP - grant 2022/05743-0 for P.B.F.S., project n° 2021/12058-0) for the financial support to this work. E.M.A. (Proc. 405800/2022-3) thanks Conselho Nacional de Pesquisa Científica e Tecnológica (CNPq) for her post-doctoral grant. M.A.F. also acknowledges the Fundação de Amparo à Pesquisa do Estado do Rio de Janeiro (FAPERJ) for financial support. H.O.P. thanks CNPq for the scholarship. Coordenação de Aperfeiçoamento de Pessoal de

Nível Superior (CAPES) - Financial Code 001 is also acknowledged. Also, the authors thank the LIRMN (IQ-UNICAMP) for the NMR analyses, Dr. Erica Munsignatti (GMP^3/UNICAMP) for all her experimental support in the development of this work, and Dr. V.W. Faria (INT) for his experimental support in the catalytic tests using furfuryl alcohol.

Conflict of interest

The authors declare no competing financial interest.

References

[1] S. Vortmann, J. Rius, S. Siegmann, and H. Gies. Ab initio structure solution from X-ray powder data at moderate resolution crystal structure of a microporous layer silicate, ***J. Phys. Chem. B***, 101, (1997), 1292-1297.

[2] M. Borowski, O. Kovalev, and H. Gies. Structural characterization of the hydrous layer silicate Na-RUB-18, $Na_8Si_{32}O_{64}(OH)_8 \cdot 32H_2O$ and derivatives with XPD-, NPD-, and SS NMR experiments, ***Microporous Mesoporous Mater.***, 107 (1-2), (2008), 71-80.

[3] T. Sirinakorn, K. Imwiset, S. Bureekaew, and M. Ogawa. Inorganic modification of layered silicates toward functional inorganic-inorganic hybrids, ***Appl. Clay Sci.***, 153, (2018), 187-197.

[4] T. Selvam, A. Inayat, and W. Schwieger. Reactivity and applications of layered silicates and layered double hydroxides, ***Dalton Trans.***, 43, (2014), 10365.

[5] G.L. Paz, E.C.O. Munsignatti, and H.O. Pastore. Novel catalyst with layered structure: Metal substituted magadiite, ***J. Mol. Catal. A: Chem.***, 422, (2016), 1-8.

[6] G.B. Superti, E. C. Oliveira, H. O. Pastore, G. Gatti and L. Marchese. Aluminum Magadiite: an Acid Solid Layered Material, ***Chem. Mater.***, 19, (2007), 4300-4315.

[7] Y. Ide, N. Kagawa, M. Sadakane and T. Sano. Precisely designed layered silicate as an effective and highly selective CO_2 adsorbent, ***Chem. Commun.***, 49, (2013), 9027.

[8] N. Alam and R. Mokaya. Strongly acidic mesoporous aluminosilicates prepared via hydrothermal restructuring of a crystalline layered silicate. ***J. Mater. Chem. A***, 3, (2015), 7799.

[9] F.S.O. Ramos, E.C.O. Munsignatti, and H.O. Pastore. 2D–3D structures: The hydrothermal transformation of a layered sodium silicate, Na-RUB-18, into mordenite zeolite, ***Microporous Mesoporous Mater.***, 177, (2013), 143-150.

[10] F.S.O. Ramos, and H.O. Pastore, 2D-to-disguised 3D materials with built-in acid sites: H+-[Al]-RUB-18, ***Dalton Trans.***, 46, (2017), 11728-11737.

[11] G.P. Campos, G.B. Báfero, and H.O. Pastore, Vapor adsorption experiments as a characterization tool for layered catalysts, ***New J. Chem.***, 44, (2020), 9998.

[12] G.B. Báfero, E.C.O. Munsignatti, and H.O. Pastore, Lamellar-zeolitic transformations mediated by diffusionless and recrystallization mechanisms, ***Microporous Mesoporous Mater.***, 323, (2021), 111189.

[13] G.B. Báfero, B.N.N. Silva, A.A. Leitão, and H.O. Pastore, The behavior of aluminum sites in H-[Al]-RUB-18 catalysts: A theoretical-experimental investigation, ***Mol. Catal.***, 535, (2023), 112870.

[14] G.P. Campos, E.M. Albuquerque, M.A. Fraga, and H.O. Pastore. Continuous Cellobiose Hydrolysis over Lamellar Aluminosilicates—Unveiling [Al]-magadiite Water-Tolerant Acid Sites, ***Ind. Eng. Chem. Res.***, 60 (13), (2021), 4794−4805.

[15] A. Corma. From Microporous to Mesoporous Molecular Sieve Materials and Their Use in Catalysis. ***Chem Rev.***, 97 (6), (1997), 2373-2420.

[16] T. Ennaert, J. Van Aelst, J. Dijkmans, R. De Clercq, W. Schutyser, M. Dusselier, D. Verboekend, and B.F. Sels. Potential and challenges of zeolite chemistry in the catalytic conversion of biomass, ***Chem. Soc. Rev.***, 45, (2016), 584-611.

[17] J. Huo, Jean-Philippe Tessonnier, and B. H. Shanks. Improving Hydrothermal Stability of Supported Metal Catalysts for Biomass Conversions: A Review. ***ACS Catalysis***, 11(9), (2021), 5248-5270.

[18] R. A. Sheldon, Green chemistry, catalysis and valorization of waste biomass, ***J. Mol. Catal. A: Chem.***, 422, (2016), 3-12.

[19] M. Niakan, C. Qian, and S. Zhou. Highly Efficient One-Pot Conversion of Glucose to 5-Hydroxymethylfurfural over Acid-Base Bifunctional MCM-41, Mesoporous Silica under Mild Aqueous Conditions. ***Energy & Fuels***, 37 (21), (2023), 16639-16647.

[20] A. Kruse and A. Gawlik, Biomass conversion in water at 330− 410 C and 30− 50 MPa. Identification of key compounds for indicating different chemical reaction pathways, ***Ind. Eng. Chem. Res.*** 42 (2), (2003), 267-279.

[21] Y.B. Huang and Y. Fu, Hydrolysis of cellulose to glucose by solid acid catalysts, ***Green Chem.***, 15, (2013), 1095-1111.

[22] D. Song, et al. Efficient conversion of levulinic acid or furfuryl alcohol into alkyl levulinates catalyzed by heteropoly acid and ZrO2 bifunctionalized organosilica nanotubes, ***J. Catal.***, 333, (2016), 184-199.

[23] C.R. Patil, S.P. Kamble, and C.V. Rode, Single-Pot Alcoholysis of Furfuryl Alcohol to Alkyl Levulinates Using Heterogenized p-TSA Catalyst. ***ChemistrySelect***, 6, (2021), 6636-6643.

[24] S.H. Chung, S. de Haart, R. Parton, N. R. Shiju, Conversion of furfuryl alcohol into alkyl-levulinates using solid acid catalysts, ***Sustain. Chem. Clim. Action***., 1 (2022), 100004.

[25] Y. J. Wee, J. N. Kim, and H. W. Ryu, Biotechnological production of lactic acid and its recent applications. ***Food Technol. Biotechnol***., 44(2), (2006), 163-172.

[26] C. Antonetti, D. Licursi, S. Fulignati, et al., New frontiers in the catalytic synthesis of levulinic acid: from sugars to raw and waste biomass as starting feedstock, ***Catalysts***, 6, (2016) 196.

[27] K.M.A. Santos *et al.*, Discussing Lewis and Brønsted acidity on continuous pyruvaldehyde Cannizzaro reaction to lactic acid over solid catalysts, ***Mol. Catal.***, 458(B), (2018), 198-205.

[28] K.M.A. Santos *et al.*, The Role of Brønsted and Water-Tolerant Lewis Acid Sites in the Cascade Aqueous-Phase Reaction of Triose to Lactic Acid, ***ChemCatChem***, 11, (2019), 3054-3063.

[29] E.M. Albuquerque, L.E.P. Borges, and M.A. Fraga, Lactic acid production from aqueous-phase selective oxidation of hydroxyacetone, ***J. Mol. Catal. A Chem.***, 400, (2015), 64-70.

[30] A.H. Van Pelt, O.A. Simakova, S.M. Schimming, J.L. Ewbank, G.S. Foo, E.A. Pidko, E.J.M. Hensen, and C. Sievers, Stability of functionalized activated carbon in hot liquid water, ***Carbon***, 77, (2014), 143-154.

[31] R.K.S. Almeida, G.L. Paz, G.B. Báfero, and H.O. Pastore, Properties of Layered [Al]- and [V,Al]-Magadiite Catalysts as Revealed by Ethanol Dehydration, ***Microporous Mesoporous Mater.***, 284, (2019), 1-9.

[32] E.G. Derouane, J.C. Védrine, R.R. Pinto, P.M. Borges, L. Costa, M.A.N.D.A. Lemos, F. Lemos, and F.R. Ribeiro. The Acidity of Zeolites: Concepts, Measurements and Relation to Catalysis: A Review on Experimental and Theoretical Methods for the Study of Zeolite Acidity, ***Catal. Rev.***, 55, (2013), 454–515.

[33] M. Niwa, N. Katada, M. Sawa, Y. Murakami. Temperature-Programmed Desorption of Ammonia with Readsorption Based on the Derived Theoretical Equation, ***J. Phys. Chem. A***, 99, (1995), 8812-8816.

[34] M. Tamura, K. Shimizu, A. Satsuma. Comprehensive IR study on acid/base properties of metal oxides, ***Appl. Catal. A - Gen.***, 433–434, (2012), 135-145.

[35] A. Zheng, S. Liu, and F. Deng. Acidity characterization of heterogeneous catalysts by solid-state NMR spectroscopy using probe molecules, ***Solid State Nucl. Magn. Reson.***, 55-56, (2013), 12-27.

[36] A. Zheng, Shing-Jong Huang, Wen-Hua Chen, Pei-Hao Wu, H. Zhang, Huang-Kuei Lee, Louis-Charles de Ménorval, F. Deng, and Shang-Bin Liu. ^{31}P Chemical Shift of Adsorbed Trialkylphosphine Oxides for Acidity Characterization of Solid Acids Catalysts, ***J. Phys. Chem. A***, 112 (32), (2008), 7349-7356.

[37] J. Guan, X. Li, G. Yang, W. Zhang, X. Liu, X. Han, and X. Bao. Interactions of phosphorous molecules with the acid sites of H-Beta zeolite: Insights from solid-state NMR techniques and theoretical calculations, ***J. Mol. Catal. A Chem.***, 310(1-2), (2009), 113-120.

[38] Y. Seo, K. Cho, Y. Jung, and R. Ryoo. Characterization of the Surface Acidity of MFI Zeolite Nanosheets by 31P NMR of Adsorbed Phosphine Oxides and Catalytic Cracking of Decalin, ***ACS Catal.***, 3, (2013), 713–720.

[39] C. Bornes, M. Sardo, Z. Lin, J. Amelse, A. Fernandes, M. Ribeiro, C. Geraldes, J. Rocha, and L. Mafra. 1H–31P HETCOR NMR elucidates the nature of acid sites in zeolite HZSM-5 probed with trimethylphosphine oxide, ***Chem. Comm.***, 55(84), (2019), 12635-12638.

[40] Y. Wang, S. Xin, Y. Chu, J. Xu, G. Qi, Q. Wang, Q. Xia, and F. Deng. Influence of trimethylphosphine oxide loading on the measurement of zeolite acidity by solid-state nmr spectroscopy, ***J. Phys. Chem. C***, 125(17), (2021), 9497-9506.

[41] C. Bornes, M. Fischer, J. Amelse, C. Geraldes, J. Rocha, and L. Mafra. What Is Being Measured with P-Bearing NMR Probe Molecules Adsorbed on Zeolites?, ***J. Am. Chem. Soc.***, 143(34), (2021), 13616-13623.

[42] D. Zasukhin, I. Kasyanov, Y. Kolyagin, A. Bulygina, K. Kharas, and I. Ivanova. Evaluation of Zeolite Acidity by 31P MAS NMR Spectroscopy of Adsorbed Phosphine Oxides: Quantitative or Not?, ***ACS Omega***, 7(14), (2022), 12318-12328.

[43] X. Yi, H. Ko, F. Deng, S. Liu, and A. Zheng. Solid-state ^{31}P NMR mapping of active centers and relevant spatial correlations in solid acid catalysts, ***Nat. Protoc.***, 15 (10), (2020), 3527-3555.

[44] D. Zasukhin, I. Kostyukov, I. Kasyanov, Y. Kolyagin, and I. Ivanova. ^{31}P NMR Spectroscopy of Adsorbed Probe Molecules as a Tool for the Determination of the Acidity of Molecular Sieve Catalysts (A Review), ***Pet. Chem.***, 61 (8), (2021), 875-894.

[45] National Institute of Standards and Technology., ***NIST Chemistry WebBook***. https://webbook.nist.gov/chemistry/, (Accessed: Feb 10, 2023).

[46] V.W. Faria, K.M.A. Santos, A.M. Calazans, and M.A. Fraga, Hydrolysis of Furfuryl Alcohol to Angelica Lactones and Levulinic Acid over Nb-based Catalysts, ***ChemCatChem***, 15, (2023), e202300447.

[47] E.L. Albuquerque, L.E.P. Borges, and M.A. Fraga, Relationship between Acid-Base Properties and the Activity of ZrO_2-Based Catalysts for the Cannizzaro Reaction of Pyruvaldehyde to Lactic Acid, ***ChemCatChem***, 9, (2017), 2675-2683.

[48] K.M.A. Santos, E.M. Albuquerque, T.L. Coelho *et al.* Continuous aqueous-phase cascade conversion of trioses to lactic acid over Nb_2O_5 catalysts. ***Biomass Conv. Bioref.***, 13, (2023), 11865-11878.

[49] F.S.O. Ramos, R. K. S. Almeida, C.A. Lopes Júnior, M.A.Z. Arruda, and H. O. Pastore. A Straightforward Method for Determination of Al and Na in Aluminosilicates Using ICP OES, ***J. Braz. Chem. Soc.***, 28 (8), (2017), 1-7.

[50] M. Borowski, B. Marler, and H. Gies. The crystal structure determination of the crystalline layered silicic acid H-RUB-18, ***Z. Krist.*** 217, (2002), 233–241.

[51] G. Engelhardt and D. Michel, ***High-resolution Solid State NMR of Silicates and Zeolites***, Wiley, Chichester, 1987.

[52] S. Mintova, V. Valtchev, T. Onfroy, C. Marichal, H. Knözinger, and T. Bein. Variation of the Si/Al ratio in nanosized zeolite Beta crystals, ***Microporous Mesoporous Mater.***, 90(1-3), (2006), 237-245.

[53] H.M. Moura, F.A. Bonk, R.C.G. Vinhas, R. Landersb, and H.O. Pastore. Aluminium-magadiite: from crystallization studies to a multifunctional material, ***CrystEngComm***, 13, (2011), 5428-5438.

[54] M. Jin, M. Ravi, C. Lei, C. Heard, F. Brivio, Z. Tošner, L. Grajciar, and J.A. van Bokhoven. Dynamical Equilibrium between Brønsted and Lewis Sites in Zeolites: Framework-Associated Octahedral Aluminum, ***Angew. Chem. Int. E.***, 62, (2023), e202306183.

[55] A. Zheng, S.B. Liu, F. Deng. ^{31}P NMR Chemical Shifts of Phosphorus Probes as Reliable and Practical Acidity Scales for Solid and Liquid Catalysts. ***Chem. Rev.***, 117 (19), (2017), 12475-12531.

[56] P.A. Wright, ***Microporous Framework Solids***, RSC Publishing, Cambridge, 2008.

[57] K. Chen, S. Horstmeier, Vy.T. Nguyen, B. Wang, S.P. Crossley, T. Pham, Z. Gan, I. Hung, and J.L. White. Structure and Catalytic Characterization of a Second Framework Al(IV) Site in Zeolite Catalysts Revealed by NMR at 35.2 T, ***J. Am. Chem. Soc.***, 142 (16), (2020), 7514−7523.

[58] S. Xin, *et al.* The acidic nature of “NMR-invisible” tri-coordinated framework aluminum species in zeolites. ***Chem. Sci.***, 10, (2019), 10159–10169.

[59] Q. Zhao, Wen-Hua Chen, Shing-Jong Huang, Yu-Chih Wu, Huang-Kuei Lee, and Shang-Bin Liu. Discernment and quantification of internal and external acid sites on zeolites. ***J. Phys. Chem. B***, 106, (2002), 4462–4469.

[60] I. Wolf, H. Gies, and C.A. Fyfe. Ordering of Silicate Layers by Hydrogen-Bonding Networks: Solid State NMR Investigation of the Perfect Three-Dimensional Registration in the Layer Silicate RUB-18. ***J. Phys. Chem. B***, 103, (1999), 5933-5938.

[61] M. Borowski, I. Wolf, and H. Gies. Investigation of Proton Dynamics within the Hydrogen-Bond Network of the Layer Silicate Na-RUB-18, ***Chem. Mater.***, 14, (2002), 38-43.

[62] Q. Zhao, W. Chen, S. Huang, Y. Wu, H. Lee, and S. Liu. Discernment and Quantification of Internal and External Acid Sites on Zeolites, ***J. Phys. Chem. B***, 106 (17), (2002), 4462-4469.

[63] R. Zhao, Z. Zhao, S. Li, and W. Zhang. Insights into the Correlation of Aluminum Distribution and Brönsted Acidity in H-Beta Zeolites from Solid-State NMR Spectroscopy and DFT Calculations, ***J. Phys. Chem. Lett.***, 8 (10), 2017, 2323-2327.

[64] C. Bornes, C.F.G.C. Geraldes, J. Rocha, and L. Mafra. Investigating trimethylphosphine oxide interactions with Brønsted and Lewis acid sites in zeolites: A comparative solid-state NMR study of wet-phase and gas-phase adsorption techniques, ***Microporous Mesoporous Mat.***, 360, (2023), 112666.

[65] C. Bornes, D. Stosic, C.F.G.C. Geraldes, S. Mintova, J. Rocha, L. Mafra. Elucidating the Nature of the External Acid Sites of ZSM-5 Zeolites Using NMR Probe Molecules, ***Chem. Eur. J.***, 28, (2022), e202201795.

[66] G.C. Pimentel, and A.L. McClellan. ***The Hydrogen Bond***. W. H. Freeman; trade distributor: Reinhold Publishing Corporation, New York, 1960.

[67] D. Song, *et al.* Efficient conversion of levulinic acid or furfuryl alcohol into alkyl levulinates catalyzed by heteropoly acid and ZrO_2 bifunctionalized organosilica nanotubes, ***J. Catal.***, 333, (2016), 184-199.

[68] C.R. Patil, S.P. Kamble, and C.V. Rode, Single-Pot Alcoholysis of Furfuryl Alcohol to Alkyl Levulinates Using Heterogenized p-TSA Catalyst. ***ChemistrySelect***, 6, (2021), 6636-6643.

[69] Y. Li, S. Wang, S. Fan, B. Ali, X. Lan, and T. Wang, Nano-H-ZSM-5 with Short b-Axis Channels as a Highly Efficient Catalyst for the Synthesis of Ethyl Levulinate from Furfuryl Alcohol. ***ACS Sustain. Chem. Eng.***, 10, (2022), 3808-3816.

[70] H. Tian, Y. Shao, C. Liang, Q. Xu, L. Zhang, S. Zhang, S. Liu, and X. Hu. Sulfated attapulgite for catalyzing the conversion of furfuryl alcohol to ethyl levulinate: Impacts of sulfonation on structural transformation and evolution of acidic sites on the catalyst, Renew. Energy, 2020, 162, 1576-1586.

[71] Y. Ma, J. Ding, L. Yang, X. Wu, Y. Gao, R. Ran, and D. Weng. Flexible Al Coordination with H_2O Explaining the Deviation of Strong Acid Amount from the Framework Al Content in Al-Rich SSZ-13, ***J. Phys. Chem. C***, 127 (33), (2023), 16598-16606.

[72] C. Lei, A. Erlebach, F. Brivio, L. Grajciar, Z. Tošner, C. Heard, and P. Nachtigall. The need for operando modelling of ^{27}Al NMR in zeolites: the effect of temperature, topology and water. ***Chem. Sci.*** 14 (34), (2023), 9101.

[73] T. Yagasaki, K. Iwahashi, S. Saito, I. Ohmine. A theoretical study on anomalous temperature dependence of pKw of water, ***J. Chem. Phys.***, 122(14), (2005), 144504.

[74] P. Bhaumik, P.L. Dhepe. Effects of careful designing of SAPO-44 catalysts on the efficient synthesis of furfural, ***Catal. Today***, 251, (2015), 66-72.

Supplementary Information

Partial framework-Al in lamellar H-[Al]-RUB-18: acidity by probe TMPO adsorption and catalytic study in the presence and absence of water

Paulla B. F. Sousa[1,2], Elise M. Albuquerque[2], Marco A. Fraga[2,3*], and Heloise O. Pastore[1*]

[1]*Micro and Mesoporous Molecular Sieves Group, Institute of Chemistry, University of Campinas, Campinas-SP,13083-862, Brazil.*
[2]*Instituto Nacional de Tecnologia (INT), Laboratory of Catalysis, Rio de Janeiro-RJ, 20081-312, Brazil.*
[3]*Department of Chemical and Materials Engineering, Pontifical Catholic University of Rio de Janeiro (PUC-Rio), 22453-900 Rio de Janeiro, RJ, Brazil.*

*Corresponding authors: marco.fraga@int.gov.br (M.A. Fraga); lolly@unicamp.br (H.O. Pastore)

1. Experimental procedures

PREPARATION OF ACIDIC SEEDED LAMELLAR RUB-18

Synthesis of Na-[Al]-RUB-18 induced by crystal seeds: Following the synthesis procedure adopted in this work, a second mixture of silica (0.16 mol) and metasilicate solution (molar composition: 0.05 SiO_2: 0.10 NaOH: 1.31 H_2O) was mechanically stirred at 22 °C for 30 min. Subsequently, Na-RUB-18 was then added to the second mixture as a seed (0.8% w/w equivalent to 0.16 mol of silica) and maintained under mechanical stirring for an additional 5 min. The homogeneous, viscous, and bright gels (molar composition 0.05 Na_2SiO_3: 0.16 SiO_2: 1.36 H_2O) were completely transferred to a stainless-steel autoclave lined with Teflon® and hydrothermally treated in the oven for 14 days at 100 °C. The products (named *Na-R18$_{(seeded)}$*) were washed with distilled water, filtered until neutral pH and dried in hot air for 12 h. The incorporation of Al^{3+} ions on lamellar silicates (Si/Al nominal ratio = 15 and 30) was applied sequentially using the same method described in *Section 2.1 (Syntheses of acidic lamellar silicate and aluminosilicate)*. The final products were named *Na-[Al z]-R18$_{(seeded)}$*, with *z* as the Si/Al experimental ratio.

Ion exchange procedure in Na-[Al y]- and Na-R18$_{(seeded)}$ samples: each lamellar solid was exchanged with a 1 mol L^{-1} of NH_4Cl solution [1], dispersing 100 mL g^{-1} under magnetic stirring at 22 °C for 24 h. Then, the samples were washed and filtered with distilled H_2O until a negative test for chloride ions with $AgNO_3$ (Synth, 0.1 mol L^{-1}). The NH_4^+ products were dried in hot air for 12 h. This procedure was employed in triplicate for each sample. Subsequently, a thermal treatment was carried out by ramping the temperature to 200 °C under an N_2 atmosphere (1 °C min^{-1}) and then maintaining this temperature for 1 h. The sample was then heated to 300 °C under O_2 (1 °C min^{-1}) and kept at this temperature for another 2 h period. The acidic samples were named *H-R18*$_{(seeded)}$ and *H-[Al z]-R18*$_{(seeded)}$, with *z* as the Si/Al experimental ratio.

EXPERIMENTAL APPARATUS FOR TMPO ADSORPTION PROCEDURE

Figure S.1: Digital image of home-built Schlenk: **(a)** valves and taps to achieve high vacuum; **(b)** main cell; **(c)** secondary cell.

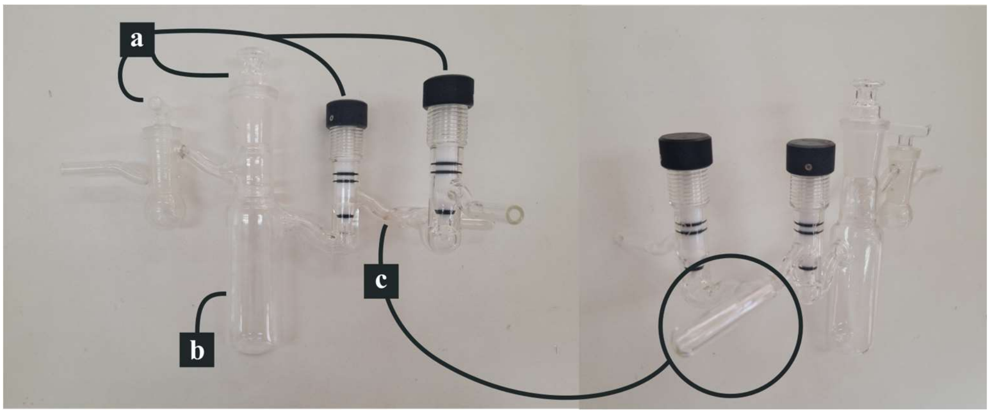

COMPLEMENTARY ANALYSIS

FTIR spectra for seeded lamellar samples: The FTIR spectra were collected by using a Thermo Electron Corporation Spectrophotometer (Nicolet 6700 model, detector DTGS), in the mid-infrared region (λ^{-1} = 400 a 4000 cm^{-1}), by accumulating 128 scans at 4 cm^{-1} of resolution. The samples were prepared with KBr and pressed into pellets.

Dehydration of non-seeded lamellar samples and FTIR spectra: The self-supporting wafers (0.025 g of sample) were placed into an IR cell equipped with KBr windows permanently attached to a high-vacuum line (~ 10^{-6} mmHg). The samples were heated from room temperature to 100 °C and held at this temperature for 1 h under a high dynamic vacuum. This procedure was repeated until 350 °C was reached. After that, the sample was maintained at this temperature (350 °C) for 15 h. *In situ* FTIR spectra were collected using a Thermo Electron Corporation Spectrophotometer (Nicolet 6700 model, detector DTGS), accumulating 128 scans at 2 cm^{-1} of resolution.

Method of GC-MS analysis: The liquid aliquots obtained from the FFA alcoholysis reaction were analyzed by an Agilent 7890A, with an Agilent 5975C (Inert XL MSD) mass spectrometer (GC-MS) detector. The inlet temperature was set at 280 °C, with 0.5 µL of injection volume and a split ratio of 300:1. The product separations were conducted on a Carbowax 20M (30 m x 0.25 mm x 0.25 µm) poly(ethylene glycol) column with He flown of

150 mL min^{-1}. The oven temperature was maintained at 50 °C, and a heating ramp to 220 °C at 10 °C min^{-1} was employed. The temperatures for the GC apparatus were 280 °C for the interface, 150 °C for the quadrupoles, and 275 °C for the ions source. The Scan analysis mode was employed with a scanning rate of 40 to 600 u.m.a. The identified products were achieved using the MSD Productivity ChemStation (Wiley7Nist05 spectra library).

2. Experimental data - additional results:

Table S.1: Determination of Si^{4+} and Al^{3+} species molar ratios and the molar chemical composition of the unit cell for acidic non-seeded lamellar materials.

Samples	Molar ratios				Empirical molecular formula $^{(v)}$
	Si/Al$^{(i)}$	Si/Al $^{(ii)}$	Q^3/Q^4 $^{(iii)}$	Al_{Td}/Al_{Oh} $^{(iv)}$	
H-R18	∞	∞	0.96	-	$H_{7.92}\,Na_{0.08}\,[Si_{32}\,(OH)_8\,O_{64}]$
H-[Al32]-R18	60	32	1.06	3.38	$H_{7.54}\,Na_{0.46}\,[Si_{31.04}\,Al_{0.96}\,(OH)_8\,O_{64}]$
H-[Al29]-R18	30	29	1.20	0.78	$H_{7.35}\,Na_{0.65}\,[Si_{30.95}\,Al_{1.05}\,(OH)_8\,O_{64}]$
H-[Al16]-R18	15	16	1.28	0.45	$H_{7.31}\,Na_{0.69}\,[Si_{30.14}\,Al_{1.86}\,(OH)_8\,O_{64}]$

(i) Nominal Si/Al molar ratio. Measured by: (ii) XRF; (iii) ^{29}Si- and (iv) ^{27}Al-NMR; (v) ICP-OES analysis.

Figure S.2: TG and differential TG curves of (A) sodium and (B) acidic seeded lamellar RUB-18, with different Si/Al molar ratios. To guarantee the maintenance of the structure with -OH groups on the lamellar surface of RUB-18, the maximum temperatures used for the treatment of these materials were as follows: 140 °C (*H-R18*), 250 °C (*H-[Al32]-R18*), 280 °C (*H-[Al29]-R18*), and 290 °C (*H-[Al16]-R18*).

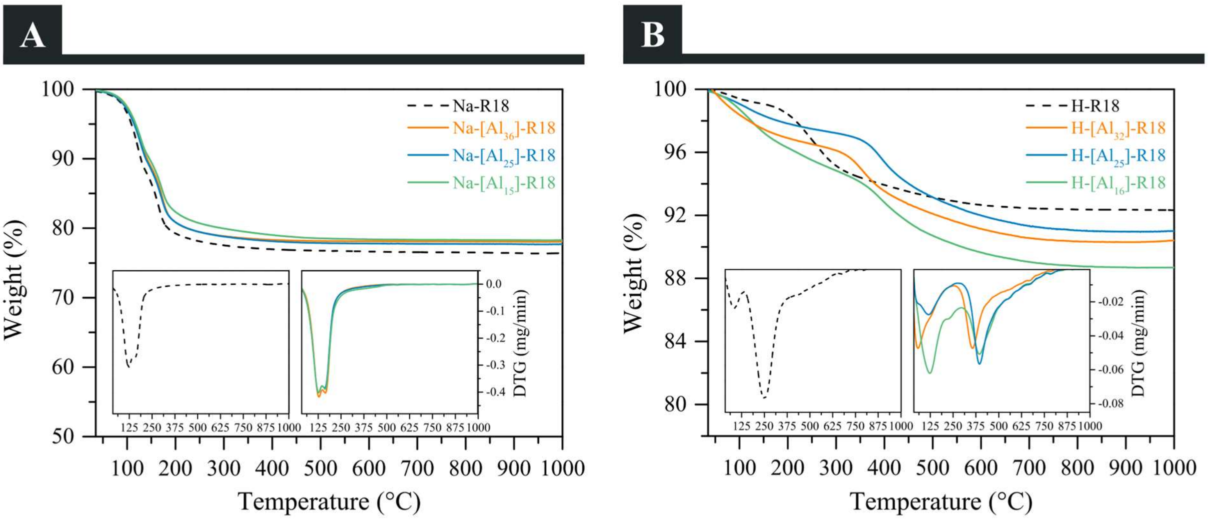

Table S.2: Percentage of resonance signals for ^{31}P-NMR spectra of dehydrated and hydrated lamellar materials. The values between parentheses are the respective chemical shifts.

Samples		**TMPO (Phys.)**	**-SiOH/-AlOH or LAS**	**BAS(1)**	**BAS(2)**
Dehydrated non-seeded samples **P/Al = 1.20**	H-R18	100.0% (43.8)	-	-	-
	H-[Al32]-R18	61.9% (41.3)	12.1% (49.4)	19.0% (67.0)	7.0% (71.4)
	H-[Al29]-R18	59.9% (41.4)	14.0% (51.6)	14.7% (66.0)	11.4% (70.5)
	H-[Al16]-R18	63.9% (41.2)	13.4% (51.7)	14.2% (66.1)	8.5% (70.8)
Dehydrated non-seeded samples **P/Al = 0.50**	H-R18	-	-	-	-
	H-[Al32]-R18	4.8% (48.0)	4.7% (52.2)	39.8% (64.7)	50.7% (69.4)
	H-[Al29]-R18	12.6% (48.8)	5.8% (54.0)	47.6% (64.2)	34.0% (68.2)
	H-[Al16]-R18	40.9% (44.6)	18.5% (51.7)	24.2% (64.6)	16.5% (69.0)
Hydrated non-seeded samples (2H_2O:1Al_{Oh}) **P/Al = 0.50**	H-R18	-	-	-	-
	H-[Al32]-R18	4.3% (45.1)	8.1% (51.5)	62.2% (64.1)	25.4% (68.7)
	H-[Al29]-R18	11.0% (48.7)	12.7% (54.4)	46.8% (64.2)	29.4% (67.7)
	H-[Al16]-R18	3.8% (46.0)	9.2% (51.0)	46.9% (64.2)	40.1% (68.7)
Dehydrated seeded samples **P/Al = 1.40**	H-R18$_{(seeded)}$	82.4% (43.7)	17.6% (49.9)	-	-
	H-[Al47]-R18$_{(seeded)}$	87.0% (43.8)	7.8% (53.0)	3.4% (66.7)	1.8% (70.7)
	H-[Al25]-R18$_{(seeded)}$	91.0% (42.3)	2.4% (52.9)	4.0% (67.0)	2.6% (71.2)
Dehydrated seeded samples **P/Al = 0.50**	H-R18$_{(seeded)}$	100.0% (46.9)	-	-	-
	H-[Al47]-R18$_{(seeded)}$	77.8% (44.9)	12.2% (51.8)	6.0% (65.9)	4.0% (70.7)
	H-[Al25]-R18$_{(seeded)}$	63.4% (46.4)	16.7% (51.9)	12.2% (65.4)	7.7% (70.2)
Dehydrated seeded samples **P/Al = 0.25**	H-R18$_{(seeded)}$	100.0% (47.5)	-	-	-
	H-[Al47]-R18$_{(seeded)}$	72.4% (45.8)	16.9% (51.6)	6.3% (65.6)	4.3% (69.9)
	H-[Al25]-R18$_{(seeded)}$	24.7% (45.7)	37.7% (50.1)	27.1% (64.6)	10.5% (69.7)
Hydrated seeded samples (Sat. H_2O) **P/Al = 1.40**	H-R18$_{(seeded)}$	89.3% (44.6)	10.7% (51.2)	-	-
	H-[Al47]-R18$_{(seeded)}$	72.5% (43.4)	14.7% (53.8)	8.9% (68.8)	3.9% (73.0)
	H-[Al25]-R18$_{(seeded)}$	75.9% (42.8)	14.2% (55.3)	5.2% (66.9)	4.7% (71.3)
Hydrated (Sat. H_2O) **P/Al = 0.25**	H-[Al47]-R18$_{(seeded)}$	26.7% (47.4)	30.3% (51.7)	27.0% (66.3)	16.0% (71.1)
Hydrated (Sat. H_2O) **P/Al = 1.40**	H-[Al16]-R18	29.4% (41.7)	13.8% (50.3)	37.5% (66.3)	19.3% (71.5)

(-) Values not found.

Figure S.3: XRD patterns spectra of sodium and acidic lamellar acidic seeded lamellar RUB-18.

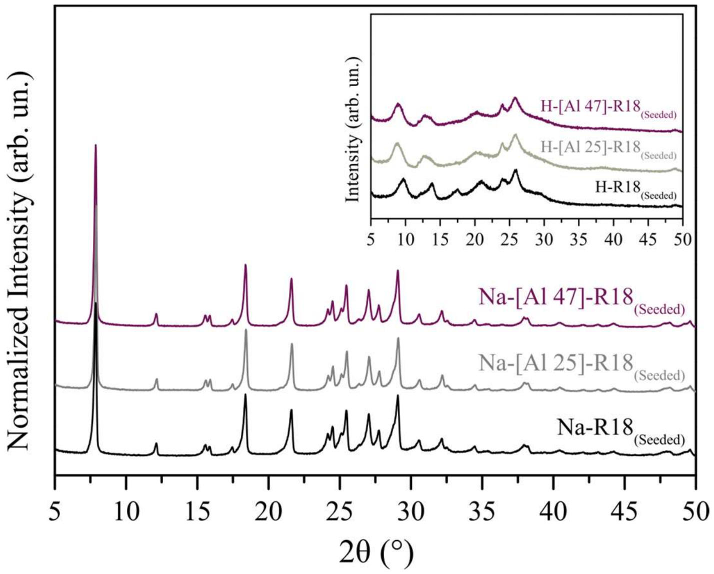

Figure S.4: FTIR spectra of sodium lamellar samples. The inner graph corresponds to samples after ion exchange (— *solid curve*) and acid form (--- *dashed curve*): **(ii)** NH_4- and **(i)** H-R18$_{(Seeded)}$; **(iv)** NH_4- and **(iii)** H-[Al25]-R18$_{(Seeded)}$; **(vi)** NH_4- and **(v)** H-[Al47]-R18$_{(Seeded)}$.

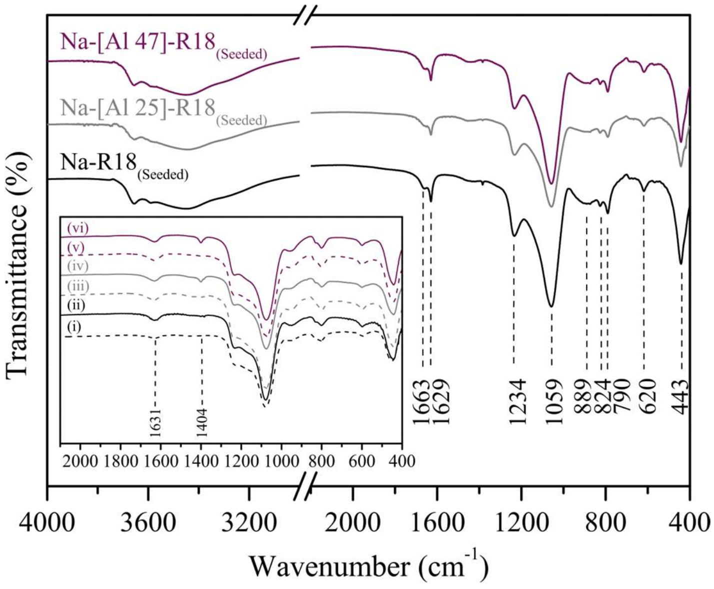

Figure S.5: ^{27}Al- and ^{29}Si-MAS-NMR spectra of sodium and acidic lamellar acidic seeded lamellar RUB-18.

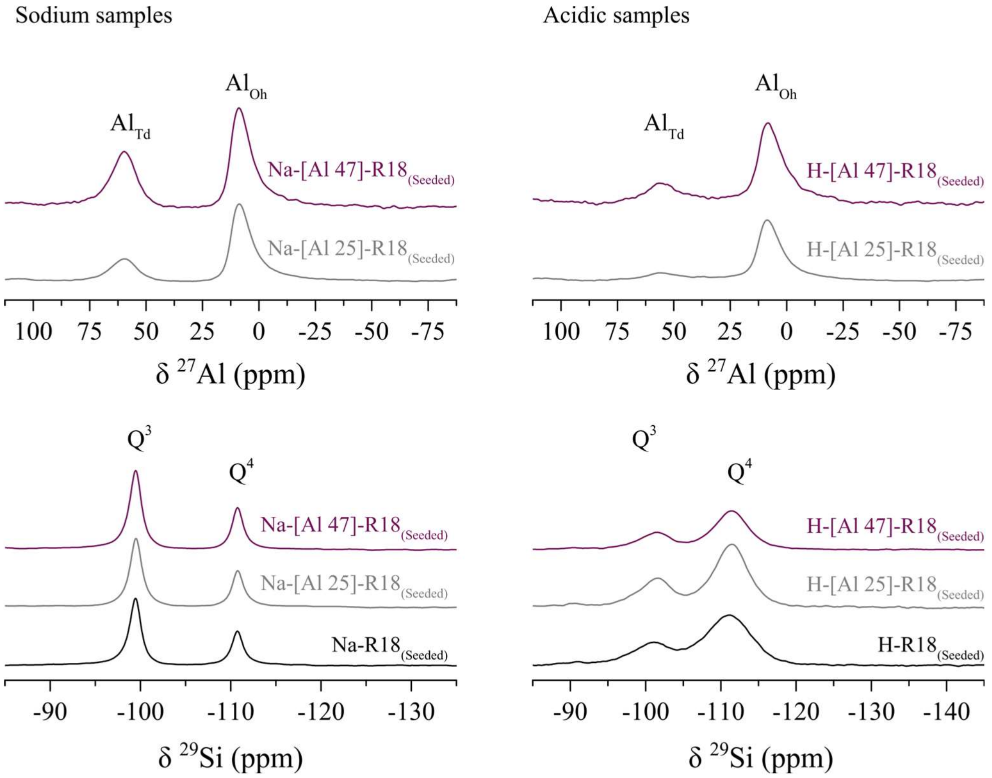

Figure S.6: TG and differential TG curves of sodium and acidic seeded lamellar RUB-18, with different Si/Al molar ratios: Na- and H-R18$_{(Seeded)}$ (— *solid curves*); Na- and H-[Al25]-R18$_{(Seeded)}$ (--- *dashed curves*); Na- and H-[Al47]-R18$_{(Seeded)}$ (··· *dotted curves*). *To guarantee the maintenance of the structure with -OH groups on the lamellar surface of RUB-18, the maximum temperature used for thermal treatment of these materials was 250 °C.

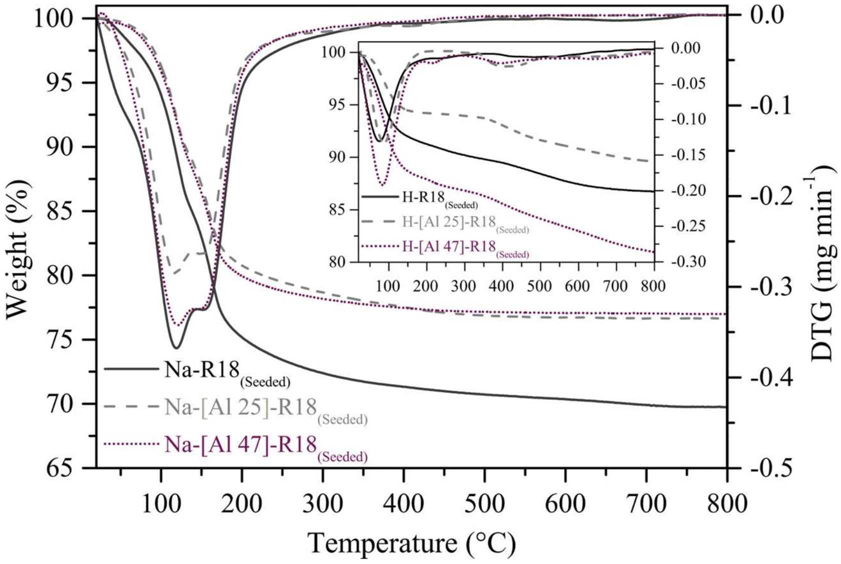

Table S.3: Si/Al and Al_{Td}/Al_{Oh} molar ratios, and concentration of Al species before and after catalytic reactions.

Catalysts	**Molar ratios**		**Concentration (mmol g^{-1})$^{(i,ii)}$**	
	Si/Al $^{(i)}$	**Al_{Td}/Al_{Oh} $^{(ii)}$**	**Al_{Td}**	**Al_{Oh}**
Before reaction				
H-[Al32]-R18	32	3.38	0.789	0.236
H-[Al29]-R18	29	0.78	0.503	0.646
H-[Al16]-R18	16	0.45	0.630	1.386
Post-DHA reaction$^{(*)}$				
H-[Al32]-R18	32.41 ± 0.32	0.65 ± 0.06	0.408 ± 0.018	0.628 ± 0.030
H-[Al29]-R18	26.99 ± 2.56	0.38 ± 0.05	0.344 ± 0.003	0.909 ± 0.116
H-[Al16]-R18	13.76 ± 0.21	0.14 ± 0.02	0.289 ± 0.033	2.075 ± 0.010
Post-PA reaction				
H-[Al32]-R18	131	0.57	0.093	0.164
H-[Al29]-R18	57	0.24	0.075	0.525
H-[Al16]-R18	21	0.04	0.055	1.484

(*) Average values ± standard deviation. Measured by: (i) XRF and (ii) ^{27}Al-NMR analysis.

Figure S.7: Proposal for reaction pathways to the alcoholysis of furfuryl alcohol, according to the compounds observed by GC-MS.

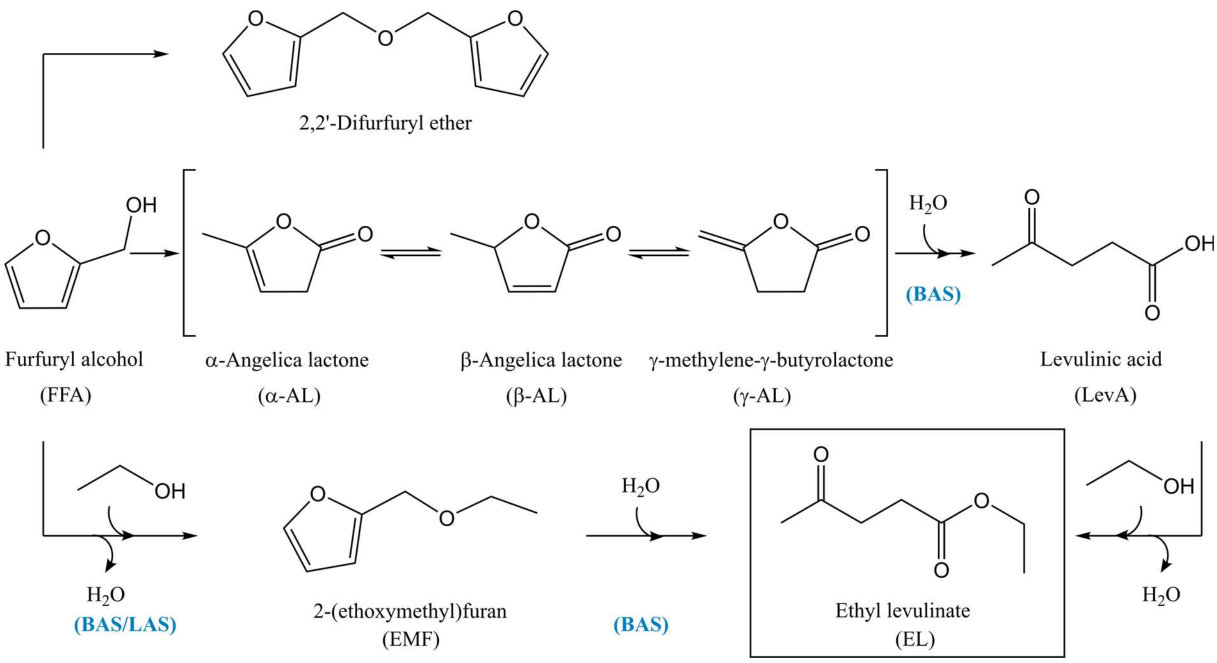

Figure S.8: Structural characterization by XRD analysis of catalysts before (--- *dashed curves*) and post-DHA (— *solid curves*) and PA (··· *dotted curves*) reactions, with different experimental Si/Al molar ratios before reaction.

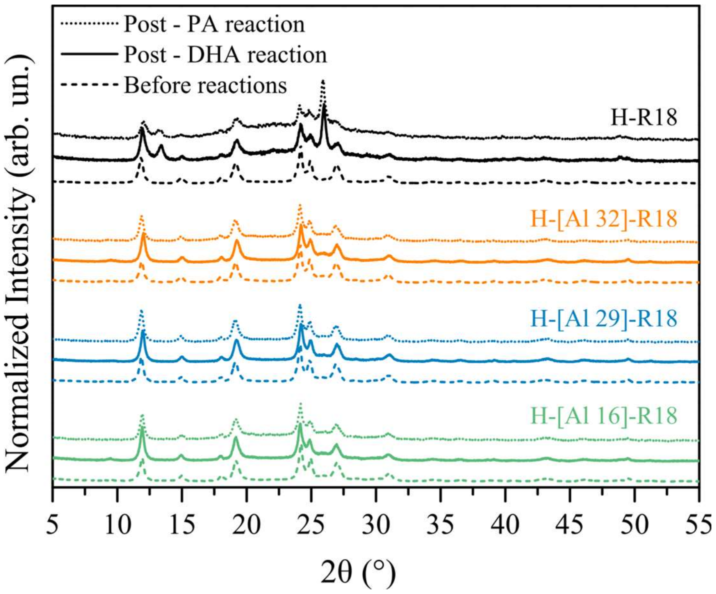

Figure S.9: Structural characterization by ^{27}Al-MAS-NMR analysis of catalysts before (--- *dashed curves*) and post-DHA (— *solid curves,* ··· *dotted curves* = reactions in duplicate), and PA reactions (— *solid curves*), with different experimental Si/Al molar ratios before reaction.

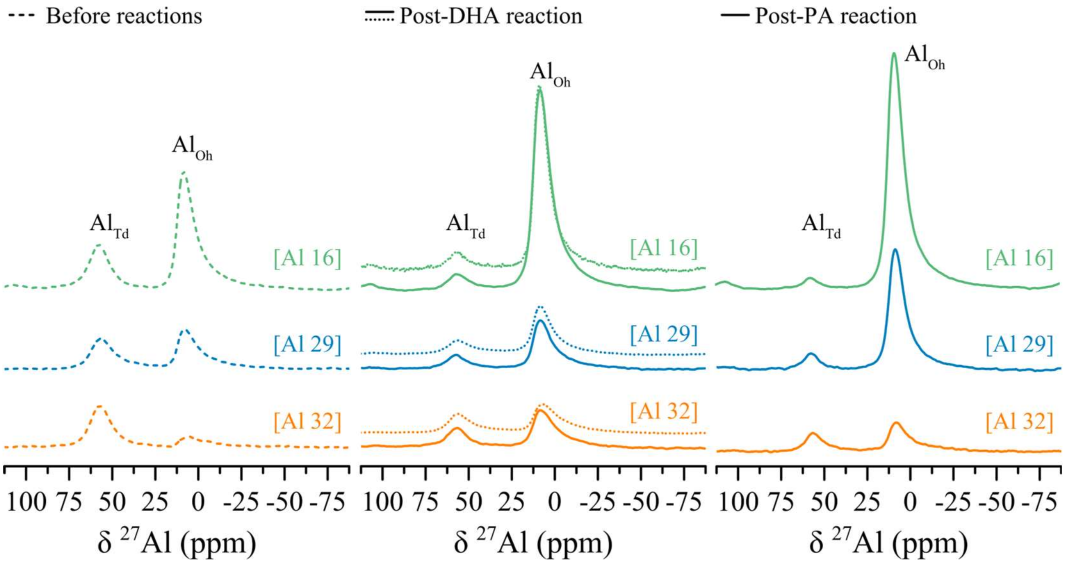

Figure S.10: Evaluation of variation of the tetrahedral and octahedral Al species concentration for each catalyst in the function of total Al concentration (mmol g^{-1}) before reaction: **(A)** data from the DHA reaction (average values ± standard deviation), and **(B)** data from the PA reaction.

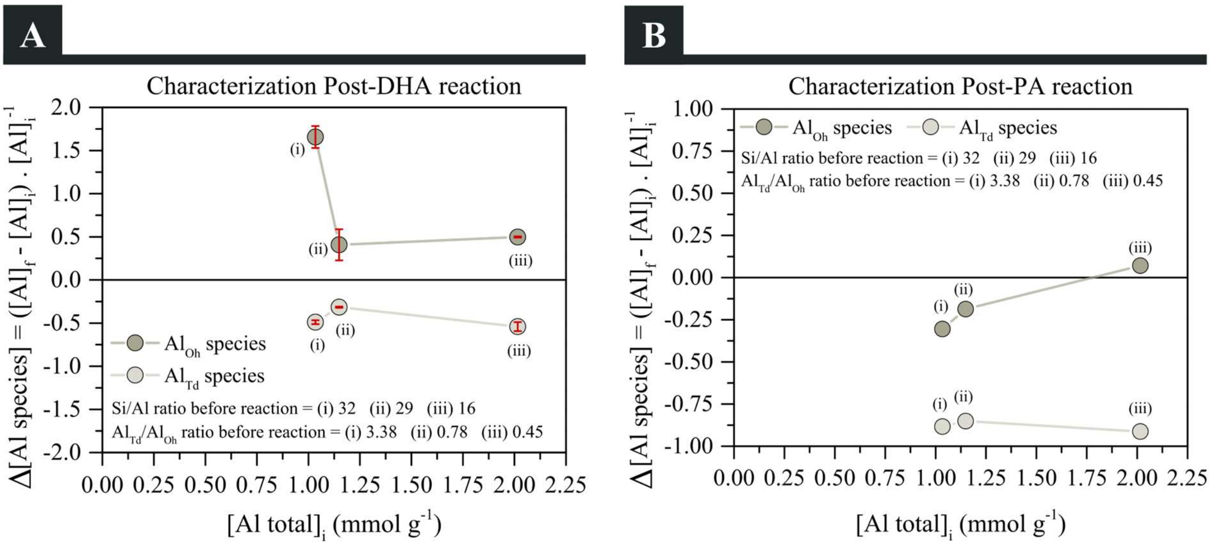

3. References

[1] G.B. Báfero, V.A. Araújo, R.K.S. Almeida, and H.O. Pastore. Catalytic performance of ferrierite and omega zeolites obtained through 2D-3D-3D transformation from Na-RUB-18 layered silicate, ***Microporous Mesoporous Mat.***, 302, (2020), 110216.

3. FINAL CONSIDERATIONS

3.1. Conclusions

The present work shows that the experiments carried out using the ^{31}P-NMR technique on dehydrated and hydrated TMPO-loaded samples in combination with catalytic tests provide new insights into the acidic properties of partial framework-Al sites on non-seeded and seeded H-[Al]-RUB-18.

Firstly, Na-RUB-18 materials were synthesized with a larger concentration of silanol or silanolate groups than usual. The larger presence of these Q^3 sites suggests structural defects and probably smaller crystal sizes than standard RUB-18. The Si^{4+} to Al^{3+} isomorphous substitution process was influenced by a direct correlation between the Si/Al ratio in the synthesis and aluminum species in the RUB-18 structure. This process mainly occurred on the lamellar surface. Framework-Al (Al_{Td}) and partial framework-Al (Al_{Oh} or aluminol sites) species were identified in the lamellar aluminosilicate samples, in different proportions. A higher content of Al_{Td} species was found when decreasing Al content, proving a better dispersion of these species on the lamellar structure. Otherwise, an increase in Al_{Oh} concentration in relation to Al_{Td} species content occurred for higher Al loading.

According to the ^{31}P-MAS-NMR data, we believe that some factors lead to changes in the resonance signals, such as crystallinity degree of the structure, the amount of aluminum (Si/Al ratio), completely and partially framework-Al species, adsorption under wet or dry conditions, and varying TMPO loadings. The spectroscopic analysis of the ^{31}P nucleus indicates that the resonance signals arise from TMPO adsorbed on the lamellar surface ($\delta^{31}P$ = 40 – 49 ppm), silanol/aluminol sites ($\delta^{31}P$ = 49 – 56 ppm), and Brönsted acid sites (60 – 75 ppm). In lower TMPO concentrations, the spectral data revealed at least the existence of two types of BAS with different strengths at ca. 64 ppm and 68 – 69 ppm. Upon exposure to humidity, the coordination of water molecules to aluminol sites enhanced the adsorption capacity of the active sites. This resulted in an increase in the resonance peak intensities, for both the Al_{Td} and Al_{Oh} species, associated with the peaks at 69 and 64 ppm, respectively. A water and TMPO-saturated environment induced changes in the signals above 50 ppm, implying no loss of acidity, and possibly no deactivation, occurs in the presence of water. This would result in enhanced catalytic activity when subjected to similar experimental conditions.

Additional characterizations of the acid properties of non-seeded H-[Al]-RUB-18 materials were performed by model reactions for biomass-derivative conversion. Batch ethanolysis of furfuryl alcohol and fixed-bed continuous flow reactions in aqueous phase for dihydroxyacetone and pyruvaldehyde conversions were performed. The objective of these experiments was to evaluate the activity, strength, and nature of the active centers. The Al_{Oh} and Al_{Oh} species present in the RUB-18 structure played a crucial role in these reactions. The H-[Al32]-R18 catalyst has a better performance in producing ethyl levulinate in ethanolysis reaction and pyruvaldehyde in DHA dehydration. This is attributed to the uniform distribution of Al_{Td} species due to the smaller Al content in the RUB structure, which facilitates the insertion of stronger BAS. Conversely, the H-[Al16]-R18 catalyst exhibited a significant selectivity towards 2-ethoxymethyl-furan (an intermediate in the ethanolysis reaction) and lactic acid (the final product of DHA and PA conversions). This indicates that the BAS sites are not sufficiently strong for complete 2-ethoxymethyl-furan hydrolysis to ethyl levulinate and, additionally, that Al_{Oh} sites in the aqueous medium act as LAS, producing lactic acid.

The ^{31}P-NMR spectroscopic analyses and catalytic tests approach reinforce the improvement in acidity under wet conditions and highlight the acid behavior of partial framework-Al sites in the RUB-18 structure. This work initiates the effort to create a consistent protocol for acidity analysis in lamellar solids, comparable to the existing ones for zeolites, and brings the importance of evaluating the acidity characteristics of solid catalysts under aqueous-phase conditions.

3.2. Future perspectives

Two-dimensional homo/heteronuclear correlation NMR experiments of adsorbed probe molecules allow the mapping of active centers and the determination of the spatial correlations among various acid sites. The experiments most explored in the literature are 2D ^{1}H-^{31}P, ^{27}Al-^{31}P, ^{1}H-^{27}Al HETCOR NMR, and ^{27}Al multiple-quantum MAS-NMR.

Also, the incorporation of computational modeling, such as Density Functional Theory (DFT) and *ab initio* molecular dynamics (AIMD) calculations, to the spectroscopic experimental data provides details about the configurations of probe molecules, their interactions with acid centers, the prediction of deprotonation energy values (DPE or proton affinity) and its correlations with chemical shift values for ^{31}P nucleus.

Therefore, a detailed characterization of the acidity of the lamellar materials will be obtained by combining experimental, including 1D and 2D NMR analyses in the presence and absence of water, and theoretical methods.

REFERENCES

[1] S. Vortmann, J. Rius, S. Siegmann, and H. Gies. Ab Initio Structure Solution from X-ray Powder Data at Moderate Resolution: Crystal Structure of a Microporous Layer Silicate, ***J. Phys. Chem. B***, 101, (1997), 1292-1297.

[2] I. Wolf, H. Gies, and C. Fyfe. Ordering of Silicate Layers by Hydrogen-Bonding Networks: Solid State NMR Investigation of the Perfect Three-Dimensional Registration in the Layer Silicate RUB-18, ***J. Phys. Chem. B***, 103, (1999), 5933-5938.

[3] M. Borowski, I. Wolf, and H. Gies. Investigation of proton dynamics within the hydrogen-bond network of the layer silicate Na-RUB-18, ***Chem. Mater.***, 14, (2002)38–43.

[4] M. Borowski, O. Kovalev, and H. Gies. Structural characterization of the hydrous layer silicate Na-RUB-18, Na8Si32O64(OH)8·32H2O and derivatives with XPD-, NPD-, and SS NMR experiments, ***Microporous Mesoporous Mater.***, 107, (2008), 71-80.

[5] M. Borowski, B. Marler, and H. Gies. The crystal structure determination of the crystalline layered silicic acid H-RUB-18, ***Z. Krist.***, 217, (2002), 233-241.

[6] T. Sirinakorn, K. Imwiset, S. Bureekaew, and M. Ogawa. Inorganic modification of layered silicates toward functional inorganic-inorganic hybrids, ***Appl. Clay Sci.***, 153, (2018), 187-197.

[7] T. Selvam, A. Inayat, and W. Schwieger. Reactivity and applications of layered silicates and layered double hydroxides, ***Dalton Trans.***, 43, (2014), 10365.

[8] Y. Oumi, T. Takeoka, T. Ikeda, T. Yokoyama, and T. Sano. Convenient conversion of crystalline layered silicate octosilicate into RWR-type zeolite by acetic acid intercalation, ***New J. Chem.***, 31, (2007), 593-597.

[9] T. Ikeda, Y. Oumi, T. Takeoka, T. Yokoyama, T. Sano, and T. Hanaoka. Preparation and crystal structure of RUB-18 modified for synthesis of zeolite RWR by topotactic conversion, ***Microporous Mesoporous Mater.***, 110, (2008), 488-500.

[10] N. Alam, and R. Mokaya. Super-micropore/small mesopore composite pillared silicate and aluminosilicate materials from crystalline layered silicate Na-RUB-18, ***Microporous Mesoporous Mater***., 143, (2011), 104-114.

[11] N. Alam, and R. Mokaya. Strongly acidic mesoporous aluminosilicates prepared via hydrothermal restructuring of a crystalline layered silicate, ***J. Mater. Chem. A,*** 3, (2015), 7799.

[12] G. Paz, E. Munsignatti, and H. Pastore. Novel catalyst with layered structure: Metal substituted magadiite, ***J. Mol. Catal. A: Chem.***, 422, (2016), 1-8.

[13] G. Superti, E. Oliveira, H. Pastore, A. Bordo, C. Bisio, and L. Marchese. Aluminum Magadiite: an Acid Solid Layered Material, ***Chem. Mater.***, 19, (2007), 4300-4315.

[14] Y. Ide, N. Kagawa, M. Sadakane, and T. Sano. Precisely designed layered silicate as an effective and highly selective CO_2 adsorbent, ***Chem. Commun.***, 49, (2013), 9027.

[15] F. Ramos, E. Munsignatti, and H. Pastore. 2D-3D structures: The hydrothermal transformation of a layered sodium silicate, Na-RUB-18, into mordenite zeolite, ***Microporous Mesoporous Mater.***, 177, (2013), 143-150.

[16] F. Ramos, and H. Pastore. 2D-to-disguised 3D materials with built-in acid sites: H+-[Al]- RUB-18, ***Dalton Trans.***, 46, (2017), 11728-11737.

[17] G. Campos, G. Báfero, and H. Pastore. Vapor adsorption experiments as a characterization tool for layered catalysts, ***New J. Chem.***, 44, (2020), 9998.

[18] G. Báfero, E. Munsignatti, and H. Pastore. Lamellar-zeolitic transformations mediated by diffusionless and recrystallization mechanisms, ***Microporous Mesoporous Mater.***, 323, (2021), 111189.

[19] G. Báfero, B. Silva, A. Leitão, and H. Pastore. The behavior of aluminum sites in H-[Al]-RUB-18 catalysts: A theoretical-experimental investigation, ***Mol. Catal.***, 535, (2023), 112870.

[20] G. Campos, E. Albuquerque, M. Fraga, and H. Pastore. Continuous Cellobiose Hydrolysis over Lamellar Aluminosilicates-Unveiling [Al]-magadiite Water-Tolerant Acid Sites, ***Ind. Eng. Chem. Res.***, 60, (2021), 4794-4805.

[21] A. Corma, From Microporous to Mesoporous Molecular Sieve Materials and Their Use in Catalysis, ***Chem Rev.,*** 97, (1997), 2373-2420.

[22] J. Liang, Z. Liang, R. Zou, and Y. L. Zhao. Heterogeneous Catalysis in Zeolites, Mesoporous Silica, and Metal-Organic Frameworks, ***Adv. Mater.***, 29, (2017), 1701139.

[23] T. Ennaert, J. V. Aelst, J. Dijkmans, R. D. Clercq, W. Schutyser, M. Dusselier, D. Verboekend, and B. Sels. Potential and challenges of zeolite chemistry in the catalytic conversion of biomass, ***Chem. Soc. Rev.***, 45 (2016), 584-611.

[24] J. Huo, J.-P. Tessonnier, and B. H. Shanks. Improving Hydrothermal Stability of Supported Metal Catalysts for Biomass Conversions: A Review, ***ACS Catalysis***, 11, (2021), 5248-5270.

[25] R. Sheldon. Green chemistry, catalysis and valorization of waste biomass, ***J. Mol. Catal. A: Chem.***, 422, (2016), 3-12.

[26] M. Niakan, C. Qian, and S. Zhou. Highly Efficient One-Pot Conversion of Glucose to 5-Hydroxymethylfurfural over Acid-Base Bifunctional MCM-41, Mesoporous Silica under Mild Aqueous Conditions, ***Energ. Fuel.***, 37, (2023), 16639-16647.

[27] A. Kruse, and A. Gawlik. Biomass conversion in water at 330−410 C and 30−50 MPa. Identification of key compounds for indicating different chemical reaction pathways, ***Ind. Eng. Chem. Res.***, 42, (2003), 267-279.

[28] Y. Huang, and Y. Fu. Hydrolysis of cellulose to glucose by solid acid catalysts, ***Green Chem.***, 15, (2013), 1095-1111.

[29] A.V. Pelt, O. Simakova, S. Schimming, J. Ewbank, G. Foo, E. Pidko, E. Hensen, and C. Sievers. Stability of functionalized activated carbon in hot liquid water, ***Carbon***, 77, (2014), 143-154.

[30] R.A. Sheldon. Green solvents for sustainable organic synthesis: state of the art, ***Green Chem.***, 7(5), (2005), 267-278.

[31] **IUPAC Compendium of Chemical Terminology**. International Union of Pure and Applied Chemistry: 3rd edition, 2006 (Online version: 3.0.1, 2019).

[32] G.L. Miessler, P.J. Fischer, and D.A. Tarr. **Inorganic Chemistry**. Pearson Education: 5th edition, 2013.

[33] G. Yang, L. Zhou, and X. Han. Lewis and Brönsted acidic sites in $M4^+$-doped zeolites (M = Ti, Zr, Ge, Sn, Pb) as well as interactions with probe molecules: A DFT study, ***J. Mol. Catal. A Chem.***, 363-364, (2012), 371-379.

[34] L.G. A. van de Water, M.A. Zwijnenburg, W.G. Sloof, J. C. van der Waal, J.C. Jansen, and T. Maschmeyer. The Effect of Ge Incorporation on the Brønsted Acidity of ZSM-5, ***ChemPhysChem***, 5, (2004), 1328-1335.

[35] R. Almeida, G. Paz, G. Báfero, and H. Pastore. Properties of Layered [Al]- and [V,Al]-Magadiite Catalysts as Revealed by Ethanol Dehydration, ***Microporous Mesoporous Mater.***, 284, (2019), 1-9.

[36] E.P.L. Hunter, and S.G. Lias. Evaluated Gas Phase Basicities and Proton Affinities of Molecules: An Update, ***J. Phys. Chem. Ref. Data***, 27(3), (1998), 413-656.

[37] E. Derouane, J. Védrine, R. Pinto, P. Borges, L. Costa, M. Lemos, F. Lemos, F. Ribeiro. The Acidity of Zeolites: Concepts, Measurements and Relation to Catalysis: A Review on Experimental and Theoretical Methods for the Study of Zeolite Acidity, ***Catal. Rev.***, 55, (2013), 454-515.

[38] M. Niwa, N. Katada, M. Sawa, and Y. Murakami. Temperature-Programmed Desorption of Ammonia with Readsorption Based on the Derived Theoretical Equation, ***J. Phys. Chem. A***, 99, (1995), 8812-8816.

[39] M. Tamura, K. Shimizu, A. Satsuma. Comprehensive IR study on acid/base properties of metal oxides, ***Appl. Catal. A - Gen.***, 433-434, (2012), 135-145.

[40] A. Zheng, S. Liu, and F. Deng. Acidity characterization of heterogeneous catalysts by solid-state NMR spectroscopy using probe molecules, ***Solid State Nucl. Magn. Reson.***, 55-56, (2013), 12-27.

[41] X. Yi, H.H. Ko, F. Deng, S.B. Liu, and A. Zheng. Solid-state ^{31}P NMR mapping of active centers and relevant spatial correlations in solid acid catalysts, ***Nature Protocols***, 15, (2020), 3527-3555.

[42] A. Zheng, S.J. Huang, W.H. Chen, P.H. Wu, H. Zhang, H.K. Lee, L.C.D. Ménorval, F. Deng, and S.B. Liu, ^{31}P chemical shift of adsorbed trialkylphosphine oxides for acidity characterization of solid acids catalysts, ***J. Phys. Chem. A***, 112, (2008), 7349-7356.

[43] A. Zheng, H. Zhang, X. Lu, S.-B. Liu, and F. Deng. Theoretical Predictions of ^{31}P NMR Chemical Shift Threshold of Trimethylphosphine Oxide Absorbed on Solid Acid Catalysts, ***J. Phys. Chem. B***, 112, (2008), 4496-4505.

[44] J. Guan, X. Li, G. Yang, W. Zhang, X. Liu, X. Han, and X. Bao. Interactions of

phosphorous molecules with the acid sites of H-Beta zeolite: Insights from solid-state NMR techniques and theoretical calculations, ***J. Mol. Catal. A Chem.***, 310, (2009), 113-120.

[45] Y. Seo, K. Cho, Y. Jung, and R. Ryoo. Characterization of the Surface Acidity of MFI Zeolite Nanosheets by ^{31}P NMR of Adsorbed Phosphine Oxides and Catalytic Cracking of Decalin, ***ACS Catal.***, 3, (2013), 713-720.

[46] C. Bornes, M. Sardo, Z. Lin, J. Amelse, A. Fernandes, M. F. Ribeiro, C. Geraldes, J. Rocha, and L. Mafra. ^{1}H-^{31}P HETCOR NMR elucidates the nature of acid sites in zeolite HZSM-5 probed with trimethylphosphine oxide, ***Chem. Comm.***, 55, (2019), 12635-12638.

[47] Y. Wang, S. Xin, Y. Chu, J. Xu, G. Qi, Q. Wang, Q. Xia, and F. Deng. Influence of trimethylphosphine oxide loading on the measurement of zeolite acidity by solid-state nmr spectroscopy, ***J. Phys. Chem. C***, 125, (2021), 9497-9506.

[48] C. Bornes, M. Fischer, J. A. Amelse, C. F. Geraldes, J. Rocha, and L. Mafra. What Is Being Measured with P-Bearing NMR Probe Molecules Adsorbed on Zeolites?, ***J. Am. Chem. Soc.***, 143, (2021), 13616-13623.

[49] D.S. Zasukhin, I.A. Kasyanov, Y.G. Kolyagin, A.I. Bulygina, K.C. Kharas, and I.I. Ivanova. Evaluation of Zeolite Acidity by ^{31}P MAS NMR Spectroscopy of Adsorbed Phosphine Oxides: Quantitative or Not?, ***ACS Omega***, 7, (2022), 12318-12328.

[50] D.S. Zasukhin, I.A. Kostyukov, I.A. Kasyanov, Y.G. Kolyagin, and I.I. Ivanova. ^{31}P NMR Spectroscopy of Adsorbed Probe Molecules as a Tool for the Determination of the Acidity of Molecular Sieve Catalysts (A Review), ***Pet. Chem.***, 61, (2021), 875-894.

[51] **National Institute of Standards and Technology**. NIST Chemistry WebBook, https://webbook.nist.gov/chemistry/, (Accessed: Oct 10, 2022).

[52] E. Selli, and L. Forni. Comparison between the surface acidity of solid catalysts determined by TPD and FTIR analysis of pre-adsorbed pyridine, ***Microporous Mesoporous Mater.***, 31(1-2), (1999), 129-140.

[53] F. Jin, and Y. Li. A FTIR and TPD examination of the distributive properties of acid sites on ZSM-5 zeolite with pyridine as a probe molecule, ***Catal. Today***, 145(1-2), (2009), 101-107.

[54] K. Santos, E. Albuquerque, L. Borges, and M. Fraga. The Role of Brønsted and Water-Tolerant Lewis Acid Sites in the Cascade Aqueous-Phase Reaction of Triose to Lactic Acid, ***ChemCatChem***, 11, (2019), 3054-3063.

[55] C.A. Emeis. Determination of Integrated Molar Extinction Coefficients for Infrared Absorption Bands of Pyridine Adsorbed on Solid Acid Catalysts, ***J. Catal.***, 141(2), (1993), 347-354.

[56] S. Xin, et al. The acidic nature of “NMR-invisible” tri-coordinated framework aluminum species in zeolites. ***Chem. Sci.***, 10, (2019), 10159-10169.

[57] Q. Zhao, W.-H. Chen, S.-J. Huang, Y.-C. Wu, H.-K. Lee, and S.-B. Liu. Discernment and quantification of internal and external acid sites on zeolites. ***J. Phys. Chem. B***, 106, (2002), 4462-4469.

[58] V.W. Faria, K.M.A. Santos, A.M. Calazans, and M.A. Fraga. Hydrolysis of Furfuryl Alcohol to Angelica Lactones and Levulinic Acid over Nb-based Catalysts, ***ChemCatChem***, 15, (2023), e202300447.

[59] E.M. Albuquerque, L.E.P. Borges, and M.A. Fraga. Relationship between Acid-Base Properties and the Activity of ZrO_2-Based Catalysts for the Cannizzaro Reaction of Pyruvaldehyde to Lactic Acid, ***ChemCatChem***, 9, (2017), 2675-2683.

[60] K.M.A. Santos, E.M. Albuquerque, T.L. Coelho, and M.A. Fraga. Continuous aqueous-phase cascade conversion of trioses to lactic acid over Nb_2O_5 catalysts, ***Biomass Conv. Bioref.***, 13, (2023), 11865-11878.

[61] S. Chung, S. de Haart, R. Parton, and N. R. Shiju. Conversion of furfuryl alcohol into alkyl-levulinates using solid acid catalysts, ***Sustain. Chem. Clim. Action.***, 1, (2022), 100004.

[62] C. Patil, S. Kamble, and C. Rode. Single-Pot Alcoholysis of Furfuryl Alcohol to Alkyl Levulinates Using Heterogenized p-TSA Catalyst, ***ChemistrySelect***, 6(26), (2021), 6636-6643.

[63] D. Song, S. An, Y. Sun, and Y. Guo. Efficient conversion of levulinic acid or furfuryl alcohol into alkyl levulinates catalyzed by heteropoly acid and ZrO_2 bifunctionalized organosilica nanotubes, ***J. Catal.***, 333, (2016), 184-199.

[64] C. Antonetti, D. Licursi, S. Fulignati, G. Valentini, and A.M.R. Galletti. New frontiers

in the catalytic synthesis of levulinic acid: from sugars to raw and waste biomass as starting feedstock, ***Catalysts***, 6(12), (2016), 196.

[65] Y.J. Wee, J.N. Kim, and H.W. Ryu. Biotechnological production of lactic acid and its recent applications, ***Food Technol. Biotechnol.*** 44(2), (2006), 163-172.

[66] K.M.A. Santos, E.M. Albuquerque, L.E.P. Borges, M.A. Fraga. Discussing Lewis and Brønsted acidity on continuous pyruvaldehyde Cannizzaro reaction to lactic acid over solid catalysts, ***Mol. Catal.***, 458(B), (2018), 198-205.

[67] E.M. Albuquerque, L.E.P. Borges, and M.A. Fraga. Lactic acid production from aqueous-phase selective oxidation of hydroxyacetone, ***J. Mol. Catal. A Chem.***, 400, (2015), 64-70.

ANNEX A: EXPERIMENTAL APPARATUS FOR ADSORPTION AND CATALYTIC PROCESSES

TMPO adsorption experiments and solid-state ^{31}P-MAS-NMR spectroscopy

Figure A.1: Experimental apparatus for adsorption procedure of TMPO as probe molecule: **(a)** oven; **(b)** schlenk with sample connected to a vacuum line; and **(c)** turbomolecular pump to achieve high vacuum.

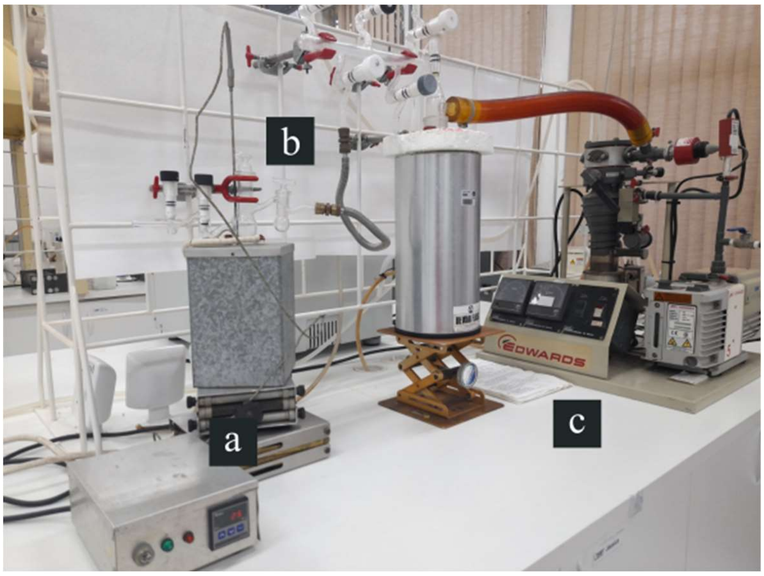

Figure A.2: Digital image of schlenk: **(a)** valves and taps to achieve high vacuum; **(b)** main cell; and **(c)** secondary cell.

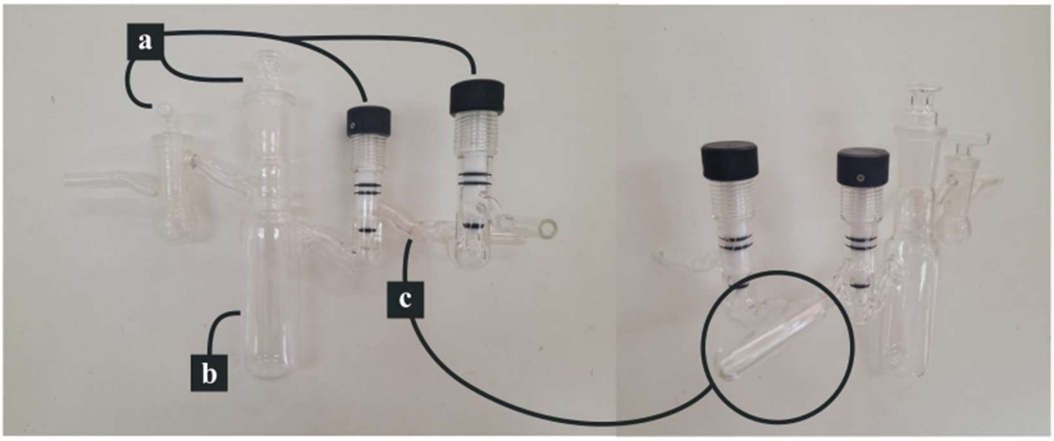

Model reaction A: alcoholysis of FFA in batch system

Figure A.3: Digital image of **(a)** batch multi-reactor system: **(b)** manometer; **(c)** gas flow; **(d)** carousel with the reactors; and **(e)** digital temperature controller.

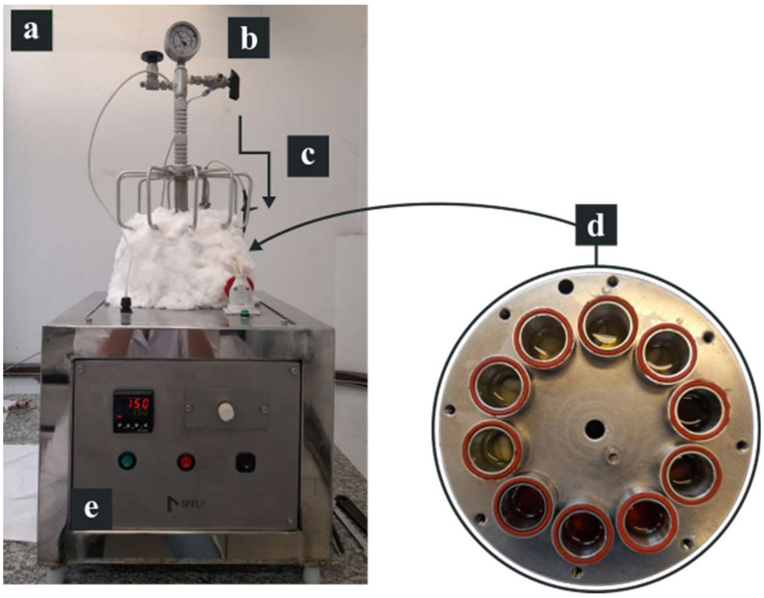

Model reaction B and C: PA and DHA conversions in continuous flow reaction system

Figure A.4: Digital image of continuous flow reaction system: **(a)** HPLC pump with the substrate solution; **(b)** digital temperature controller; **(c)** manometer; **(d)** oven with the reactor; and **(e)** sampler.

ANNEX B: ANALYTICAL CURVE FOR ICP-OES ANALYSIS

ICP-OES method: The Na element was quantified by Inductively Coupled Plasma Optical Emission Spectrometry (ICP-OES). The pre-treatment step of the samples was performed according to the methodology defined by [1]. Firstly, the thermal decompositions of the samples were carried out in a furnace by ramping the temperature to 900 °C, at a heating rate of 2 °C min^{-1}, and then maintaining the target temperature for 10 h. Next, 0.100 g of these materials were digested in a concentrated acidic mixture of 4 mL of HF (40%, Sigma Aldrich) and 4 mL of HNO_3 (65%, Synth, P.A. - A.C.S.), assisted by microwave irradiation (Provect Analitica oven, DGT - 100 Plus model, with Teflon PTFE digestion vessels). Then, diluted solutions of the totally dissolved samples were analyzed by ICP-OES. The analytical curve for the Na element was prepared to calibrate the spectrometer. The ICP-OES analyses were performed on a Perkin Elmer spectrometer (Optima 8300 model), with the following operating conditions: 1.3 kW power, a plasma gas flow rate of 0.5 L min^{-1}, λ^{-1} = 589.592 nm of emission line and axial viewing for Na element.

Figure B.1: Analytical curve for Na^+ at λ = 589.592 nm employed for quantification of the metal in synthesized lamellar samples.

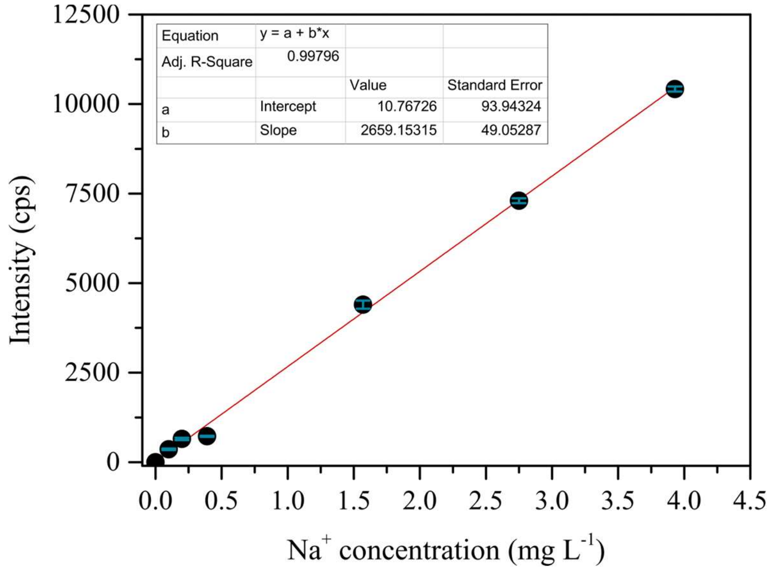

Equation	y = a + b*x		
Adj. R-Square	0.99796		
		Value	Standard Error
a	Intercept	10.76726	93.94324
b	Slope	2659.15315	49.05287

[1] F. Ramos, R. Almeida, C. Lopes, M. Arruda, and H. Pastore. A Straightforward Method for Determination of Al and Na in Aluminosilicates Using ICP-OES, ***Journal of the Brazilian Chemical Society***, 28, (2017), 1557-1563.

ANNEX C: ANALYTICAL CURVES FOR FFA, DHA, AND PA CONVERSION REACTIONS

Model reaction A: FFA conversion reaction

The analytical curve was prepared for organic compounds quantification. The standard solutions in EtOH had the following concentrations: 0.250 mol L^{-1} to 0.005 mol L^{-1}. The samples were also analyzed by GC-MS to confirm the organic compounds.

Figure C.1: Analytical curve of substrate solutions and the respective regression data for alcoholysis reactions.

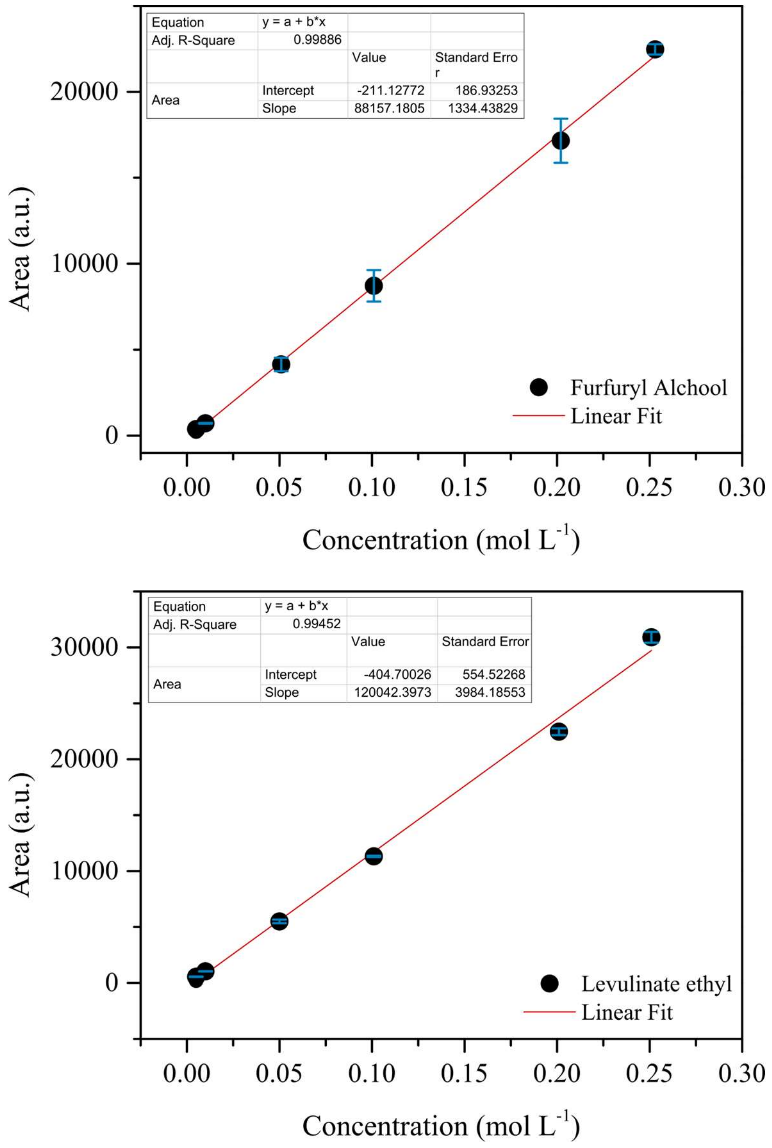

Figure C.1: (Cont.) Analytical curve of substrate solutions and the respective regression data for alcoholysis reactions.

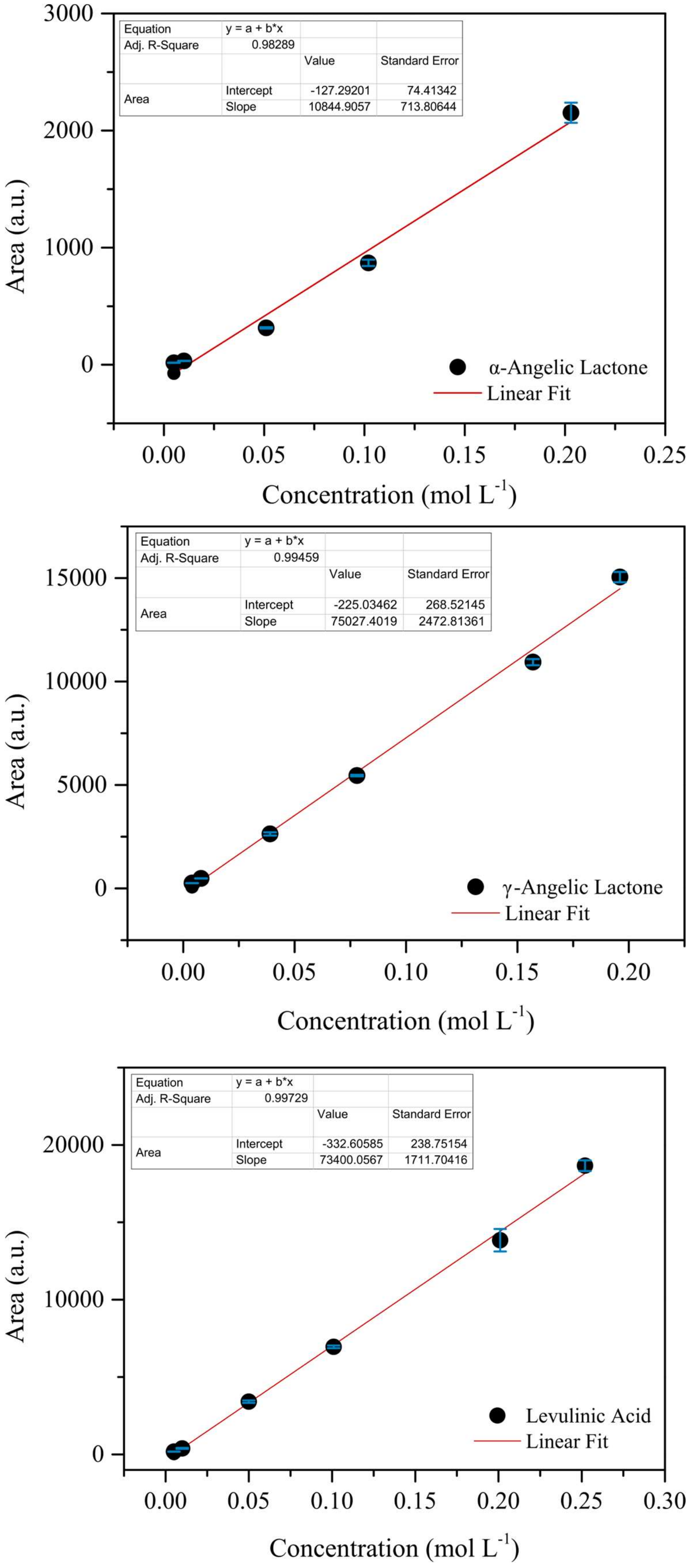

Equation	y = a + b*x		
Adj. R-Square	0.98289		
		Value	Standard Error
Area	Intercept	-127.29201	74.41342
	Slope	10844.9057	713.80644

Equation	y = a + b*x		
Adj. R-Square	0.99459		
		Value	Standard Error
Area	Intercept	-225.03462	268.52145
	Slope	75027.4019	2472.81361

Equation	y = a + b*x		
Adj. R-Square	0.99729		
		Value	Standard Error
Area	Intercept	-332.60585	238.75154
	Slope	73400.0567	1711.70416

Model reactions B and C: PA and DHA conversion reactions

The analytical curve was prepared for the quantification of organic compounds. The standard solutions had the following concentrations: 0.250 mol L^{-1}, 0.150 mol L^{-1}, 0.050 mol L^{-1}, 0.025 mol L^{-1}, 0.005 mol L^{-1}.

Figure C.2: Chromatogram of the analytical curve of 0.250 mol L^{-1} of substrate solutions and the compound retention times (RT): Pyruvaldehyde (PA, RT = 10.2 min); Lactic acid (LA, RT = 10.8 min); and Dihydroxyacetone (DHA, RT = 11.9 min).

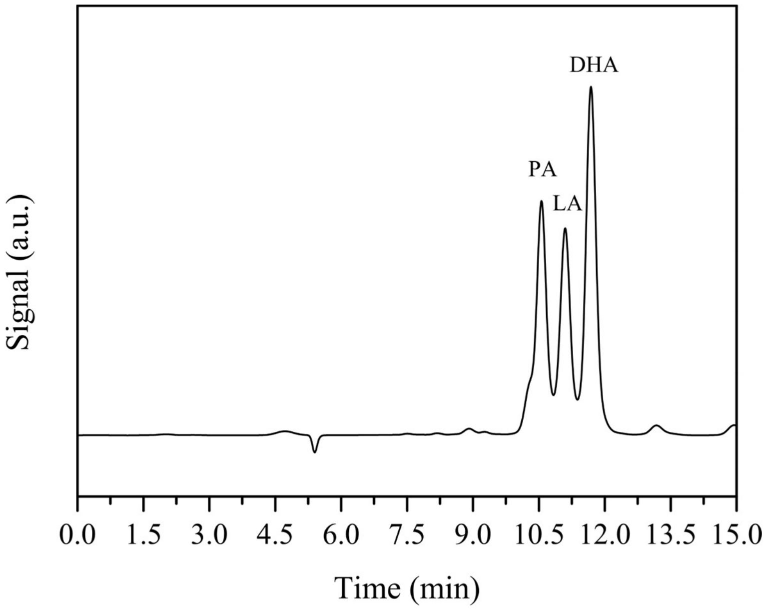

Figure C.3: Analytical curve of substrate solutions and the respective regression data for DHA and PA reactions.

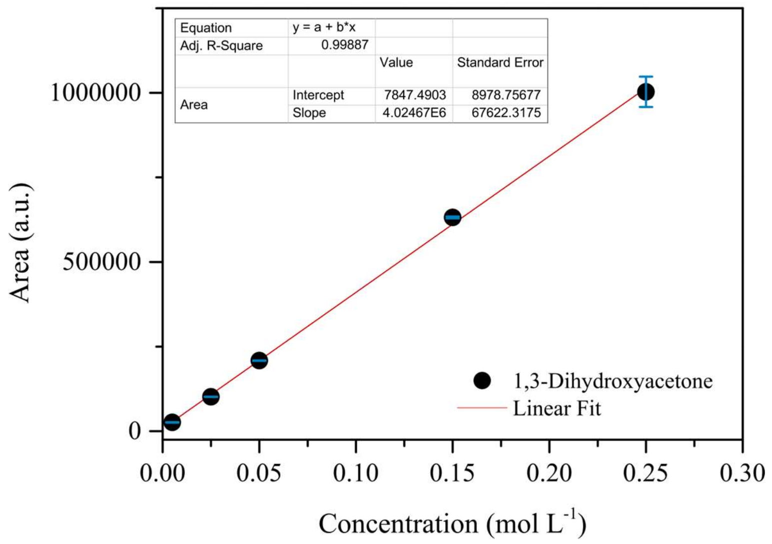

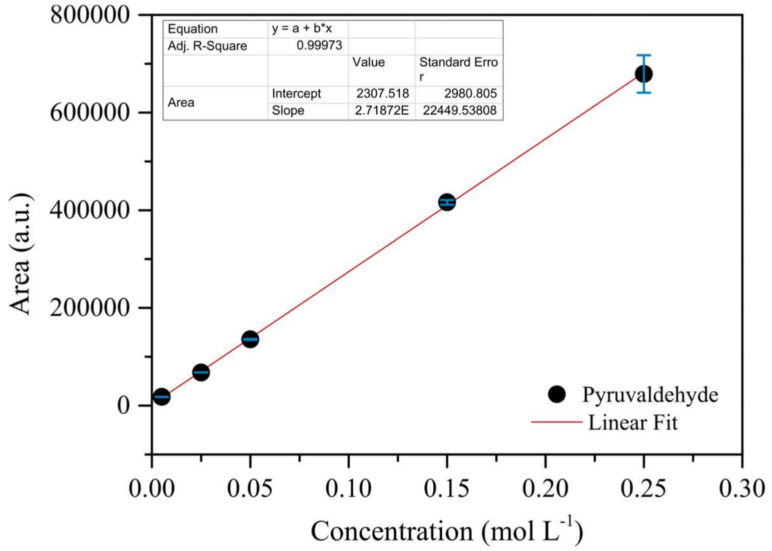

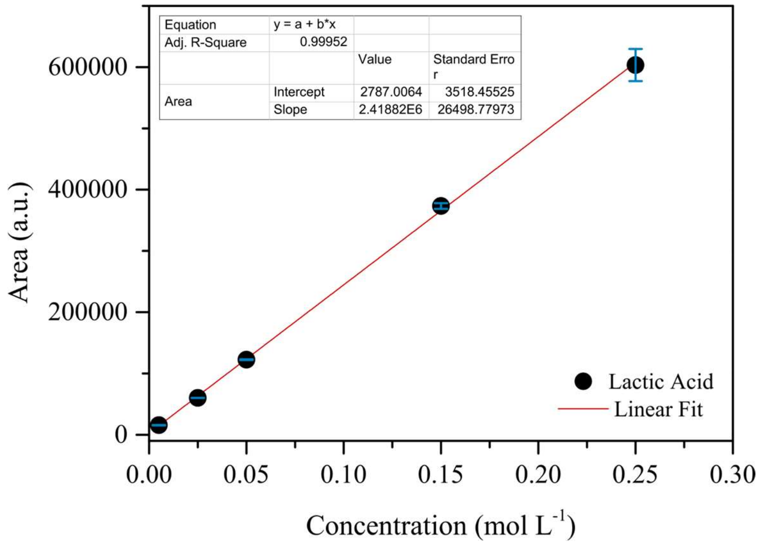

ANNEX D: ALIQUOTS AND CHROMATOGRAMS OF FFA CONVERSION REACTIONS

Figure D.1: Aliquots from FFA alcoholysis reaction (multi-reactor - batch process): 0h = blank aliquot at 0 h, r2 = H-[Al16]-R18, r4 = H-R18, r6 = H-[Al29]-R18, r8 = autothermal, r10 = H-[Al32]-R18.

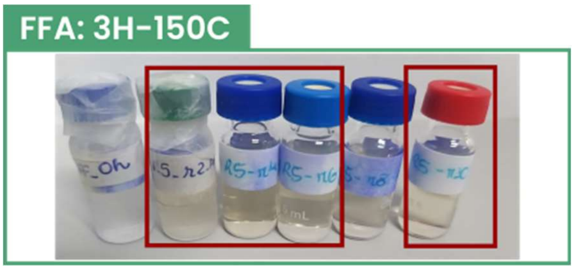

Table D.1: Compounds and the respective retention time analyzed in GC-MS (Catalyst used in FFA reaction = H-[Al16]-R18).

Name	Retention time (min)
Ethanol	1.591
2-(Ethoxy-methyl)-Furan	1.958
α-Angelica lactone	2.616
Ethyl levulinate	3.850
Furfuryl Alcohol	4.021
Difurfuryl ether	5.776

Figure D.2: Chromatogram obtained by GC-MS of the FFA to EL reaction (Catalyst = H-[Al16]-R18).

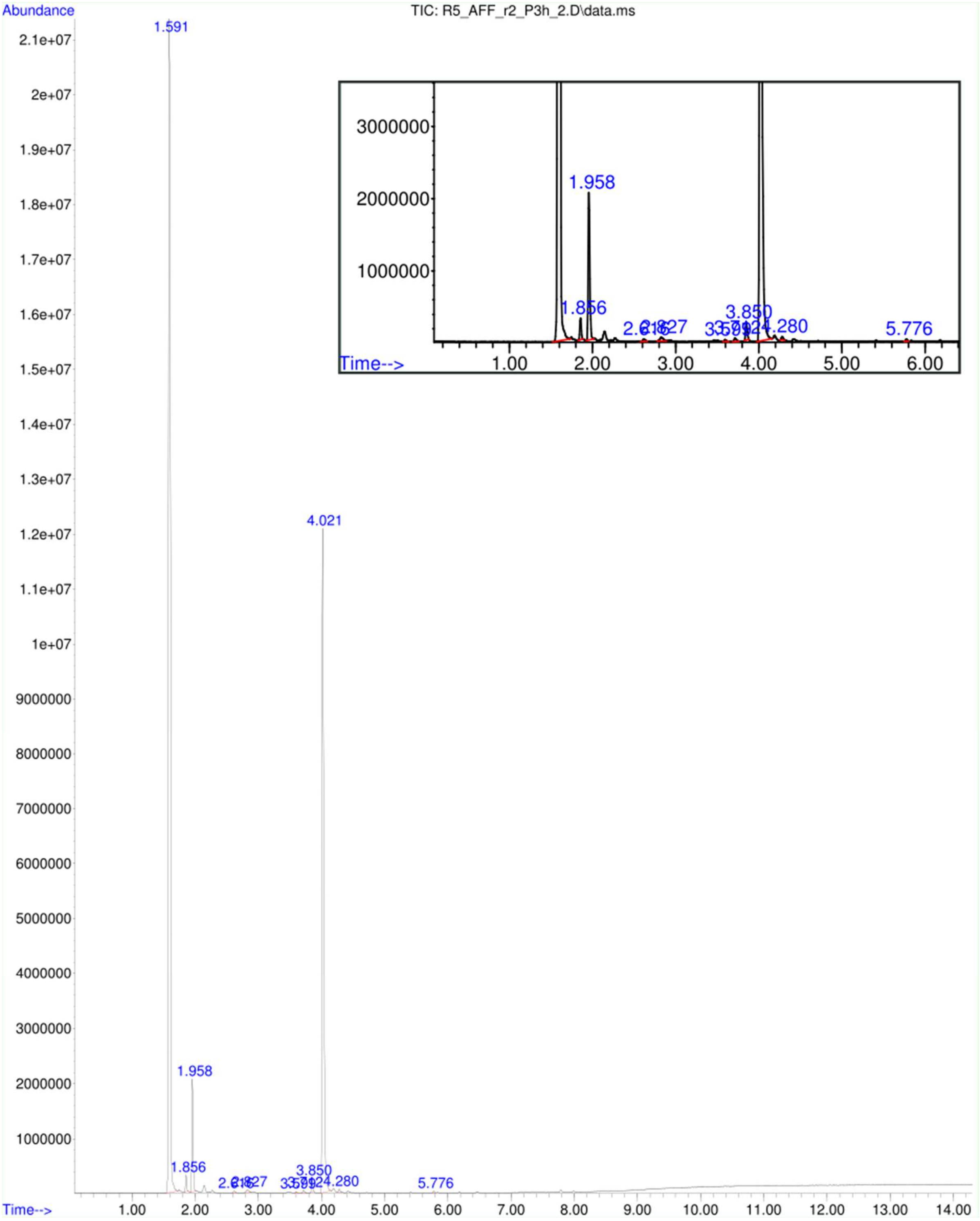

ANNEX E: CATALYSTS, ALIQUOTS AND CHROMATOGRAMS OF DHA AND PA CONVERSION REACTIONS

Figure E.1: Aspects of the catalysts before and post-PA and post-DHA reactions.

Figure E.2: Aliquots of PA in continuous flow reaction (fixed-bed in a tubular reactor).

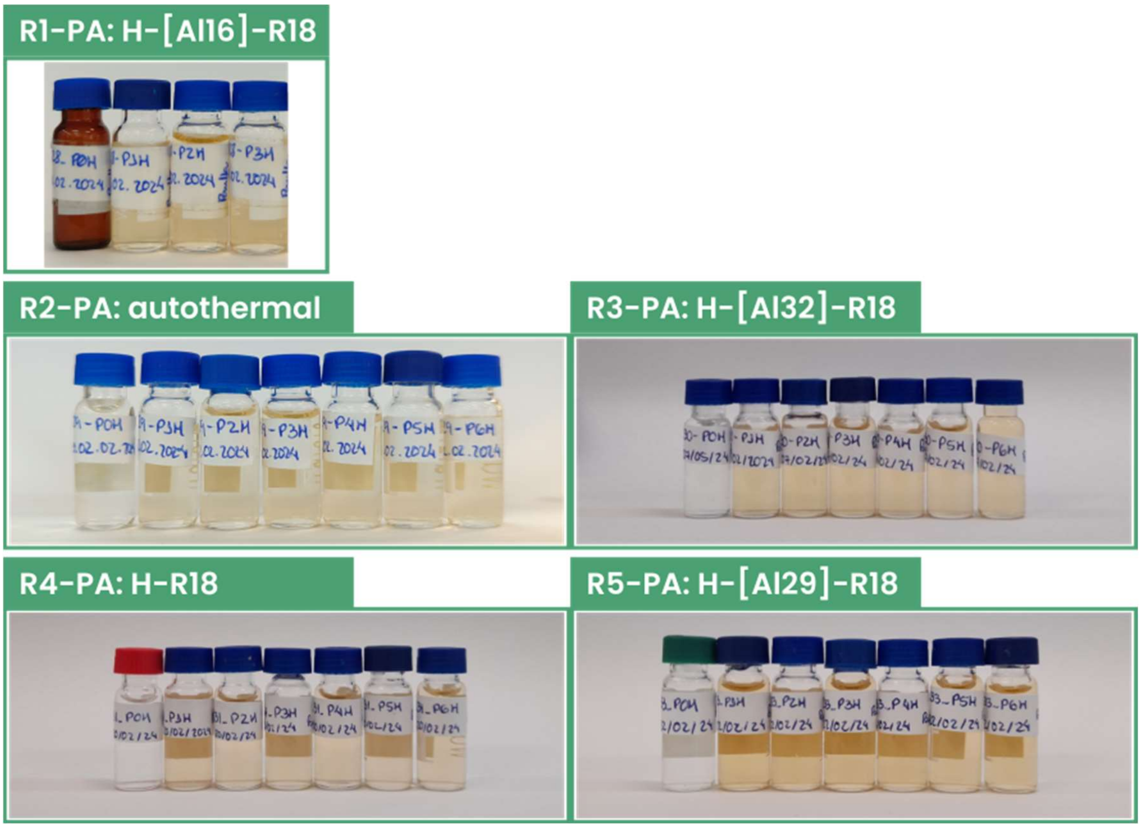

Figure E.3: Aliquots of DHA in continuous flow reaction (fixed-bed in a tubular reactor).

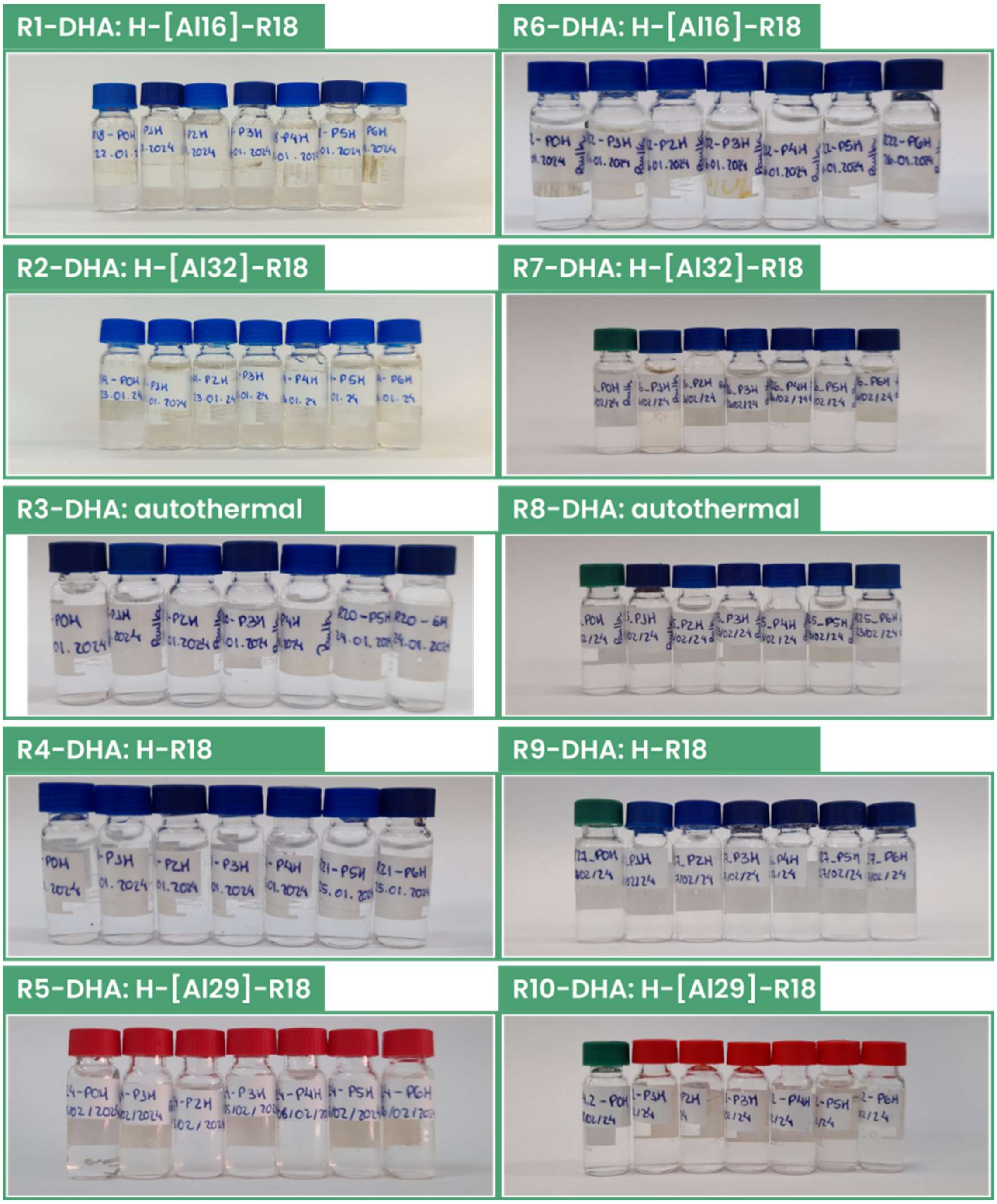

R1-DHA: H-[Al16]-R18

R6-DHA: H-[Al16]-R18

R2-DHA: H-[Al32]-R18

R7-DHA: H-[Al32]-R18

R3-DHA: autothermal

R8-DHA: autothermal

R4-DHA: H-R18

R9-DHA: H-R18

R5-DHA: H-[Al29]-R18

R10-DHA: H-[Al29]-R18

Figure E.4: Chromatograms of the pyruvaldehyde to lactic acid reactions (time of reaction = 3 h).

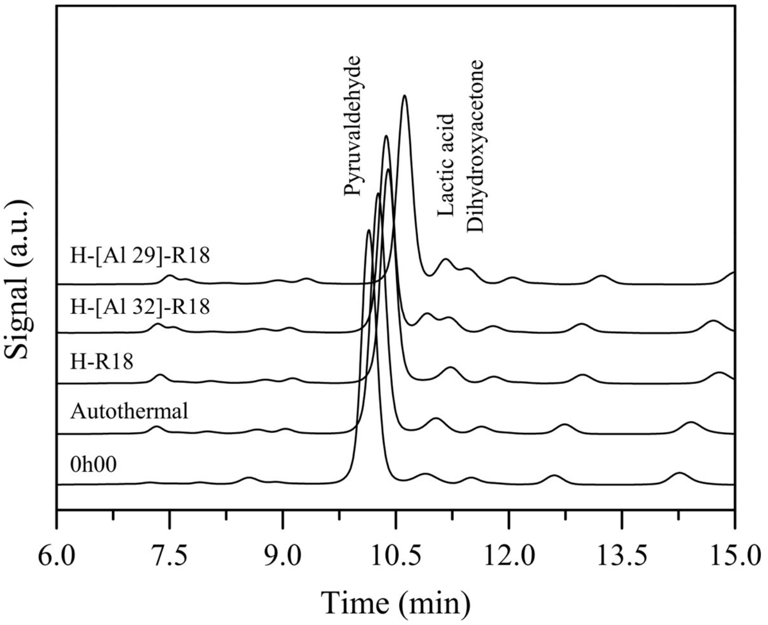

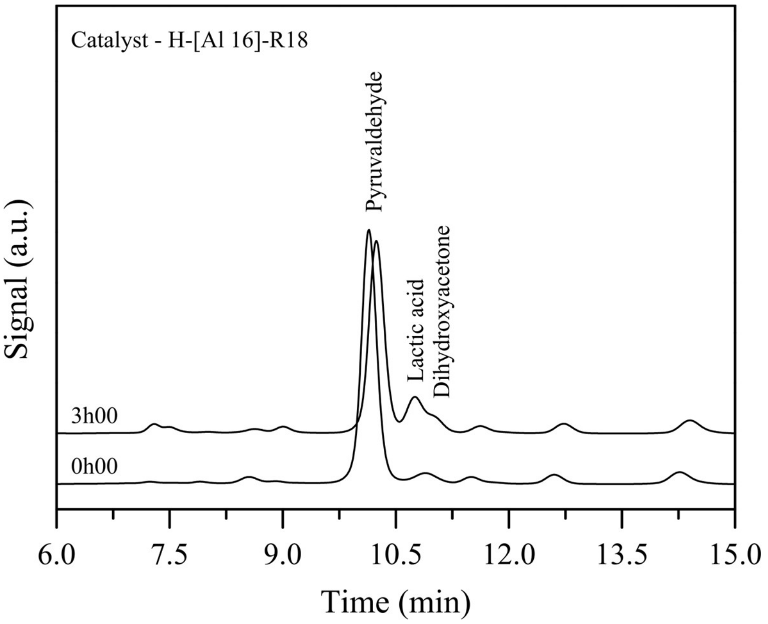

Figure E.5: Chromatograms of the dihydroxyacetone to lactic acid reactions (time of reaction = 6 h).

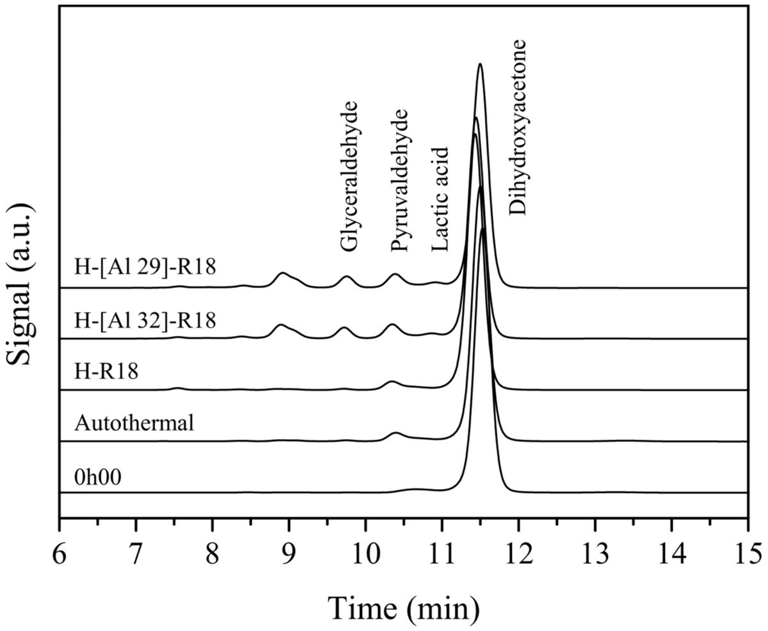

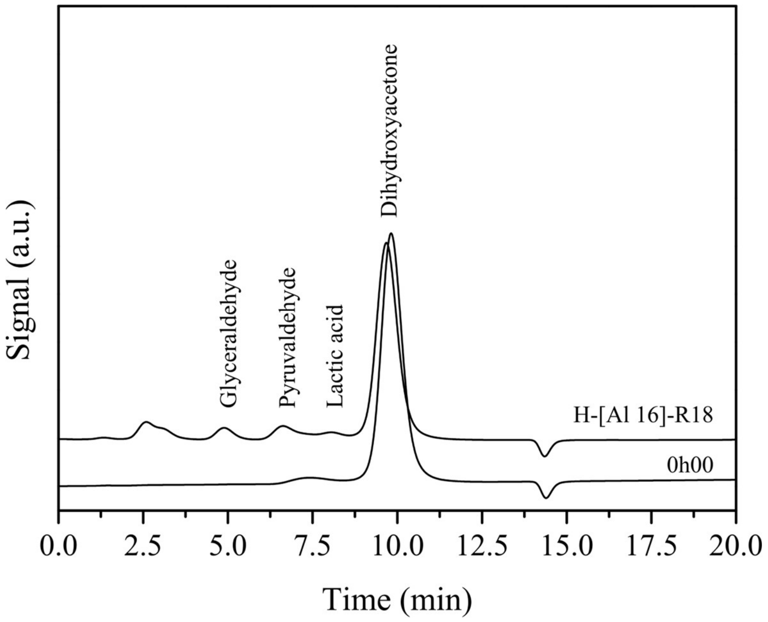

ANNEX F: DECLARATION FOR ALTERNATIVE FORMAT FOR DISSERTATION AND THESIS

DECLARAÇÃO

As cópias dos documentos de minha autoria ou de minha coautoria, já publicados ou submetidos para publicação em revistas científicas ou anais de congressos sujeitos a arbitragem, que constam da minha Dissertação/Tese de Mestrado/Doutorado, intitulada *“Acidity of 2D lamellar aluminosilicates in the presence and absence of water” (Acidez de aluminossilicatos lamelares 2D na presença e na ausência de água)* não infringem os dispositivos da Lei nº 9.610/98, nem o direito autoral de qualquer editora.

Campinas/SP, 07 de janeiro de 2025.

gov.br
Documento assinado digitalmente
PAULLA BEATRIZ FRANCA DE SOUSA
Data: 07/01/2025 14:15:56-0300
Verifique em https://validar.iti.gov.br

Autor CPF nº 103.518.804-02

gov.br
Documento assinado digitalmente
HELOISE DE OLIVEIRA PASTORE JENSEN
Data: 07/01/2025 13:33:03-0300
Verifique em https://validar.iti.gov.br

Orientador CPF n° 068.755.698-84